2010

Consequences of coaxial jet penetration performance and shaped charge design criteria

Hasenberg, David

Monterey, California. Naval Postgraduate School

NPS-PH-10-001

NAVAL POSTGRADUATE SCHOOL

MONTEREY, CALIFORNIA

CONSEQUENCES OF COAXIAL JET PENETRATION PERFORMANCE AND SHAPED CHARGE DESIGN CRITERIA

by

David Hasenberg

April 2010

Approved for public release; distribution is unlimited

THIS PAGE INTENTIONALLY LEFT BLANK

NAVAL POSTGRADUATE SCHOOL
Monterey, California 93943-5000

Daniel T. Oliver
President

Leonard A. Ferrari
Executive Vice President
Provost

This report contains the results of research conducted at the Naval Postgraduate School, under an exchange agreement with the Helmut Schmidt University (German Armed Forces), in partial fulfillment of the requirements for the Degree ”Diplom Wirtschafsingenieur” in Industrial Engineering.

This report was prepared by:

_____
David Hasenberg

Reviewed by:

_____
Andres Larraza
Department of Physics

Released by:

_____
Karl A. van Bibber
Vice President and
Dean of Research

THIS PAGE INTENTIONALLY LEFT BLANK

REPORT DOCUMENTATION PAGE		Form Approved OMB No. 0704-0188

1. AGENCY USE ONLY (Leave blank)	2. REPORT DATE	3. REPORT TYPE AND DATES COVERED
	April 2010	Diplomarbeit, Technical Report: 11/2009-04/2010

4. TITLE AND SUBTITLE: Consequences of Coaxial Jet Penetration Performance and Shaped Charge Design Criteria

5. FUNDING NUMBERS

6. AUTHOR(S): David Hasenberg

7. PERFORMING ORGANIZATION NAME(S) AND ADDRESS(ES)
Naval Postgraduate School
Monterey, CA 93943-5000

8. PERFORMING ORGANIZATION REPORT NUMBER
NPS-PH-10-001

9. SPONSORING/MONITORING AGENCY NAME(S) AND ADDRESS(ES)
Helmut Schmidt University, University of the Federal Armed Forces Hamburg; Holstenhofweg 85, 22043 Hamburg, Germany

10. SPONSORING/MONITORING AGENCY REPORT NUMBER

11. SUPPLEMENTARY NOTES: The views expressed in this thesis are those of the author and do not reflect the official policy or position of the Department of Defense or the U.S. Government.

12a. DISTRIBUTION / AVAILABILITY STATEMENT
Approved for public release; distribution is unlimited

12b. DISTRIBUTION CODE
A

13. ABSTRACT (maximum 200 words)

There are longstanding interests in multi-material shaped charge liners for purposes of, for example, diagnosing jet formation, overcoming coherent flow limitations, and enhancing behind the target effects.

This research shows the possibilities for generating stable multi-material coaxial shaped charge jets. General design criteria and guidelines for multi-material coaxial jetting and penetration are developed and investigated, based on experimental data and simulation of a 100 mm charge.

Further, the influence on jet coherency and the effect of density variation on penetration is studied. Findings are in agreement with Harisson's and Walker's coherency theory, showing that the flow velocity is the key factor for jet coherency. Multi-material design concepts are presented and tested with the finite difference code ANSYS AUTODYN.

14. SUBJECT TERMS	15. NUMBER OF PAGES
shaped charge, multi-material liner design, jet coherency, coaxial penetration, finite difference computation ANSYS AUTODYN	213
	16. PRICE CODE

17. SECURITY CLASSIFICATION OF REPORT	18. SECURITY CLASSIFICATION OF THIS PAGE	19. SECURITY CLASSIFICATION OF ABSTRACT	20. LIMITATION OF ABSTRACT
Unclassified	Unclassified	Unclassified	UU

NSN 7540-01-280-5500

Standard Form 298 (Rev. 2-89)
Prescribed by ANSI Std. 239-18

THIS PAGE INTENTIONALLY LEFT BLANK

ABSTRACT

There are longstanding interests in multi-material shaped charge liners for purposes of, for example, diagnosing jet formation, overcoming coherent flow limitations, and enhancing behind the target effects.

This research shows the possibilities for generating stable multi-material coaxial shaped charge jets. General design criteria and guidelines for multi-material coaxial jetting and penetration are developed and investigated, based on experimental data and simulation of a 100 mm charge.

Further, the influence on jet coherency and the effect of density variation on penetration is studied. Findings are in agreement with Harisson's and Walker's coherency theory, showing that the flow velocity is the key factor for jet coherency. Multi-material design concepts are presented and tested with the finite difference code ANSYS AUTODYN.

THIS PAGE INTENTIONALLY LEFT BLANK

TABLE OF CONTENTS

THIS PAGE INTENTIONALLY LEFT BLANK

LIST OF FIGURES

THIS PAGE INTENTIONALLY LEFT BLANK

LIST OF TABLES

THIS PAGE INTENTIONALLY LEFT BLANK

LIST OF SYMBOLS

Symbol	Explanation
α	Liner angle
β	Liner turning angle or liner collapsing angle
β^+	Initial liner turning angle or liner collapsing angle (PER-theory)
δ	Angle between V_0 vector and perpendicular to the initial liner
η	Base insert angle
ξ	Base insert angle
CD	Charge diameter
E	Gurney energy
$\sqrt{2E}$	Gurney velocity coefficient
M	Metall mass
C	Explosive charge mass
D or U_D	Detonation velocity
U_s	Shock velocity
V_0	Collision/ collapse velocity
v_f	Flow velocity
v_{fl}	Limiting flow Velocity
v_s	Stagnation velocity
v_{slug}	Slug velocity
v_j	Jet velocity
m	Liner mass
m_j	Liner mass flowing into jet
m_s	Liner mass flowing into slug
c or c_0	Bulk speed of sound
c_l	Longitudinal sound speed
Ma	Mach number
U	Penetration velocity
ρ_j	Density of rod/ jet
ρ_t	Density of target
l_j	horiz. distance between theoretical apex and point of maximum jet tip velocity
l_{th}	distance between theoretical apex and current apex

THIS PAGE INTENTIONALLY LEFT BLANK

LIST OF ABBREVIATIONS

Symbol	Explanation
NPS	Naval Postgraduate School
HSU	Helmut-Schmidt-University
UIUC	University of Illinois at Urbana-Champaign
CD	Charge Diameter
NM	Nitromethane

THIS PAGE INTENTIONALLY LEFT BLANK

I. INTRODUCTION

The goal of this research is to develop general criteria for generating multi-material and coaxial jetting. Specific objectives are directed towards determining the structural stability (and governing factors) of multi-material jets and applying the knowledge for purposes of recommending a design for introduction into an University of Illinois experiment.

Unpublished experimental results of copper/zirconium shaped charge configurations by Kennedy and Brown, and reported data by Chanteret are studied for purposes of validating ANSYS AUTODYN predictions and examining a critical coherency issue, respectively.

Techniques are developed for estimating mass partitioning during liner collapse, and the rate of flow of liner mass into jet.

Motivations for the research, technical approaches and interpretation of results are reported in the following sections.

THIS PAGE INTENTIONALLY LEFT BLANK

II. MOTIVATION

A. ADVANTAGES OF A BIMETALLIC LINER

There are long-standing interests in using multi-material shaped charge liners for purposes of, for example:

- Diagnosing jet formation
- Overcoming limitations imposed by mechanical response, i. e. shock velocity, coherency
- Increasing jet ductility from exothermic inter-metallic reaction between metals during jet formation
- Reducing cost of high density or high valued materials (e. g. gold, platinum, rhenium, tantalum)
- Adding materials (e. g. magnesium, aluminum, titanium, zirconium, hafnium) for enhancing behind the target effects (blast effects in the interior of penetrated targets).
- Generating coaxial bimetallic flow through the entire jet formation process for purposes of protecting an environmentally reactive core, for electro/magnetic insulation, and for application of additional chemical reactions [Duo05]
- Reducing storage hazards

In order to add specific abilities or to expand the capability of solid material liners, a second liner material can be applied to what is then called a bimetallic liner. Bimetallic liners have been considered in the past for various purposes. Many researches made experiments with different material substitutions in the liner. These are for example replacements at the apex, multi-layered stratified liners, base inserts, and sleeve configurations.

Copper is the most common material used for shaped charge liners because of its ductility, density, its relatively low cost, and machining ease. Although not unique to this research there are several other metals that can be usefully applied, particularly in combination with copper, for increasing elements of performance. Some of these combinations are highlighted in this research.

B. PREVIEW OF INITIAL RESULTS AND IMPLICATIONS TO PROJECT GOAL AND OBJECTIVE

Shaped charge simulations and rod penetration simulations were conducted, both accompanied by literature review.

The validity of the AUTODYN code to accurately predict jet formation was shown in three cases. One involving a 42° copper-lined nitromethane charge, another containing Octol explosive, and a third charge containing a 42° copper/zirconium lined charge.

The effect of liner angle decrease on jet coherency confirms findings reported by Chanteret and supports conclusions made by Harrison and Walker regarding the effect of bulk and longitudinal sound velocities. This analyses benefited from a technique used to monitor the flow and stagnation velocities during jet formation.

Based on results from set of experiments conducted by Kennedy and simulations conducted in this research it appears that it is possible to expect good adhesion between materials in a coaxial jet between onset of formation to target impact in the absence of radical differences in the charge-to-mass ratio.

General approaches for generating stable multi-material jets are shown, and a candidate solutions for a UIUC experiment is recommended.

For those cases where penetration enhancement is a motivation, it is shown that the most favorable distribution in a coaxial jet is a higher density core than the surrounding sleeve.

General techniques improving the workflow for changing geometrical setups in AUTODYN are presented, and the benefits of a CAD/ AUTODYN interface are discussed.

C. RESEARCH GOAL AND OBJECTIVE

The main focus of this research is to examine effects of multi-material jet formation and to provide guidelines for bimetallic coaxial jetting and penetration. It involves literature reviews, using the ANSYS AUTODYN code, assessment of experimental data, and a recommendation for a UIUC experiment.

The jet formation and the eventual separation of the liner materials is one of the main aspects that will be addressed in this research.Therefore the jet formation, resultant jet velocity and mass distributions of different liner designs and materials will be compared. Additionally, the importance of radial velocity gradients, shock pressures and impact forces during collapse, and thermal expansion will be investigated.

Effects of different densities over a potential range of velocities on penetration as well as the effect of basal liner substitutions (with different variations) will be studied.

THIS PAGE INTENTIONALLY LEFT BLANK

III. TECHNICAL BACKGROUND

This chapter is primarily[1] based on [ZW89] and covers the relevant technical background for shaped charge jetting and penetration in this research.

A. SHORT INTRODUCTION TO SHAPED CHARGES

The beginning of shaped charge science is relatively recent, its development did not occur in one step. A shaped charge is an explosive charge with a lined or unlined cavity. The hollow cavity effect was observed by von Foerster in Germany in 1883 and five years later by Munroe in the United States. This effect points to the partial focusing of explosive gases (detonation energy) by a void cut into a piece of explosive. The hollow cavity effect is known as the Munroe or von Foerster effect. If the cavity is unlined, a fast moving plasma will form. A lined cavity (i.e. hemishere, conical, trumpet) will deform into a fast moving jet of the lined material. In both cases the indentation in a target will be greater than that from the detonation of a solid block of explosive. All other things equal, a hollow charge with a lined cavity will cause a greater amount of target displacement than one without a liner.

The high velocity jet (usually 7-10 km/s) is generated by high pressure at the collision interface, which causes plastic flow.

Fig. 1 provides the collapse process of a conical liner. The double-dashed line represents the original liner shape and black material shows the momentary liner material shape as the detonation front travels from left to right.

The military value of the shaped charge effect and contribution of the liner were not realized until the end of the Second World War after the development of flash radiography in Germany and the United States. The development of jet formation theory and hydrodynamic penetration theories followed.

[1] Additional references are denoted accordingly

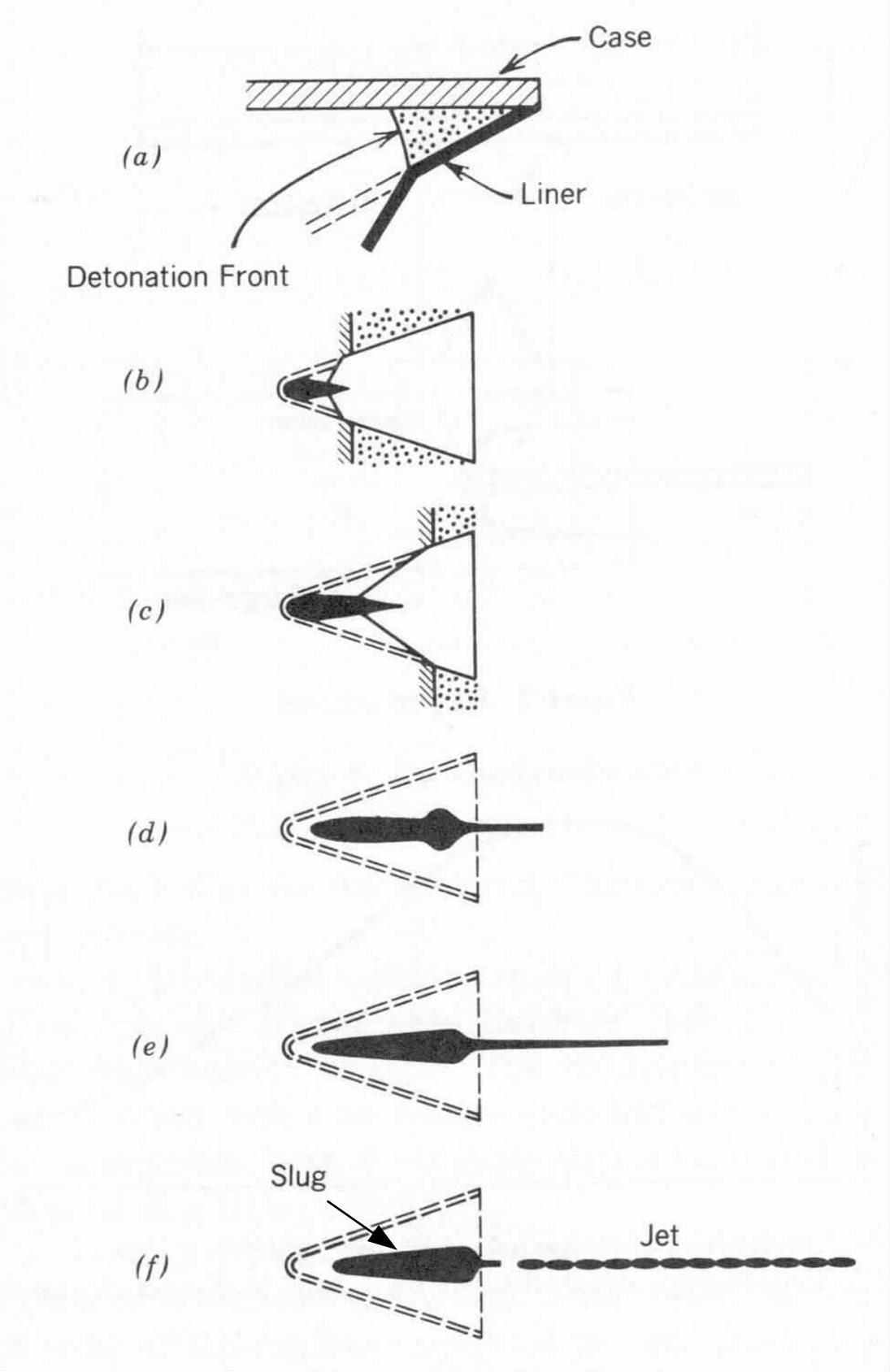

Figure 1: Progress inward collapse of a conical shaped charge liner and jet formation [ZW89]

B. JETTING THEORY

This section gives an brief overview of the development of important equations and theories for the shaped charge concept and jet formation. The leading concepts are presented and their applicability reviewed.

1. Nomenclature

For a better understanding of the subsequent presented theory, the parameters of a shaped charge will be introduced.

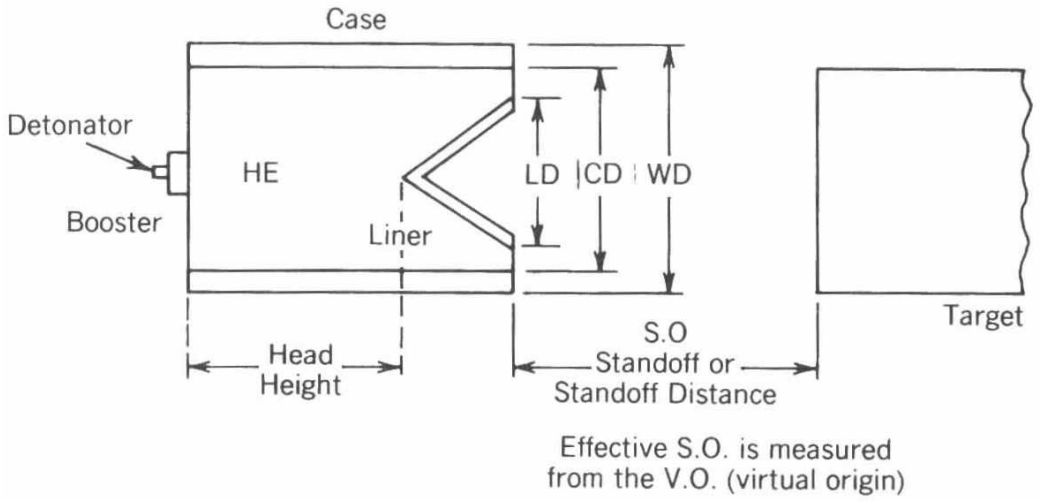

Figure 2: Principle design parameters of a shaped charge with point initiation [ZW89]

Figure 2 provides an example for a shaped charge with the parameters:

- **Case** or confinement is a metallic or fiber material (i) to help in loading the charge, (ii) to increase energy deposition from the detonation to the liner, especially along the basal portion of the liner where explosive mass decreases, and (iii) to provide fragmentation in antipersonnel devices as secondary application.
- **LD** Liner diameter is the outer diameter of the liner.

- **CD** Charge diameter is the inner diameter of the case or in unconfined setups the outer diameter of the explosive; in most cases the charge diameter is equal to the liner diameter.

- **WD** Warhead Diameter is the outer diameter of the warhead.

- **HE** High Explosive

- **Head Height** Distance between the initiation point and liner apex. The radius of curvature of the detonation front as it moves across the liner and resultant energy coupling are governed by this distance. However, effective energy coupling diminishes with distance (i.e., HE), and after approximately 1.5 CD there is very little if any contribution. For further information see [ZW89, p. 315].

- **Standoff** refers to the distance of the liner base form the target; the jet must have time and distance to form.

2. The Gurney model [ZW98]

During the 1940s, Gurney developed equations to describe effects of explosively driven metal plates. Explicit algebraic relationships for calculating the energy transformation of high explosive chemical energy to kinetic energy, is one relationship, the Gurney model covers.

The Gurney energy, E, is the energy from the detonation that is responsible for metal acceleration. Cooper and others have developed empirical relationships between E and detonation velocity. Kennedy (a different Kennedy) derived relationships for estimating the instantaneous velocities of non-fragmenting masses as functions of the Gurney Energy and the explosive mass to inert mass ratio.

The Gurney energy refers to the Gurney energy term related to the fraction of the energy released, that affects the motion of adjacent metal (e. g. flat plate, cylindrical wall, spherical wall, etc.). The physical basis for this model is the conservation of momentum and energy. Another expression, which occurs in every Gurney expression, is represented

by the Gurney velocity coefficient $\sqrt{2E}$. It is used preferential in governing equations, but values for both expressions are tabulated for explosives[2].

The applicable range of the Gurney model is given by the dimensionless ratio between metal mass M and explosive mass C: $0.1 < M/C < 10.0$ with an approximation within 10 %. Typical M/C-ratios in this research are about 0.2. A further restriction is the direction dependency of the detonation propagation which is not covered for different propagation angles. Furthermore, the equations are only for one-dimensional motion, rarefaction effects and shock characteristics of metals are ignored, and Gurney assumes instantaneous acceleration of the liner. As one can see, the simplicity of the Gurney model has inherent restrictions.

Nonetheless, in general, the final metal velocity is a direct function of the Gurney energy term (dependent on explosive) and the metal to charge mass ratio M/C, also referred as the loading factor. A higher loading factor, i. e. more metal mass or less explosive mass, results in a lower metal velocity. This basic relationship plays a role in using different liner materials with the same geometrical shape, because this results in a change of M, thus in a change of the loading factor and velocity.

However, the Gurney method does not cover the effect of curvature (compare with Fig. 1) and assumes the metal moving in a normal direction to its surface. The effect of a grazing impact and resultant metal turning, for example in the treatment of the deformation of a shaped charge liner, is more accurately covered using the Taylor angle approximation, discussed below. The ultimate treatment is covered in finite difference and/or finite element computations.

3. Taylor angle approximation

The Gurney model assumes that the detonation wave encounters the metal normal to its surface. Though, in shaped charge setups the detonation wave meets the liner in a grazing angle. The Taylor angle approximation (1941) covers grazing incidence of detonation waves encountering a metal plate.

[2] e. g. [Coo96, ZW89]

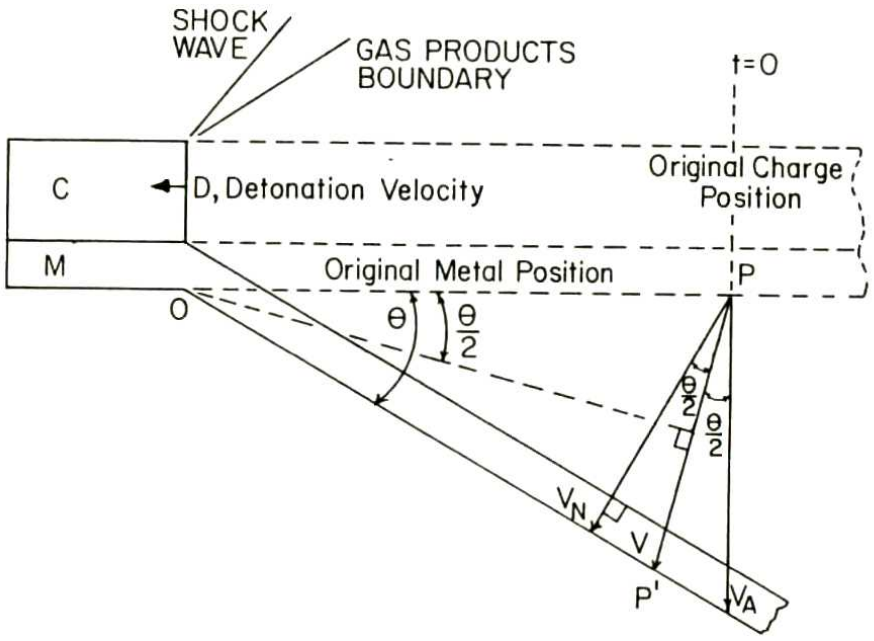

Figure 3: Taylor direction of metal projetion by a grazing detonation wave [ZW89, p. 64]

This model assumes no change in length, thickness, and shear flow. It implies that the metal plate experiences only rotation. With given geometrical relations it is possible to calculate velocity values depending on the detonation velocity and the angles. Figure 3 represents the principle for Taylor's angle approximation. The detonation wave, with a shock wave at the front, travels from right to left and forces the metal plate to deform. From the geometrical relationship one can see the rotation of the plate, as point P travels with the velocity V on the bisecting line of θ with turning point in O. $\overline{OPP'}$ is a isosceles triangle representing metal plate bending related to to leading velocity vectors.

Two-dimensional hydrocode computations are relied upon for more accurate predictions of liner collapse in this research. The Gurney treatment is used only as a guide for estimating mass substitutions.

4. Shaped charge jet formation

a. Birkhoff theory

The first theory on conical shaped charges was proposed by Birkhoff et al. (1948), assuming the pressures during the jet formation to be sufficiently high that material

strength does not play a role. The liner geometry is represented as a wedge with constant liner angle and the material is modeled as an inviscid, incompressible fluid. Birkhoff assumes a steady-state collapse model with constant liner collapsing velocity.

Constant jet lengths are predicted, by projections, as a result of the assumptions in the Birkhoff theory. But experiments show that the jet elongates due to a high-velocity jet tip and a slower moving tail, i.e. the jet has a velocity gradient decreasing from tip to tail. This important fact is covered by the Pugh, Eichelberger and Rostocker (PER theory) who implemented a velocity gradient into Birkhoff's steady-state calculations.

b. PER theory

PER theory takes into consideration the fact that the collapse of a constant thickness conically shaped liner decreases from apex to base. The geometry used in the model is illustrated in Figure 4.

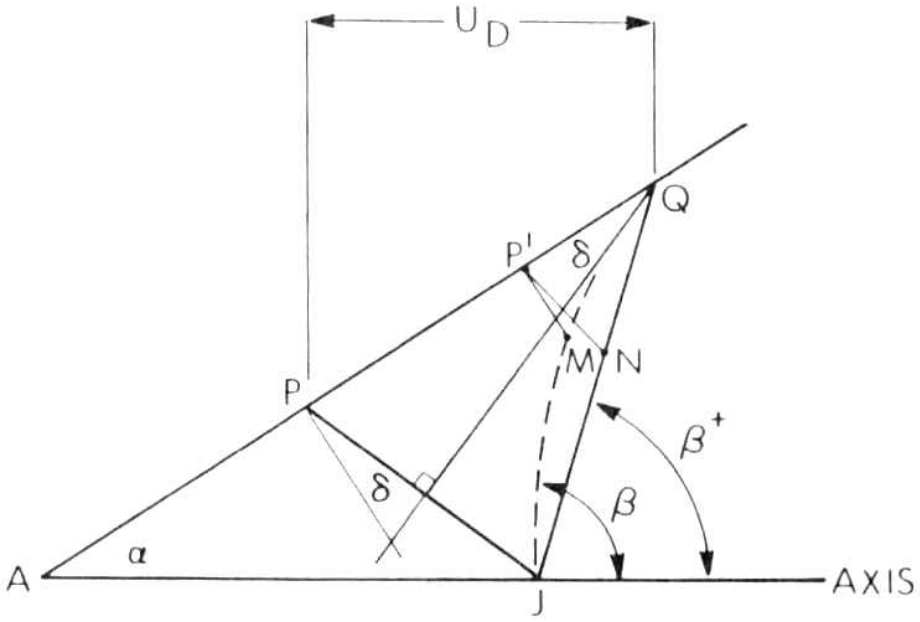

Figure 4: Collapse process for variable velocity liner [ZW89, p 78]

The denotation wave travels along the surface APQ. For example, one liner element at point P travels to J, and a second element at point P' travels to M. The element at P' starts to flow later and moves therefore slower. This is an improvement to the Birkhoff

theory. If this issue would not be taken into account, then the liner element at P' would travel to point N and the collapse velocities of both liner elements would be identical. The collapse angle increases during the formation from the steady-state β^+ to β.

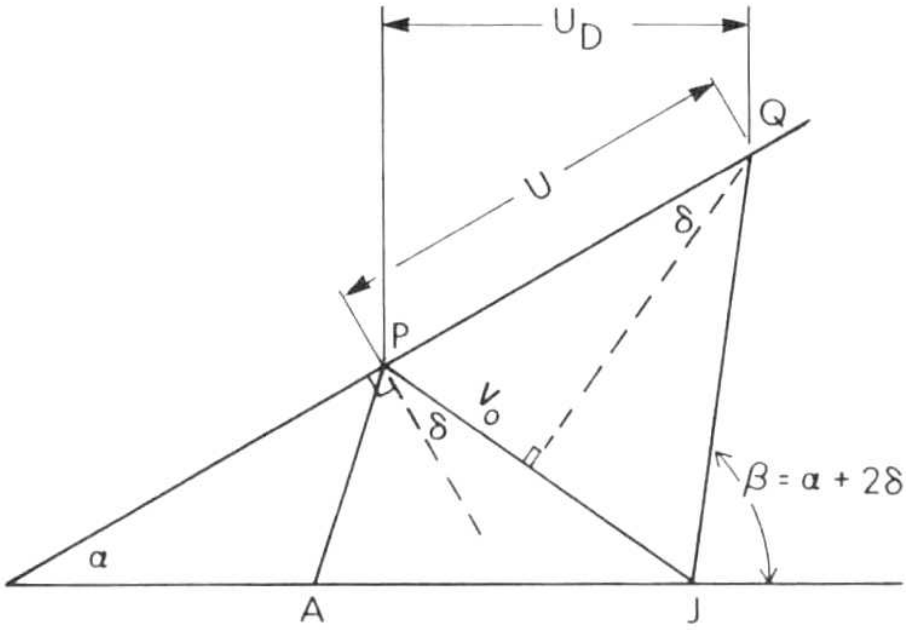

Figure 5: Velocity vectors for a collapsing process [ZW89, p. 79]

Essential geometries used to construct trigonometric relations, derived by PER, are shown in Figures 5 and 6. In Fig. 5, which shows the upper half of a symmetric conical liner, α represents the liner angle and β the liner wall collapse angle. The detonation wave needs time to move along the liner from apex to base, this results in β being greater than α. In a stationary coordinate system, the liner velocity is denoted by V_0, U_D is the detonation velocity. The liner particles move along the liner on $\overline{PQ}$ and flow into the jet along $\overline{PA}$. $\overline{PA}$ is parallel to $\overline{QJ}$; and $\overline{QJ}$ has the same magnitude as $\overline{PQ}$. This means, that in a moving coordinate system the liner element velocity entering and leaving the region P is equal.

$\overline{AJ}$ represents the velocity of the stagnation point. The stagnation point describes the high pressure region were the liner finally divides into jet and slug. This is

better represented in Fig. 6, which provides the relationship between the flow velocity v_f, the liner collapse velocity V_0, and the stagnation velocity v_s[3].

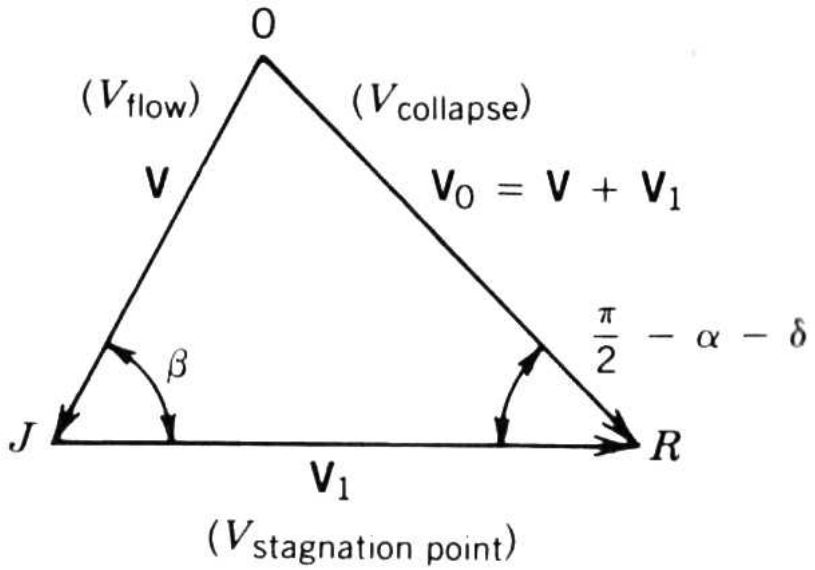

Figure 6: Relationship between velocities in the stagnation region [ZW89, p. 80]

The collapse velocity (i.e., V_0) varies approximately with the Gurney solution for a tampered unsymmetric sandwich. The velocities can be expressed as

$$v_f = \frac{V_0 \cos(\alpha + \beta)}{\sin \beta}, \tag{1}$$

and

$$v_{stag} = \frac{V_0 \cos(\beta - \alpha - \delta)}{\sin \beta}. \tag{2}$$

In fixed coordinates, the velocities for the jet v_j and the slug v_{slug} are

$$v_j = v_s + v_f, \tag{3}$$

and

$$v_{slug} = v_s - v_f, \tag{4}$$

[3]Notation used here differs from [ZW89]

Using equations (1) and (2) they become

$$v_j = V_0 \csc\frac{\beta}{2}\cos\left(\alpha+\delta-\frac{\beta}{2}\right), \tag{5}$$

and

$$v_{slug} = V_0 \sec\frac{\beta}{2}\sin\left(\alpha+\delta-\frac{\beta}{2}\right). \tag{6}$$

To solve the problem, relationships for V_0 and for the angles are needed. Values for V_0 can be calculated with the Gurney equations. Taylor's theory provides the relationships to calculate the angles. To resolve the problem, former scientists simulated the collapse of a shell and used the liner collapse data to calculate resultant relationships (e. g. velocity, mass).

A multi-dimensional finite element hydrocode allows a better estimate for the effects of acceleration, liner collapse and material response. The computations proceed in one program and allow for further analyzing techniques on several parameters.

Equations for the fraction of liner mass going into jet and slug follow from the conservation of mass and momentum, where m is the liner mass, m_j and m_s the jet and slug masses, accordingly,

$$dm = dm_j + dm_s, \tag{7}$$

$$\frac{dm_j}{dm} = \sin^2\left(\frac{\beta}{2}\right), \tag{8}$$

$$\frac{dm_s}{dm} = \cos^2\left(\frac{\beta}{2}\right). \tag{9}$$

As mentioned before, decrease in flow rate occurs because of the increase in angle (liner turning), which also results in an increase in fractional mass flowing into jet. The stagnation velocity also decreases with angle turning in accordance with Eqs. (2).

One may think that the liner angle α, and consequently the increase of β, should be as small as possible to get a fast moving jet. Practically, this can result in no jet formation. Jetting criteria and further flow limitations are covered by section III.B.C.

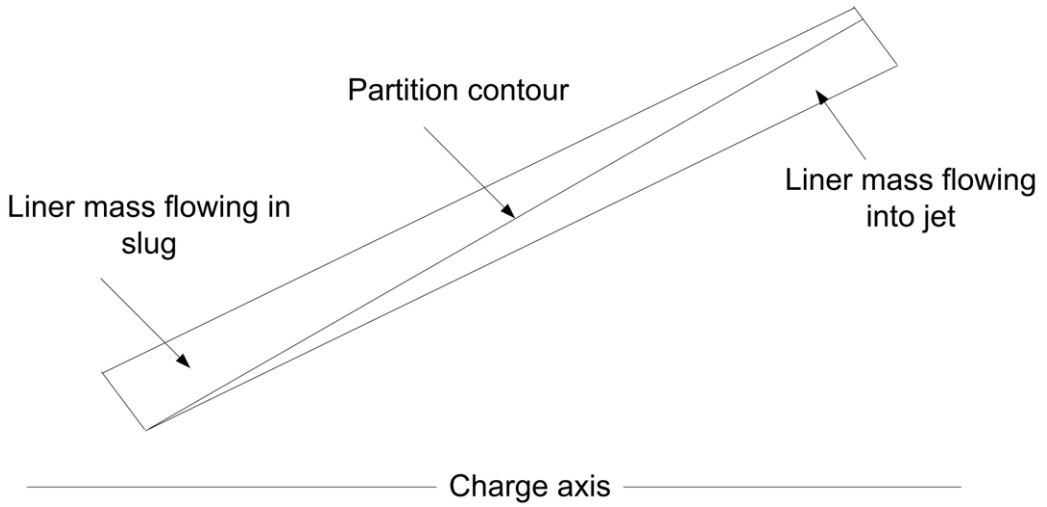

Figure 7: Mass partition of a conical liner

The general physical merit of the PER theory has been verified by several experiments and simulation calculations, hence it is the basis for all analytical shaped charge jet formation models. Of course, modifications have been made, for instance to include liner thickness, densities and other constants into the the calculations. For example, Harrison who presented the BASC[4] code at the US Army Ballistic Research Laboratory (BRL), applied modifications on the PER theory made by Defourneaux (1970) into his analytical computer code [Har81]. Further details are discussed in section IV.D.

Another issue should be pointed out here for the case of constant thickness conical shaped lined charges. The collapse velocities of liner segments about the apex and just above can not reach theoretical maximum velocities (e.g., as estimated by Gurney) because the distance from respective origins to collapse positions is too short. As a result, resultant jet velocities from this region can be slower than those that follow. This causes a so-called ”piling up” of the front jet particles and results in a negative velocity gradient. Particles behind the *first* part of the jet push the front and form the typically shaped jet tip presented in Fig. 9.

[4]BRL Analytical Shaped Charge

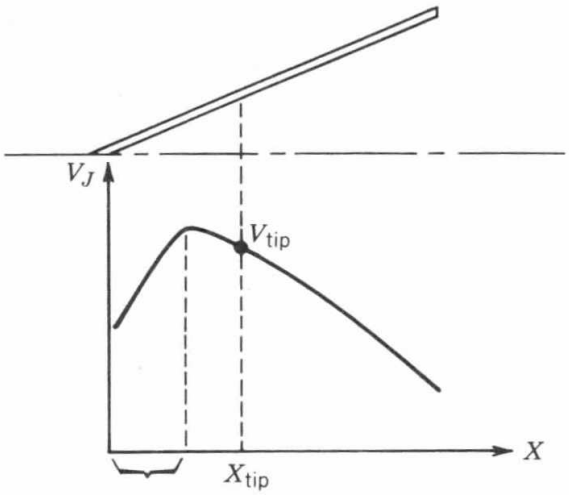

Figure 8: Jet tip velocity distribution showing a negative velocity gradient near the apex [ZW89, p. 87]

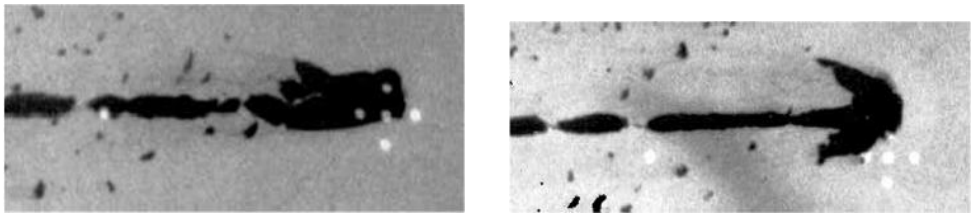

(a) FTD 13 (b) FTD 11

Figure 9: Radiographs of jet tip (both at 170 μs) illustrating the piling up of mass at the jet tip that results from an initial negative flow velocity gradient.[KB81]

c. General shaped charge model

The PER theory provides equations for a conically lined shaped charge. In this section, general relationships for shaped charge configurations will be presented. The modifications were mostly performed by Behrmann (1973) and also Carleone (1987) to reduce the assumptions in the original theory.

The equations for velocity and mass remain the same as those estimated by the PER theory. A relationship for δ is given by the Taylor angle relationship with

$$\sin \delta = \frac{V_0 cos\epsilon}{2U_D}, \tag{10}$$

where ϵ denotes the angle between the detonation front normal and the liner surface assigned at the liner surface, and U_D the detonation velocity.

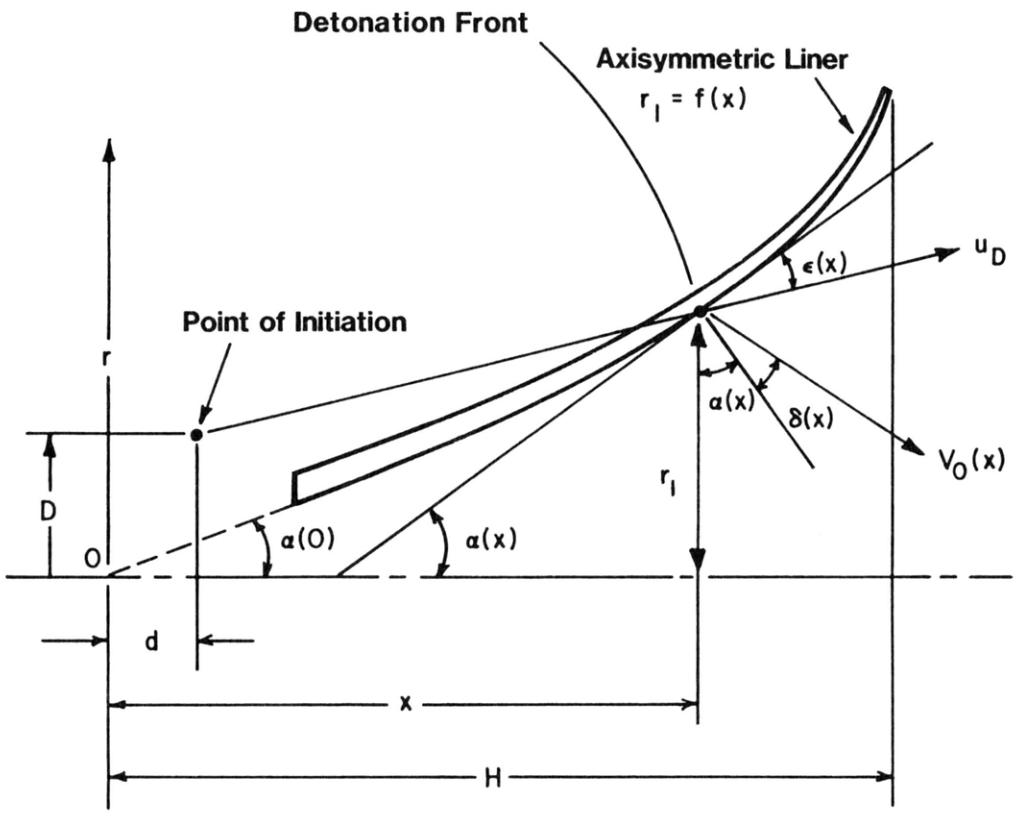

Figure 10: Geometrical shaped charge relationships in the generalized theory [ZW89, p]

In order to include variable liner angle and thickness, and other initiation types than the plane wave initiation, however, additional equations are derived by Behrmann in accordance with the geometries shown in Figure 10:

$$\tan(\alpha - \epsilon) = \frac{r_1 - D}{x - d}, \tag{11}$$

$$T(x) = \frac{1}{U_D}\left[(x-d)^2 + (r_1 - D)^2\right], \tag{12}$$

$$r(x) = r_1(x) - V_0\left[t(x) - T(x)\right] cos\left[\alpha(x) + \delta(x)\right], \tag{13}$$

$$Z(x) = x + V_0(x)\left[t(x) - T(x)\right] sin\left[\alpha(x) + \delta(x)\right], \tag{14}$$

were

r_1	radius of liner at point x
T	time for detonation wave to reach point x
t	time for a point x on the liner to reach a radius r
Z	corresponding x coordinate

The collapse angle from any given origin coordinate on the liner can be estimated from the above equations. There is implicitly assumed in this model, as in the PER theory, that the liner is incompressible and that each element of mass collapses on the axis of symmetry. Further mathematical derivations are provided by [ZW89]. The presented theories give an overview on the essential relationships of liner geometry, liner collapse, and jet formation.

C. JET COHERENCE

The selection of materials is very important in the design process. Although many applications use a copper lined charge, other materials or material combinations can be used to enhance penetration potential and/or alternatively to affect other intended effects. In order to understand the limitations on the material selection for the jet formation, it is

important to understand the physics, i.e. the leading variables of flow characteristics, jet formation and jet quality, in the jet formation region.

Fig. 11 provides the collapse region in a frame that is moving with the collapse point. It shows the collapsing (turning) angle β, flow velocity v_f, stagnation velocity v_s, and the jet velocity v_j. As mentioned in section III.B.4.b, one part of the liner is flowing into the slug, the other part flowing into the jet.

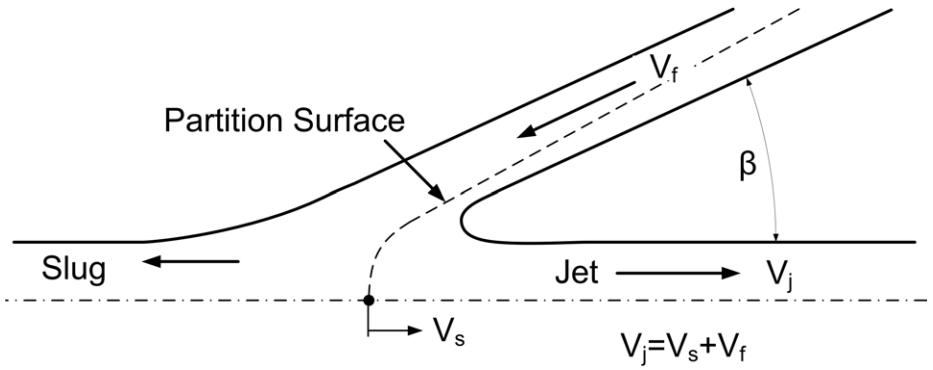

Figure 11: Flow diagram of liner material with a moving coordinate system

1. General guidelines

There are two attempts for jet coherency criteria. In the visco-plastic jet formation theory (Godunov et al. 1975) the coherency criterion is referred to the Reynolds number which has to be greater than two for a coherent jet. This won't be considered in this thesis.

Based on the fact that inviscid flow occurs during the jet formation, the jetting criteria presented in table 1 are based on the findings of Chou et al. [CCK76]. These criteria are based on impinging shells or plates but can be applied to axisymmetrical cases for conical shaped charges. The model provides limits for jet formation based on the sonic condition of liner material flow through the stagnation region and a critical collapse angle. Values of critical beta angles may be calculated for a given material with derivations and equations presented in [CCK76].

Collision Type	Velocity	Turning Angle	Jetting	Jet Type
subsonic ($Ma < 1.0$)	$v_f \leq c$	-	✓	solid coherent
supersonic ($1.0 < Ma < 5.0$)	$v_f > c$	$\beta > \beta_c$	✓	not coherent
supersonic	$v_f > c$	$\beta < \beta_c$	No	-

Table 1: Jetting criteria [CCK76]; (v_f flow velocity, c bulk speed of sound of the material)

Harrison separately postulates that there is a flow velocity threshold that can not support coherency. The difference between a coherent and incoherent jet is illustrated in Figure 12.

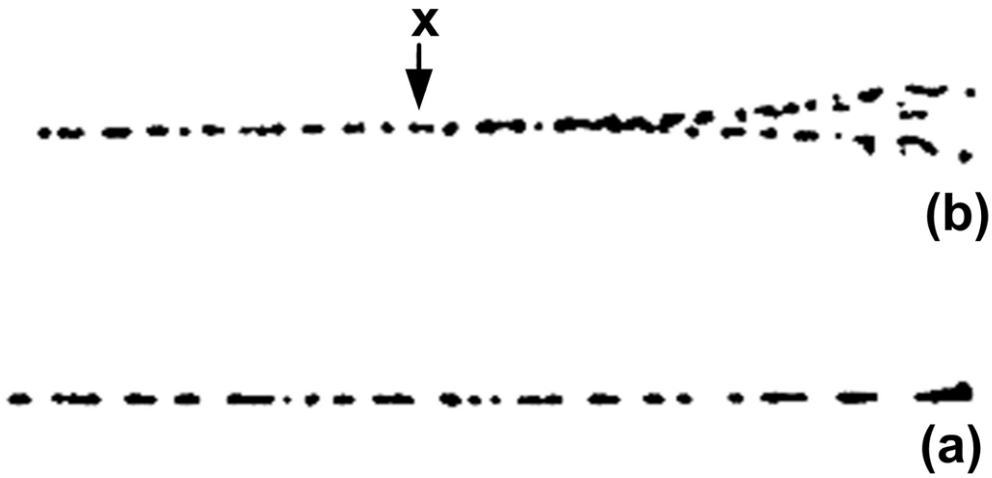

Figure 12: Radiographs of conical copper-lined charges with (a) 40° and (b) 20° liner angle. The jet from the 20° lined charge is an example of an unstable (and bifurcating) jet. [CCK76]

Harrison [Har81] postulated that the limited Mach number, Ma, for coherent flow is

$$Ma = \frac{v_f}{c_0} < 1.23 \tag{15}$$

where v_f is the flow velocity and c_0 is the bulk sound velocity of the jetting material.

Chanteret [Cha92] concluded from experimental studies that the Harrison criteria is valid for iron, nickel, and molybdenum, in addition to copper; and that this threshold for aluminum is in doubt. The aluminum jet tip expanded radially at much lower velocities than expected.

Taking the presented findings[5] into account, then the bulk sound speed is one leading parameter for applicable materials. Table 2 presents the bulk sound speed c_0, density ρ_0, and a calculated flow velocity limit (threshold parameter) $v_{fl} = 1.23\ c_0$ for various appropriate liner materials. Values for the dimensionless parameter, s, in the Hugoniot expression are also given in Table 2.

Material	c_0 (km/s)	s	ρ_0 (g/cm^3)	v_{fl}
Tungsten	4.029	1.237	19.224	4.956
Tantalum	3.414	1.201	16.654	4.199
Hafnium	2.954	1.121	12.885	3.633
Molybdenum	5.124	1.233	10.206	6.303
Copper	3.940	1.489	8.930	4.846
Nickel	4.438	1.207	8.874	5.459
Zirconium	3.296	1.271	6.505	4.054
Titanium	4.877	0.767	4.528	5.999
2024 Aluminum	5.328	1.338	2.785	6.553

Table 2: Hugoniot values for liner materials and estimates of limiting flow velocity in accordance with the Harrison Criteria.

The threshold for coherency is discussed in further detail (including recent theory) in section IV.D.

2. Opportunities of bimetallic liners

In the previous subsection limitations for coherent jetting were described. These limitations can be manipulated by the use of bimetallic liners. [CL95] examined the idea of exceeding the maximal velocity for coherent copper jets. They made experiments with two setups (the second material was nickel, partially substituting copper in both cases):

- adding material between the explosive and the copper liner (sleeve)
- replacing the apex material with a second material

[5] Many papers were published adding to the initial findings of Chou et al. and Harrison with various approaches. Anyhow, it is in general agreement that the maximum velocity for a coherent jet increases with a higher liner bulk sound speed.

Nickel was chosen due to its higher sound speed but almost the same density as copper, likely minimizing disturbances at the material interfaces. [CL95] used a 20° liner with 50 mm charge diameter to investigate means for overcoming the intrinsic coherent flow limit for copper by substituting nickel, a faster sound velocity material in the first half of the liner where flow is the fastest. In these experiments, a high sound speed material (nickel) was combined with a high ductile material (copper) with the goal of a coherent jet formation, high jet tip velocity, late jet breakup and thus high penetration performance.

For the bimetallic sleeve design, the performance did not improve, in fact the jet was less stable. In the second design, where apex material was replaced by nickel, a stable jet with nickel at the jet tip and copper at the rear was established. This bimetallic jet was coherent and with a small gap between materials.

With the aforementioned jetting criteria, a stable jet will not form if $v_f > c$. This criterion can be expanded with a bimetallic liner; the flow velocity has just to be lower than the highest sound speed material which leads to the assumption $c_I < v_f < c_{II}$. c_I denotes the lower sound speed, c_{II} the higher sound speed, accordingly. This applies for the case where the higher sound velocity partition is composed of jetting material and the other material goes into slug.

The materials, listed in table 2, are a selection of potential liner candidates for bimetallic configurations. The order of Table 2 is arranged by density and thus penetration performance which is treated in the next section. From another view, all other things equal, the order of permissible maximum coherent flow for materials of Table 2 is given by Table 3. A combination of both, high density and high permissible coherent flow is the key for successful shape charge applications.

D. PENETRATION THEORY

A utility of shaped charge devices is their ability to penetrate deeply and rapidly into structures (armor, rocks, soil, wood, ice, etc.) because of intense and focused kinetic energy output in the jets that are produced. The parameters governing penetration capability (and

Aluminum
Molybdenum
Titanium
Nickel
Tungsten
Copper
Tantalum
Zirconium
Hafnium

Table 3: Selected materials (Tab. 2) listed by maximum coherent flow (descending order)

predictability) are discussed in this section. With the given information it is possible to estimate penetration capabilities of shaped charge jets before conducting more vigorous penetration simulations.

1. Hydrodynamic penetration theory

The hydrodynamic theory of shaped charge penetration is a simplification of the Bernoulli equation where there is assume that the impact pressures far exceed the strengths of the target and penetrator, and shock reflections and target inertia do not affect the penetration process. The latter assumption imply that the penetrator is very long compared with its diameter. The theory also assumes a steady state of the penetration process which implies a infinitely long penetrator.

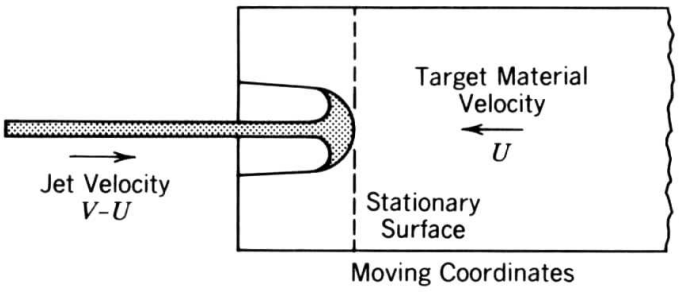

Figure 13: Jet penetration with a coordinate system moving at the penetration velocity [ZW89, p. 132]

Fig. 13 shows a penetration model with moving coordinates. Then, the motion of the penetration front can be noted as $(V - U)$ with $V = v_j$ and U representing the

penetration velocity. The rod or jet has the length l and density ρ_j, ρ_t represents the target density, respectively. Assuming a steady state, the interface pressures of jet and target must be equal, so that

$$\frac{1}{2}(V-U)^2 = \frac{1}{2}\rho_t U^2. \tag{16}$$

Using Eqs.(16) and assuming that the penetration stops instantaneously after the rear hits the target, the total penetration P is the penetration velocity times the penetration time (hydrodynamic square root density law)

$$P = U\frac{l}{V-U} \Leftrightarrow P = l\left(\frac{\rho_j}{\rho_t}\right)^{\frac{1}{2}}. \tag{17}$$

Thus penetration performance of a shaped charge is a direct function of the jet length and the square root of the densities.

This theory and simulations show that the jet velocity is less important for the penetration performance than the jet length. Consequently, the formed jet should be formed as long as possible, with minimized radial dispersion. To establish a long jet one needs a high velocity gradient within the jet, produced by a high jet tip velocity[6].

On the other hand, the hole diameter is dependent on the kinetic energy of the jet (mass and velocity squared). This energy deposition and inertia contributes to the so called second penetration, an additional penetration after the jet is dissipated.

2. Jet elongation and breakup

The presented penetration theory assumes a constant rod/ jet length. As aforementioned, a shaped charge jet has a velocity gradient, with the maximum speed at the tip and a decreasing velocity distribution along the jet until the tail (q. v. Fig. 14); except for those cases, in particular, along the jet tip that can contain a positive velocity gradient under conditions as previously mentioned. This causes the jet to stretch. Dependent on the jet

[6]Section III.C provides jetting criteria and coherency limitations for high jet tip velocities. The intention in this research is not to give detailed mathematical derivations on penetration, but to show general effects of material selection and shaped charge design. Further penetration relationships can be found in [ZW89, pp. 132]

velocity gradient, and the material density and ductility, the jet will start to break into segments and affect the penetration performance. Before breaking up, the jet develops necks and thus varies in diameter (q. v. Fig. 15).

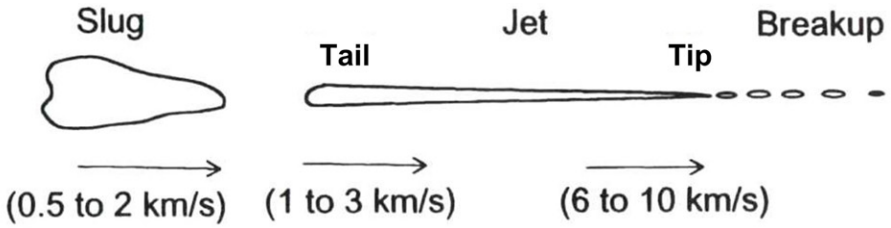

Figure 14: Ordinary velocities after jet formation

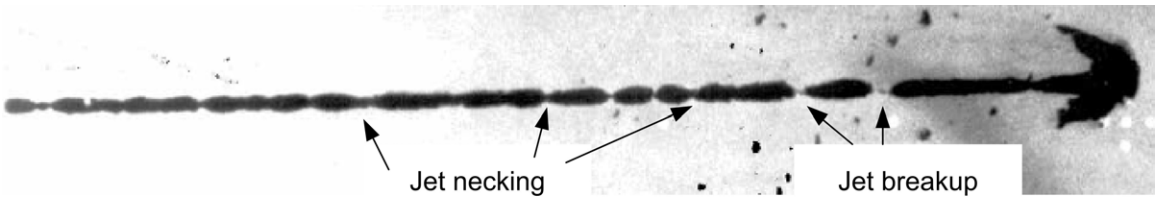

Figure 15: Radiograph showing necking and jet breakup

The factors influencing the rate and extent of jet breakup were investigated by Chou and Carleone, presenting a model describing the breakup phenomenon [ZW89, pp.123]. From their analytical results, the following policy to increase breakup time, shown in Table 4, can be concluded.

parameter	method
jet radius	↑
jet streching rate	↓
jet strength	↓
jet density	↑
jet dynamic ductility	↑

Table 4: Methods to increase breakup time

As one can see, the liner material and geometry have a major affect on the parameters showed above and should be considered in the design process. Moreover, the results

from simulations represent a mathematical solution for the breakup, but do not represent behavior of experimental results.

3. Effect of standoff

The standoff (distance) or S.O. is referred to the distance between the base of the liner and the target. It is in common to express the standoff as charge diameter (CD). The standoff dictates the space for a jet to form and to reach its characteristics (jet tip velocity, jet elongation).

At short to moderate standoffs (i.e., up to 6-10 CD), where the jet continually stretches, penetration capability increases (i.e., P increases with jet length) until the jet starts to fail in tension. Breakup is dependent on the factors shown in Table 4 in addition to the fabrication quality of the charge (incl., concentricity). When breakup occurs, there is no further increase in jet length and penetration peaks. After breakup, the jet particles tend to ablate, tumble and drift away from the axis of symmetry thereby reducing the effective jet length and as a consequence penetration effectiveness (q. v. Fig. 16). The theoretical maximum takes into account inertial effects of repetitive impacts of perfectly aligned particles after breakup.

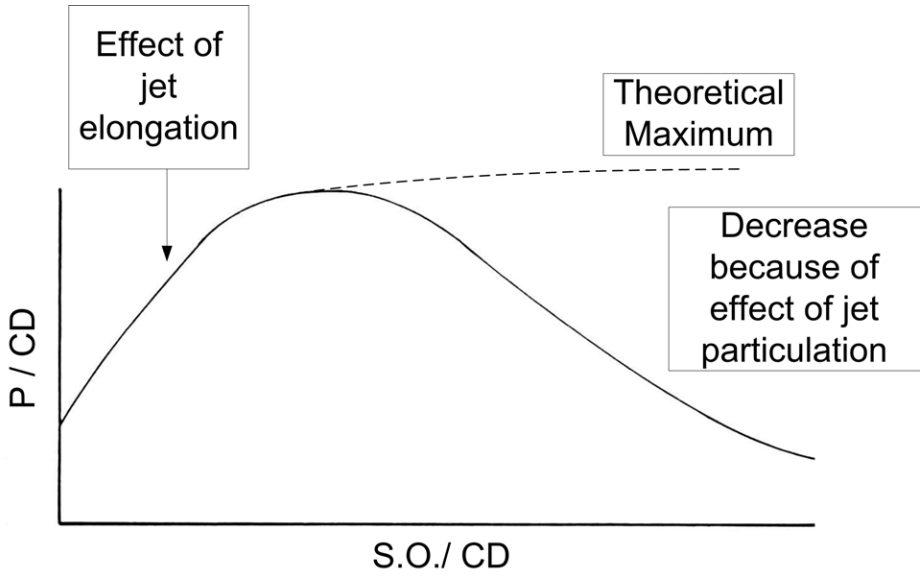

Figure 16: Effect of standoff (S.O.) on penetration P

IV. NATURE OF THE PROBLEM (TECHNICAL ISSUES)

Primary missions of this research, as previously mentioned, are to derive criterion for optimizing the design of shaped charges for generating stable multi-material jets, and to understand the potential consequences on penetration.

The role (and effect) of shaped charge components on jet formation and penetration are reviewed in the first portion of this section. This is followed by specific issues addressed.

A. DESCRIPTION OF THE PROBLEM

1. Complexity of shaped charges in general and of bimetallic configurations

The processes and parameters of shaped charges are a complex entity. Changes in material(s), geometry, initiation type, and standoff can result in a way, that was not intended nor expected. However, one can predict the primary effect of discrete changes with the help of above presented theory. Thus, it is possible to design a shaped charge with a specific characteristic (velocity gradient, jet diameter and length, coherency, penetration capability).

Although, effects of monolithic lined shaped charges are widely known, multi-material lined shaped charges have never been in the center of interest. Some scientists [CL95, WG87, KB81, Duo05] conducted bimetallic studies, most of them limited their research to materials with almost equal densities. Using materials with the same density may help (i) to avoid problems of different thermal behavior, and (ii) to decrease probability of material separation. Many studies such as those reported by Chanteret and Walters, use different materials only for purposes of studying jet formation mechanisms. Again, copper was the primarily used material, with well known behavior as baseline.

The challenge of multi-material shaped charge configurations creates a new definition of so far accepted limits. The relatively new approaches of this work exceed the area

of well known shaped charge theory. Results are based on hydrocode simulations and need to be validated by experiments.

The main goal in this research was directed towards the understanding of multi-material jet formation and coaxial jetting. 100 mm conical copper-lined shaped charge simulations were conducted to establish baseline simulation parameters. These have been compared with unpublished experiments, conducted by Kennedy and Brown, with monolithic and bimetallic setups. Further interest was performed in the effects of other bimetallic material combinations and liner designs.

2. Effect of shaped charge parameters

As mentioned in section III.B.1, a shaped charge consists of several parameters. The single effect of each parameter will be discussed in this section, for comments on the standoff see section III.D.3. Note, that liner parameters need to be adapted to any specific application. This section presents the tendency of parameters, it is not for a specific application.

a. Confinement

The confinement of a shaped charge is a metallic (e. g. steel, aluminum) or fiber material (e. g. PTFE) that has several values. It affects the explosive-liner energy coupling and has a influence on the whole shaped charge performance. The influence of the confinement increases at longer standoffs and has minor effect at short standoffs.

First, the confinement geometry influences the detonation pressures and controls the jet velocity gradient. A common shape is the tampered body (boattailing). In this design the case diameter decreases after the so called breakpoint to the warhead tail. This reduces the warhead weight, saves explosive material, and contributes in material and weight efficiency. The choice of the breakpoint affects the wave propagation and must be chosen carefully.

Second, one can vary the confinement material. Dependent on the aim, the material should have a tendency of fragmenting to be applied as anti-personnel device. Or,

it should have a high strength to contribute to higher detonation pressures over a longer time, what results in higher jet tail velocities. Higher density material decreases case expansion, and thus increases energy coupling.

Third, the confinement thickness can be varied. A thicker case contributes to higher energy coupling and jet velocities, especially in the jet tail. Note, that the effect can not be increased after certain, material dependent values, are reached[7]. Additionally, the jet mass increases with density and thickness.

b. High Explosive

High explosives are used in shaped charges to create necessary liner collapse conditions. Detonation pressure and detonation velocity are the two main parameters, affecting the liner collapse process. Detonation velocities, tabulated in Tab. 14, along with the Gurney velocity coefficient can be used to determine the effect on jet velocities.

Additionally, higher detonation pressures result in higher jet velocities and masses. Thus, based on explosive and liner material, the liner apex thickness must be varied. The higher the detonation pressure, the higher the tendency of the apex to break. Apex break needs to be avoided to enable a smooth jet formation process.

c. Charge length and head height

The length of the charge is called charge length. A sufficient length is required to contain enough explosive mass, and to define the space between the initiation and the liner apex, referred to as the head height. The head height must be long enough for the detonation to create a planar wave and to provide descent explosive energy. As above mentioned, a small charge length, in order to save material and mass, should be preferred.

[7]Evans (1950) found, that 1/10-CD confinement thickness is a reasonable value for steel

d. Liner parameter

In this work the focus lies on conically lined shaped charges. Mostly, conically lined charges with uniform thickness and constant angle are considered. This implies, that also tapered[8] conical liners with varying liner angle can be used to meet requirements.

Besides, there are other shapes like trumpet, tulip, hemispherical, or pyramidal, maybe with modifications in thickness and shape. Those are not considered in this research.

In a standard shape, the thickness and angle of a conical liner are constant. Changing the **liner angle** 2α results in changes of flow and jet velocity, and mass flowing into the jet. For instance, a smaller angle produces higher jet tip velocities, but jet mass decreases. A smaller angle also reduces, charge length being equal, the head height and affects the grazing angle, the angle the detonation wave travels along the liner. Fig. 17 shows a biconic liner with two different liner angles.

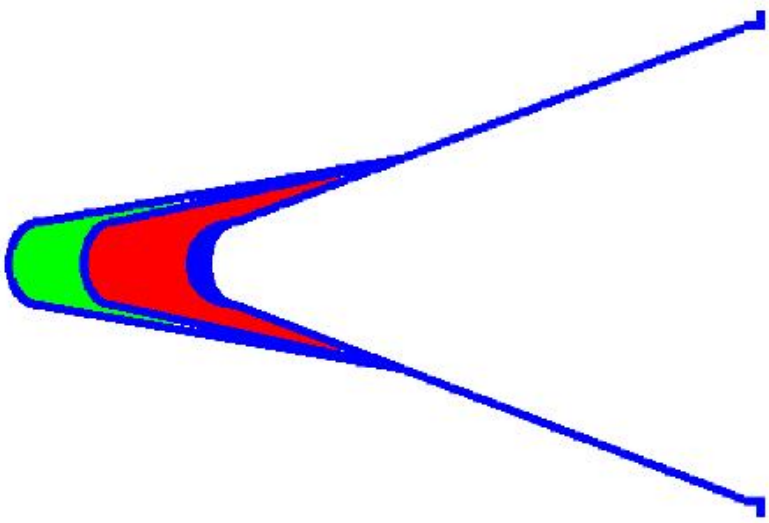

Figure 17: Effect of varying liner angle and apex thickness [Duo05]

Variation in **liner thickness** changes the liner mass and the ratio M/C. Consequently, this affects the liner collapse process, the liner mass flowing into jet, and the jet

[8]Thickness along the liner varies, e. g. apex thickness >liner thickness)

velocity. A thin liner collapses faster than a thicker liner, with higher jet tip velocity and usually lower jet mass. The jet mass may also keep constant or increase because the relative amount of liner mass flowing into the jet increases for thin liners. As aforementioned, there is a minimum liner (apex) thickness to sustain the high pressures and to avoid failure. On the other hand, a thick liner increases the M/C ratio, especially at the critical points, apex and base. Sufficient explosive energy to create optimal liner collapse conditions must be available. Usually, a liner thickness of 1-4 % of the charge diameter is applied.

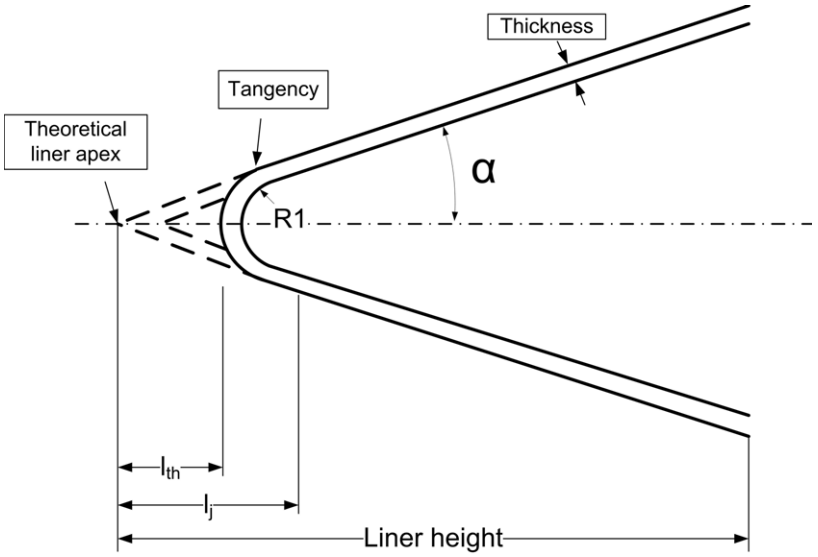

Figure 18: Liner parameter showing the effect of rounded apex

The design of the **liner apex** has several effects on other warhead parameters (q. v. Fig. 18). A conical wedge liner provides a so called theoretical apex[9]. With a rounded apex, the apex point is shifted towards the open side. The distance between the theoretical apex and the current apex is denoted by l_{th}. An increasing l_{th} leads to a smaller liner height, a bigger apex radius R1, and an decrease of the M/C ratio.

The distance l_j specifies the point, where the velocity gradient changes, i .e. where the jet tip velocity reaches the maximum. [CJC77] studied the effect of the liner apex with a constant conical copper liner. Overall, their findings state that the apex design affects the jet tip velocity and mass, the velocity gradient, and the mass distribution. Unreported

[9]The apex is rounded due to manufacturing.

simulations with a conical copper liner, conducted by [HW10], show that the distance l_{th} should be as small as possible to get a fast jet tip. With this approach, the inverse velocity gradient can be minimized and l_j shifted towards the apex. Dependent on the used liner material and explosive, one should design the apex to meet the application requirements because a massive jet tip can be more important than a higher jet tip velocity or vice versa.

3. Tradeoff

The main focus of this thesis lies on the improvement of shaped charge efficiency. The efficiency can be measured in several ways and again, it is only dependent on the application. Therefore, designing a shaped charge application implies a tradeoff situation, where one must set priorities and accept their consequences.

The are many points to start the improvement, e. g. the design of the body and the liner, the used materials, the standoff distance, and the target. Although, shaped charges are a complex system, Chanteret [CL95], Walters [WG87], Brown [BML95], and others have showed that it is possible to improve specific performance parameters of shaped charges.

There will always be a tradeoff in the shaped charge design, whether this will be because of (i) the total dimensions and weight (portability of warheads), (ii) the velocity or mass distribution, (iii) or because of cost efficiency for materials or manufacturing processes.

This research concentrates on the usage of multi-material shaped charge liners and on the enhancement of liner design as well as penetration. The interest lies in understanding multi-material liner collapse and jet coherency, with additional interest in the consequences of changes in jet characteristics with respect to resultant penetration potential. It is important to note, however, that the study of coaxial jetting and jet stability are the main focus of work.

B. GEOMETRICAL INPUT AND ZONING

1. Geometrical input

Inputting parametric liner variation into AUTODYN, required for these studies, can be very time consuming. Thus, a sub-task of the effort has been dedicated to constructing an input processor to facilitate this operation.

Although AUTODYN is relatively user-friendly, it is not easily adapted for CAD-type inputs. Using different geometrical designs, or conducting parametrical studies requires a relatively easy way to implement appropriate changes to the design. Hence, the user should avoid to start over with the setup after every parametrical change. A workflow for parametrical (geometrical) changes, computation and post-processing is a major challenge to increase efficiency, to decrease input errors and to perform high quality simulation studies. The improvement of workflow was an ongoing effort during this research.

The geometrical simulation setup in AUTODYN is not very user friendly, because the geometry has to be translated in X and Y coordinates and the geometry cannot be adjusted, i.e. the software has no *undo* functionality. To create a geometry, one can use the geometrical shapes rectangle, quad, ellipse, and parabola. The input of complex geometry or changes is very troublesome or not feasible. Some changes are only realizable with a start-over.

Therefore, interest lies in a parametrical CAD-model combined with simulation software. This would allow to be able to change parameters in a very efficient way, e.g. with a parameter list. The parameter list contains absolute input values and constrained values, calculated dependent on absolute values. Updated geometry data would need to be meshed and imported to the simulation software where a new simulation can be conducted.

As alternative, other ways to support geometrical input were examined. Approaches are presented in section V.B.

2. Required zoning

In this research warhead setups with 100 mm charges were conducted. In order to model the problem and to get required data, the grid dimensions for the charge had at least a x-y-dimension of 422 mm $\times$ 120 mm. To calculate the liner collapse and jet formation in a high definition, a minimum resolution of 4 cells/mm was chosen. Then, the number of cells results in about 0.8 Mio. To detect the liner partition and to improve the jet formation calculation, the number of cells needed to be increased up to 6 or 8 cells/mm, at least in the area of interest ($>$ 1.8 Mio. cells). With 6 cells/mm, a 1.5 mm thick liner was modeled with 9 cells. Accurate computations with multi-material liners required also a high resolution to account for very small amounts of mass in the liner.

A higher number of cells resulted not just in a long computational time, but also in very slow processing/responding of the simulation software.

C. KENNEDY EXPERIMENT

As aforementioned, Kennedy and Brown performed experiments with copper and copper/zirconium liner in the DRAGON warhead, mostly directed towards enhancing behind the target effects. This unreported experimental data was very relevant and useful to meet the research objectives. It supported the computational validation and model setup, the potential integrity of coaxial (bi-metallic) jetting, and the mechanisms that affect integrity with respect to collision rebound and thermal expansion as well as jet elongation. Therefore, the DRAGON data along with simulation were used as baseline for further design studies. Further description of the experiment and simulation models is provided in section V.D.

D. JET COHERENCY THEORY VALIDATION

Jet coherency is a critical issue of the research. Classical work by Harrison and Chou are outlined in Section III.C. In this section, more recent efforts by Walker and Murphy are also included.

The theory of Chou et al. (1976) states that a non coherent jet is formed, if the flow velocity exceeds the bulk sound speed and if the collapse angle does not under-run a critical collapse angle β_c. Five years later, Harrison developed the analytical shaped charge code BASC and his findings are known as the so called Harrison criteria. His criteria for a coherent jet, obtained from comparing radiographic, is that stable jetting requires that the flow velocity does not exceed the bulk velocity of the material. If $v_f > 1.23c_0$, a incoherent or bifurcated jet will be formed. Harrison [Har81] used a modified PER theory, in which he included a model for non-linear velocity increase V_0, with more modifications related to work performed by Defourneaux. The materials are treated as inviscid, incompressible fluid and allow to calculate jet and slug velocity with Bernoulli equations. Since, the Harrison criteria is the most accepted and validated criterion on jet coherency.

[Mur90] examined coherency criteria (Harrison, PER, Chou et al.) for high-velocity jets. He refers not to the sound speed of the material but to the shock velocity U_s related together with pressure (q. v. Fig. 19). A higher pressure in the formation region would allow for higher flow velocity, and consequently for a coherent jet. However, from geometrical analysis, Murphy provides the following equation for a maximum coherent jet velocity,

$$\frac{V_{mcj}}{U_s} = 1 + \cos(\beta) + sin(\beta)tan(\alpha + \delta), \tag{18}$$

with a maximum at following angle configuration,

$$\beta = (\alpha + \delta), \tag{19}$$

$$(\alpha + \delta) = 90deg. \tag{20}$$

Eqs. (20) is the theoretical maximum obtained by geometrical analysis, but it would result in an unrealistically value for coherent jet velocity ($V_{mcj} \rightarrow \infty$).

Murphy concludes in his paper that an upper limit for the maximum coherent jet velocity does not exist for geometric or kinematic constraints. He points out that the maxi-

mum measured coherent jet velocity is usually lower than the theoretical maximum coherent jet velocity provided by coherency criteria. Anyway, Eqs. (19) shows angle combinations for maximum coherent jet velocities.

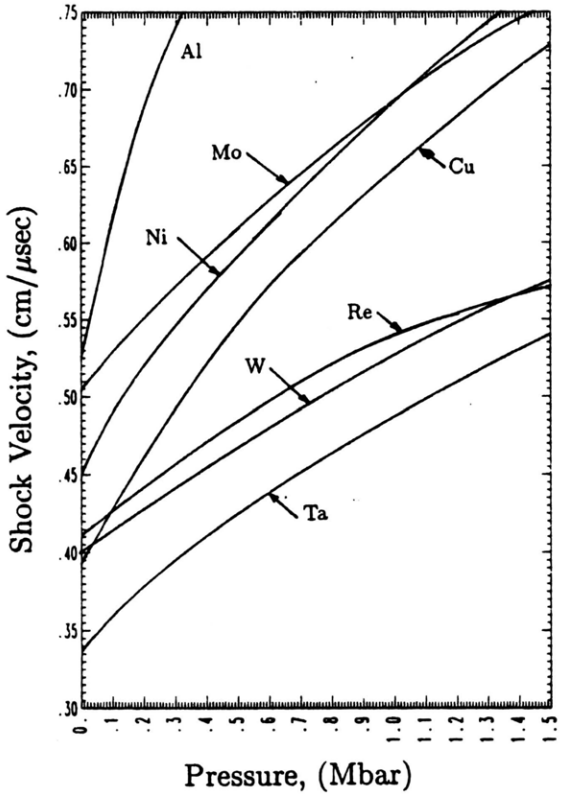

Figure 19: Shock velocity vs. pressure for several materials; 1 Mbar = 100 GPa [Mur90]

Moreover, [Cha92] conducted experiments and analytical calculations to study the maximum velocity for coherent jets. Simulation data were calculated with the finite element DYNA2DJET code, developed by Murphy. This code calculates the collapse angle with a shell collapse simulation. Chanteret estimates the maximum jet velocity with $c^\star = 1.23c_0 = v_f$ and Eqs. (19) to

$$V_{j^\star} = c^\star \left[1 + \frac{1}{\cos(\alpha + \delta)}\right], \tag{21}$$

and relates the flow velocity as a function of collision velocity V_0 and δ (q. v. Fig. 5 or 10). With this relationship, the limit for a coherent jet is proportional to the material sound

speed and increases with increasing liner angle and δ. However, this relationship would estimate lower coherent jet velocities than observed in experiments. Increasing the liner angle would result in higher coherent jet velocities, but in contradiction, the jet velocity decreases with increasing α. This problem was also mentioned by Chanteret, so the given relationship represent a theoretical analysis. Consequently, there would be a chance to form a coherent, high speed jet, if the jet velocity could be increased, not being a result of changes of the liner angle. An attempt to increase the jet velocity could be by using other (combinations of) explosives or increasing the pressure to increase collapse velocities at large liner angles.

The incoherence of shaped charges was also studied by [Wal93]. He conducted hydrocode computations with conical aluminum lined shaped charges, using aluminum with two different sound speeds. In his theory, he is using v as collapse velocity, and c_l as low pressure longitudinal sound speed of the liner material, which is different from the bulk sound speed c_0.

$$c_l = \sqrt{3\frac{1-\nu}{1+\nu}}c_0, \tag{22}$$

with

$$c_0 = \sqrt{\frac{K}{\rho}}, \tag{23}$$

where K denotes the bulk modulus, ν the Poisson's ratio, respectively. He states that the collapse region, forming the high speed jet, is determining the coherency and concludes the following coherency criteria:

- if $v > c_l$, then a incoherent jet forms;
- if $v < c_l$ (subsonic), then the jet is coherent;
- if $v \approx c_l$, then a hollow jet forms.

Due to this statements and theory, simulations to validate proposed theory or to detect other key factors for coherent jet formation were conducted as part of this thesis, inasmuch jet coherency is a leading factor for successful shaped charge design.

E. DIAGNOSING PROBLEMS ASSOCIATED WITH JET STABILITY

Multi-material liner design has been a subject of continuing interest, however, dedicated attention has been lacking. Brown for example examined behind the target incendiary effects from charges containing copper liners cladded with magnesium, aluminum and zirconium. Zernow and Lieberman studied the similar effects from zinc cite. Versions of the Quantic Industries in the 1970's and early 1980's investigated the addition of epoxy-zirconium claddings in research studies. The developers of Swedish AT-4 manufactured a version of the warhead with a bi-material liner, also for apparently adding incendiary effects [Bro10].

Unreported experiments of copper and copper/zirconium lined charges by Kennedy and Brown [KB81] provide data that should be profitably employed for initial investigations of multi-material jetting. An illustration of the multi-material liner used in these experiments is illustrated in Figure 20; and a x-radiograph of the resultant jet is shown in Figure 21. The effect of the basal zirconium insertion is apparent in the radiograph. The large particle just ahead of the zirconium shrouded copper jet most likely originates from the liner position adjacent to the material transition.

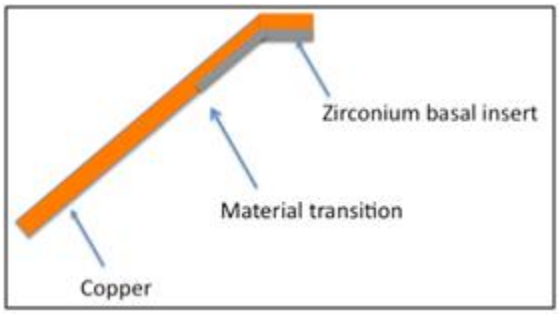

Figure 20: Schematic of copper liner with zirconium basal insert. Resultant jet shown in Figure 21

In this research, the conducted simulations, especially multi-material setups, require a high resolution at the material junction to permit qualitative and quantitative statements.

The main challenge is to diagnose problems associated with jet stability. This are for instance:

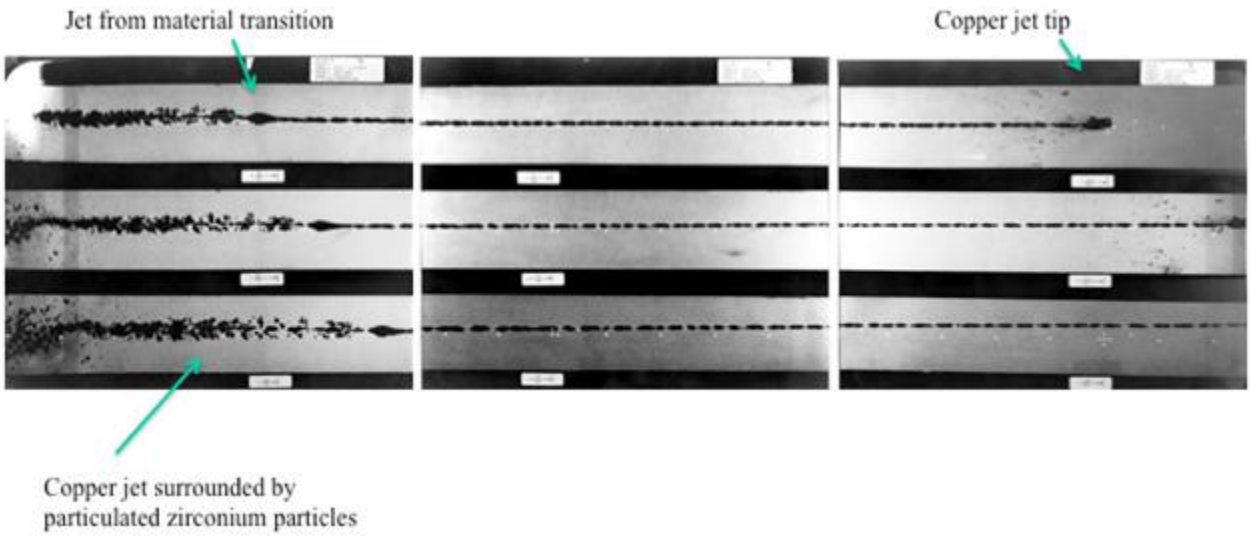

Figure 21: Radiograph of copper/zirconium-lined experiment

- Physical rebound following liner collapse; detection of radial velocity gradients in the collapse region and in the formed jet
- Potential material separations resulting from differences in thermal elongation and expansion
- Instabilities resulting from material partitioning within the liner

Velocity gradients, flow and stagnation velocities, as well as instabilities within the liner can not be reviewed by visual simulation results, hence, they represent mathematical solutions and are not 1:1 predictions for experimental results. Therefore, techniques to measure the jet quality using a configuration of fixed and moving gauges were applied. Fixed and moving gauges, placed accordingly along the axis of symmetry and in the liner, monitor valuable data (velocity, position, pressure, etc.) that is useful for subsequent analysis. However, the number of gauge points is limited to 200, which forces to place gauges strategically and to accept loss of detail. Regardless, the monitored data along with visual results enable to (i) predict jet elongation, (ii) detect radial velocities, (iii) post-process velocity, pressure and mass distributions, and (iv) predict penetration performance.

Nonetheless, realizing that there are large radial as well as axial velocity gradients during early stages of jet formation, it might be very difficult to generate conditions that can maintain material attachment. Material separation in bimetallic liner simulations can not be detected directly with gauges. It is possible to monitor the gauge position in time or space, but this is no clear indication for material cohesiveness. For statements of material separation, it is only possible to evaluate the visual results and to see effects on penetration. In most cases, consequences of other instabilities within the liner can be seen as recently as by calculating the jet for a long time (150-200 μs) or during penetration simulations.

F. EFFECTS OF MULTI-MATERIAL (COAXIAL) JETTING

There are at least three multi-material schemes worth studying. The Type I scheme is one which produces a jet composed of two material segments: Material A (I) followed by material B (II) (q. v. Fig. 23). If the two materials have the same or close to the same density then the second material can be substituted one for one in a proven single material design composed of the first material. That is all issues relative to producing a stable and well function jet have been proven. An example of this bi-material solution is the nickel-copper jetting charge demonstrated by Chanteret [CL95], for purposes of showing how the coherent limit of copper could be overcome by inserting the faster sound propagating nickel, into the first part of the liner.

The major challenge of this scheme is precision machining and mechanical connection between the materials, which was adequately accomplished by Chanteret as shown in Figure 22 (the arrow points to the material transition).

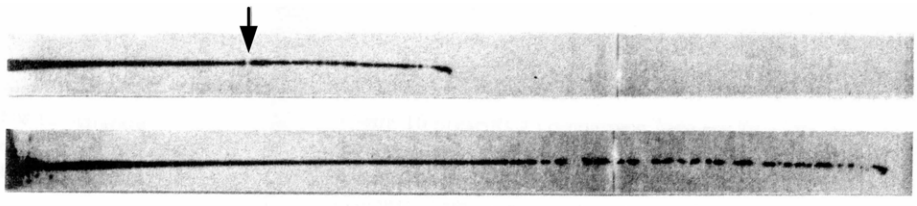

Figure 22: Jet obtained from Ni insert at apex with laser welded trumpet liner [CL95]

This jetting solution can also be satisfied by using an entire copper liner substrate with a partial nickel substrate along the apex region or a nickel substrate with a copper insert above the region that must be avoided to satisfy coherent jetting, as shown in the illustrations included in Figure 23. In both of these subset schemes accurate and reproducible fabrication is required in mating the material together without air gaps and any other discontinuity.

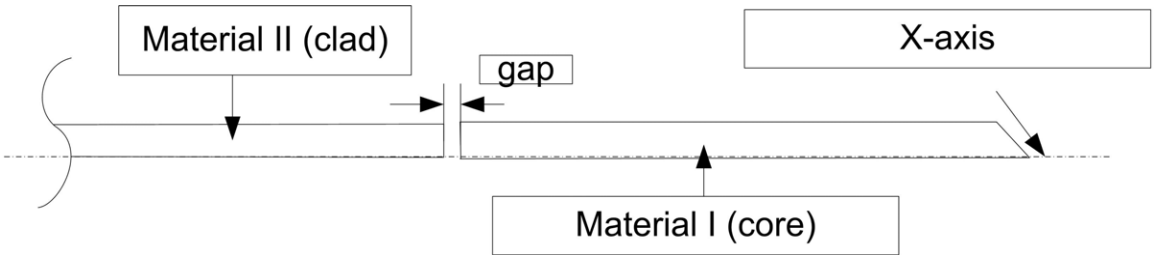

Figure 23: Principle of bimetallic type I: following jet

A major challenge of the Type I design is when the densities of the two materials are very different. In this case, adjustment to the liner geometry and thickness are required in order to avoid disruptive liner deformation and jet formation.

The Type II design is for generating a coaxial jet. In this case the two materials must be layered in the liner in such a manner that they both jet, as illustrated in Figure 24.One of the materials (the one flowing into the core of the jet) can make up the the remaining portion of the liner or a third material can be used as a substrate to support the ”active” jetting materials. These two alternatives are also illustrated in Figure 24.

The ability to estimate definitively the partitioning of jet and slug formation is essential to the design of either of these liner jetting types.

In order to examine which material should form as the core and which as the clad, a rod penetration study was performed in the initial phase of the thesis. The placement of liner material is crucial to obtain a coaxial bimetallic jet to achieve one of the following goals:

- Protection of core material from jet breakup and contribute to penetration.

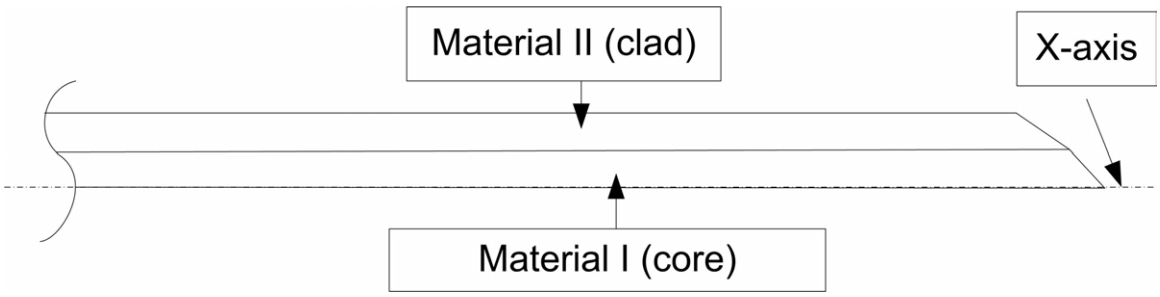

Figure 24: Principle of bimetallic type II: coaxial jet

- Protection of core material from reactions with surrounding environment during storage and application.
- Control penetration capability in order to increase penetration depth or hole diameter

A jet core with a shrouded material, assuming no separation occurs, might be protected better against radial dispersion and jet breakup. The resulting coaxial jet would increase in penetration capability because the core jet length would not decrease, compared to a jet with breakup. Furthermore, the core material could be protected in specific environments (e. g. naval applications) or the clad could contribute to underwater performance[10]. Additionally, a second material can avoid reactions (e. g. corrosion) during storage.

A guideline, how the materials should be arranged to manipulate penetration capability is provided by a rod penetration study with copper and tungsten. More details and results are provided in section V.F.

G. UIUC DESIGN GUIDELINE

UIUC is conducting an investigation of the effects of aluminum versus copper rod impacts against targets submerged in various fluids. They are using shaped charges as a means to launch the material at hypervelocity and would like to be able to control the features of the jets. The type of jetting desired fits into the Type I class [Mas10].

It is an objective of this research to recommend one or more designs with performance predictions.

[10]Further details in [Duo05]

V. TECHNICAL APPROACHES (SOLUTION ISSUES)

This section provides developed and applied approaches to perform shaped charge jet formation and penetration simulations. First, the general setup for simulations will be presented. Next, approaches directed to detect liner mass partition, effects of coaxial penetration, and approaches for stagnation as well as flow velocity estimation will be provided.

A. COMPUTATIONAL METHODOLOGIES

Initial work on this project was dedicated towards developing procedures for simulating shaped charge jetting and hypervelocity penetration problems, demonstrating an accurate shaped charge jetting solution, and investigating the effect of bi-material compositions in coaxial rods on penetration efficiency. Some attention was also given towards developing means for facilitating the input of geometric changes in parametric investigations.

The computational methodologies employed during this research are based on recommended procedures in technical notes on the general procedures for setting up and operating the suite of finite difference processors in the ANSYS AUTODYN code, performing shaped charge computations, and using ANSYS Workbench 12.0 ([ANS97, ANS07, ANS09]). This most recent version of the AUTODYN finite difference software package offers a CAD-file input that is being evaluated as a possible tool for creating parametric simulation design workflow, which would make systematic charge component changes much easier than having to construct an entire setup for each parametric change. This is covered in further detail in section V.B.

Different techniques need to be considered to improve the computational time. For relatively simple problems, the simulations run fairly fast, but for more detailed and realistic problems (higher accuracy) the computations can run for several weeks. Accordingly, techniques like graded, i.e. variable, zoning, removal of used materials, and using subgrids

were integrated into the design of the simulation layouts, resulting in the reduction of the total run time of typical simulation setups in this research.

Key features of the menu-driven setup and specific details that have to be considered for setting up axi-symmetric shaped charge and penetration computations are discussed in appendix B. There, the discussions focus on the initial 25 mm shaped charge-jetting simulation but are fully transferable to other setups. Additionally, appendix H covers code validation for the applied AUTODYN version 12.0, and compares simulation results with fellow researchers [HW10].

It is important to note that it is only necessary to construct half of the problem geometry because of cylindrical symmetry.

B. GEOMETRICAL INPUT AUTODYN

A combined CAD/AUTODYN workflow was examined at the beginning of the thesis. The current version of ANSYS Workbench supports CAD input of typical file types. However, the preprocessing does not allow to fill the parts with explosives, or to setup initial conditions needed for shaped charges in ANSYS Workbench. After a successful import[11] of the geometry into AUTODYN, problems occurred while assigning material properties and both, ANSYS Workbench and AUTODYN terminated with an unknown problem. According to information of ANSYS, a CAD support might be available in a later release[12].

As alternative, an algorithm, implemented with MATLAB, was developed during this research to support the geometrical input. The code calculates[13] the parameters for AUTODYN with a list format output. The results are serialized for the AUTODYN Fill command. This allows, for instance to externally setup a liner profile for input into AUTODYN. It increases the geometry setup speed and avoids errors, but does not offer the same potential as an integrated CAD workflow. The author provides the source code on request.

[11] data linked between workbench and AUTODYN
[12] Private communication with ANSYS Horsham, UK
[13] warhead design can be specified

The use of macros in AUTODYN for simulations with the same geometry was examined. In this case the possibilities of linking input parameters calculated with the MATLAB code were considered. AUTODYN creates a **.adc*-file and monitors geometrical input, deployment of boundaries and setting of gauge points. With a beta option one can open a **.adc*-file, highlight commands, and process these commands on the current simulations. To use this feature, the materials and boundaries need to be setup before and they must have exactly the same identifier. This macro was useful for simulations where the geometry was equal but the materials or interest changed (other placement of gauges).

Problems occurred while setting gauges with the macro option. Only one part of fixed gauges was applied successfully, the rest and moving gauges could not be applied with success. Probably this is an issue of the beta option.

C. LINER MASS PARTITION

In this research the interest lies in liner substitution with a second material. Objectives of this work focus on (i) detecting effects of substitution and (ii) mitigating any harmful effects. To estimate possible substitution areas, the actual liner mass partitioning of a monolithic liner needs to be studied. From former work, one knows that the liner mass is increasing along the way from the apex to the base, while the jet velocity decreases (see Fig. 25).

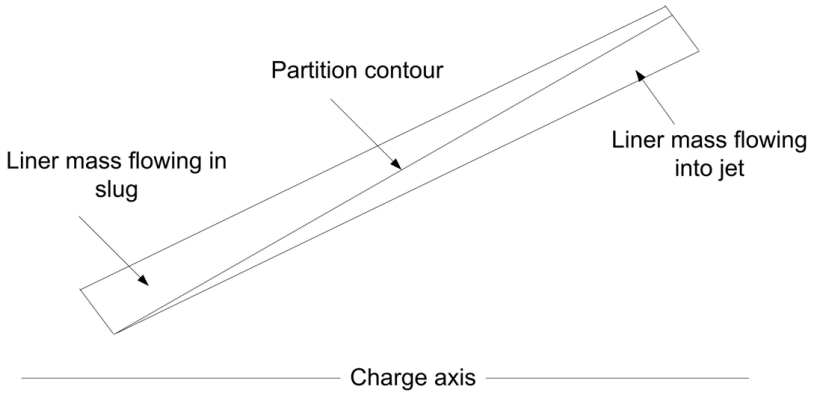

Figure 25: Liner Mass Partition

To quantitatively follow the liner collapse of a simulation, moving gauges are placed on the bottom side of the liner. The first gauge is placed at the bottom (liner air interface) and the next gauges are placed at selected spacings from each other e.g. 0.1 mm. An example is shown in Fig. 26. In the gauge plot *abs. velocity vs. time* one can determine the gauges flowing into the jet or slug as provided by Fig. 27. If this procedure is deployed with a set of rows of moving gauges equidistant along the liner, the mass partition can be established. This information provides a detailed idea for the substitution with a second material. However, the interactions between the two materials have to be investigated, as the materials have different densities and bulk sound speeds. This can result in change of the liner collapse and thus affect the jet formation, cohesiveness, coherency, and consequently the terminal ballistics. Subsequently, the partition contour is called partition interface.

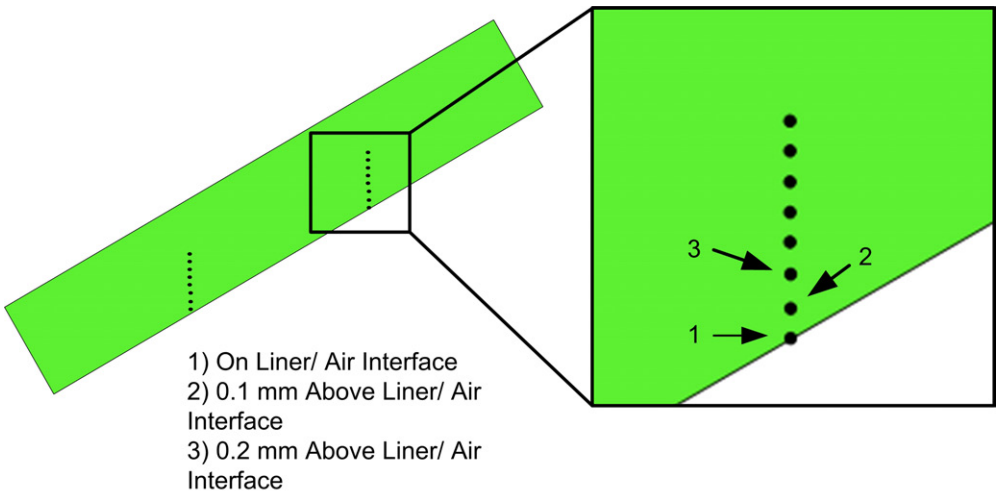

Figure 26: Lagrangian (moving) gauges inserted in a liner for purposes of monitoring collapse and jet flow

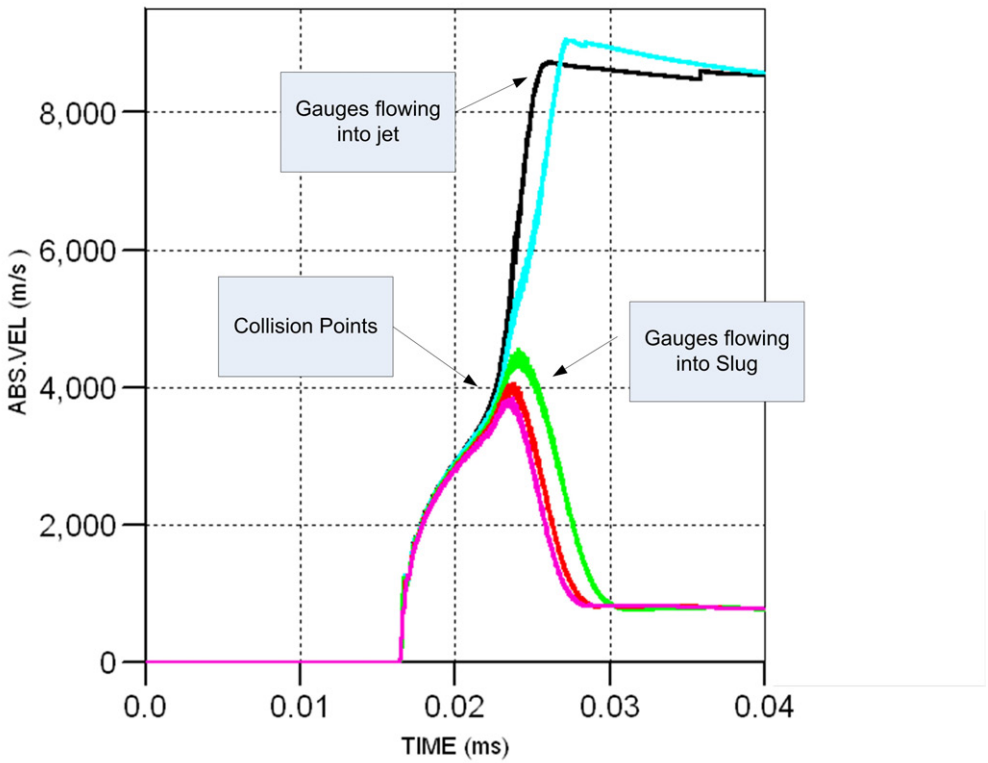

Figure 27: Absolute velocity vs. Time plot for detection of liner partition; Gauges near the liner/ air interface flow into jet, other flow into slug (q.v. Fig. 26)

D. DRAGON GEOMETRICAL SETUP

The main geometry setup for almost all conducted simulations was provided by experiments with the DRAGON warhead, conducted by Kennedy and Brown in 1980/81 [KB81]. They used a modified DRAGON warhead as basis and wanted to improve behind the target effects with a basal insert of zirconium. They also investigated effects of confinement geometry and thickness on penetration.

Experimental results were used to validate simulation results, and to provide a setup baseline for further simulations.

1. DRAGON baseline

The standard DRAGON simulation with a conical copper liner and a thin case is called DRAGON baseline. Fig. 28 provides the model setup with zoning and boundary conditions in AUTODYN (q. v. mechanical drawing of DRAGON experiment in appendix C.B). Note, that only one half of the problem needs to be modeled due to rotatory symmetry of the x-axis.

The main parameters are:

parameter	[mm]
body length	222.25
case thickness	1.27
warhead diameter	104.14
head height	99.5
charge diameter CD	100.2
liner thickness	1.5
liner angle α	21°
standoff	2 CD
initiation type	point

Table 5: DRAGON baseline parameter

Fixed gauges along the x-axis and at standoff distance were placed to monitor the velocity and mass distribution (q.v. Fig. 29 and Tab. 6). From the data at the standoff, the velocity vs. cumulative mass plot can be created. It shows the velocity distribution along the jet mass with a light, fast jet tip and a massive, slower jet tail.

With information from fixed gauges along the x-axis one gains information to estimate the jet elongation and jet length for various times. This approach allows to calculate the jet length at several standoffs and to provide information for jet breakup and penetration studies.

Moving gauges along the liner were placed to detect the partition surface (q.v. Fig. 29). The distance between the rows was 10 mm with an increasing number of gauges per row from apex to base. Simulations with vertical gauge distance of 0.1 mm and 0.05 mm were conducted in order to examine the required resolution to get satisfactory results. With

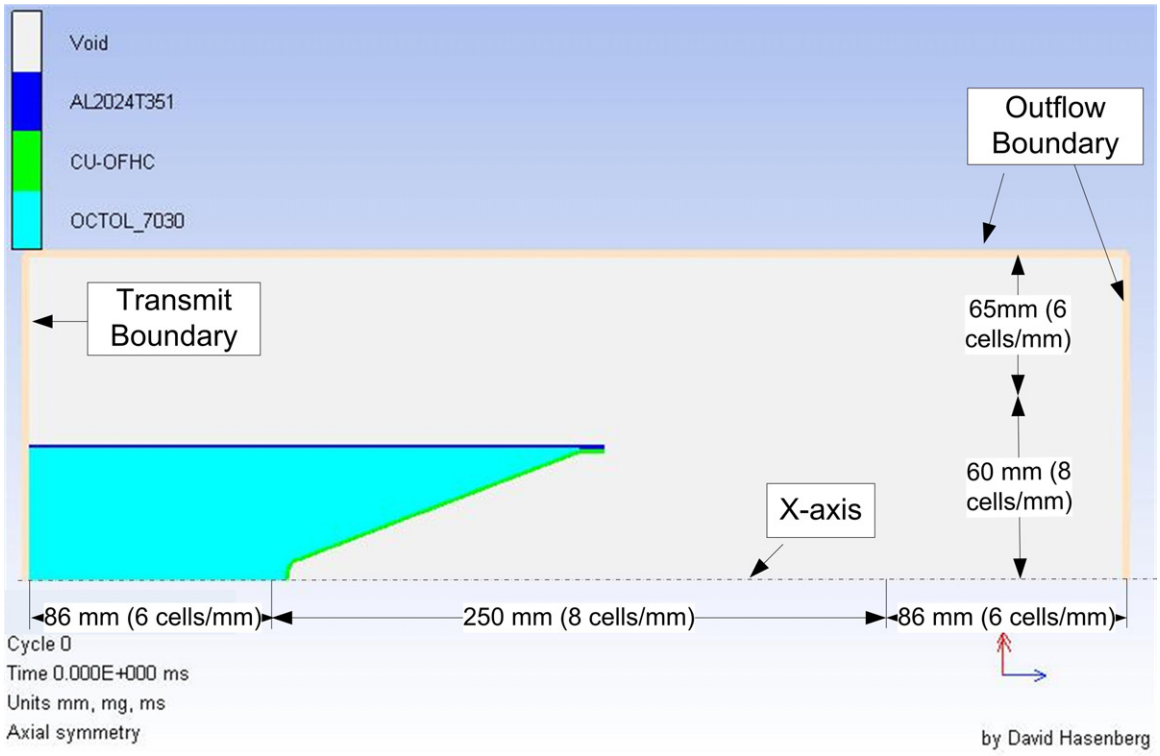

Figure 28: DRAGON baseline simulation layout

Fixed gauges	x(mm)	y(mm)	gap(mm)
1-33	-320..0	0	10
34-74	0	0..8.2	0.2
Moving gauges			
75-79	-320	6.346..6.746	0.1
80-84	-310	10.185..10.585	0.1
85-89	-300	14.023..14.423	0.1
90-95	-290	17.862..18.362	0.1
96-101	-280	21.700..22.200	0.1
102-107	-270	25.539..26.039	0.1
108-120	-260	29.377..30.577	0.1
121-133	-250	33.216..34.416	0.1
133-146	-240	37.054..38.254	0.1
147-159	-230	40.893..42.093	0.1
160-174	-220	44.731..46.131	0.1
175-189	-210	48.570..49.970	0.1

Table 6: Gauge position DRAGON

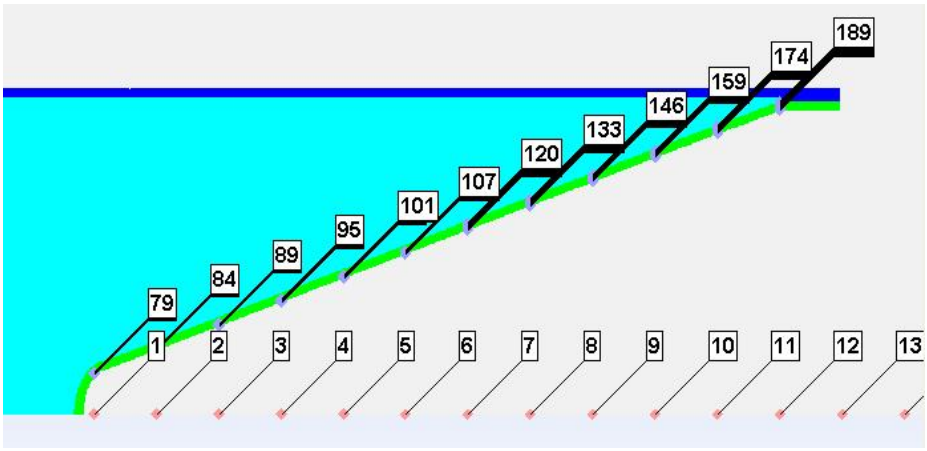

Figure 29: Placement of fixed (red) and moving (purple) gauges in the jet formation region

the knowledge of the partition surface one can get indication for the mass flowing into the jet. Moreover, moving gauges provide information about y-velocity and position, and show effects of radial velocity gradients.

2. Base insert modification

The simulations parameters and placement of gauges was identical to the DRAGON baseline simulation. The base insert was modeled as shown in Fig. 30 (q. v. mechanical drawing in appendix C.B). In the experiments, two insert heights H were used. The simulation was conducted with the 0.5 in (12.7 mm) insert. The effect of the second insert type (0.25in) was minor in Kennedys experimental results and thus not considered in this thesis. The insert thickness was modeled with 0.76 mm (original 0.03 in).

The intention of this simulation was (i) to validate bimetallic simulations with experiment, (ii) to detect the influence of the insert on partition surface, and (iii) to examine material separation.

E. ESTIMATION OF FLOW AND STAGNATION VELOCITIES

An objective of the research is to assess the validity of previously postulated limiting conditions of coherent jet flow. A validated understanding of this issue is critical to optimizing shaped charge performance by strategic emplacement of liner materials. The

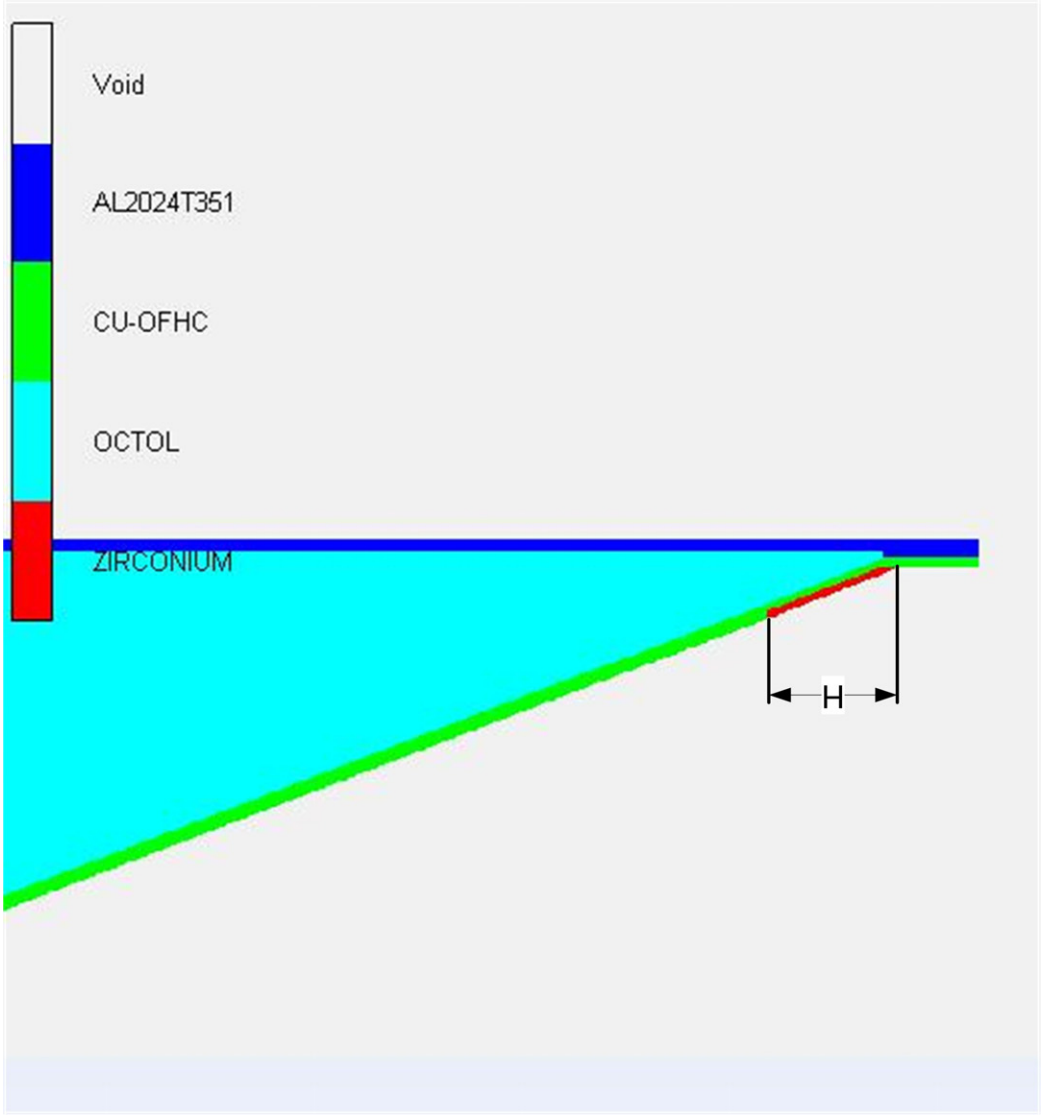

Figure 30: DRAGON base insert of zirconium (H=12.7mm)

technique developed in the research focuses on predicting jet, flow and stagnation velocities from hydrocode results. The technique for predicting jet velocity has been validated from numerous studies. This study relies on other reports that pin-point conditions for material dependent coherent-to-incoherent threshold, which provide means for comparison between estimate and observation.

1. Stagnation velocity

Two techniques are studied and tested for the stagnation velocity prediction. One uses pressure data of fixed gauges, the other uses absolute velocity data from moving gauges.

Again, the stagnation velocity is the motion of the high pressure region that result from progressive stages of liner collapse about the charge axis. A static description of the process is illustrated in Figure 33, along with an idealized view of particle motion along paths just prior to collapse to initial deposition in the jet flow stream.

The motion of the high pressure region is referred to as the stagnation front. The rate of motion along any radial surface is estimated by tracking the highest pressure along the respective surface using fixed gauges. The time of pressure maxima, measured at fixed gauges, can be referred to the velocity. Fixed gauges along the axis of symmetry were placed equidistant in the jet formation area. The pressure peak, time values, and distance between gauges were used to calculate the stagnation velocity. Every fixed gauge has one explicit maximum as shown in an example in Fig. 31 where the stagnation front passes the gauge.

The time at the pressure maximum is noted for the calculation of the estimated stagnation velocity v_{stag} and with the position of fixed gauges x:

$$v_{stag*} = \frac{x_{gauge(n)} - x_{gauge(n-1)}}{t_{gauge(n)} - t_{gauge(n-1)}} = \frac{\Delta\, x}{\Delta\, t} \tag{24}$$

The second method relies on tracking the positions of successive inflection points of moving mass points originally positioned along common planar surfaces in the liner as

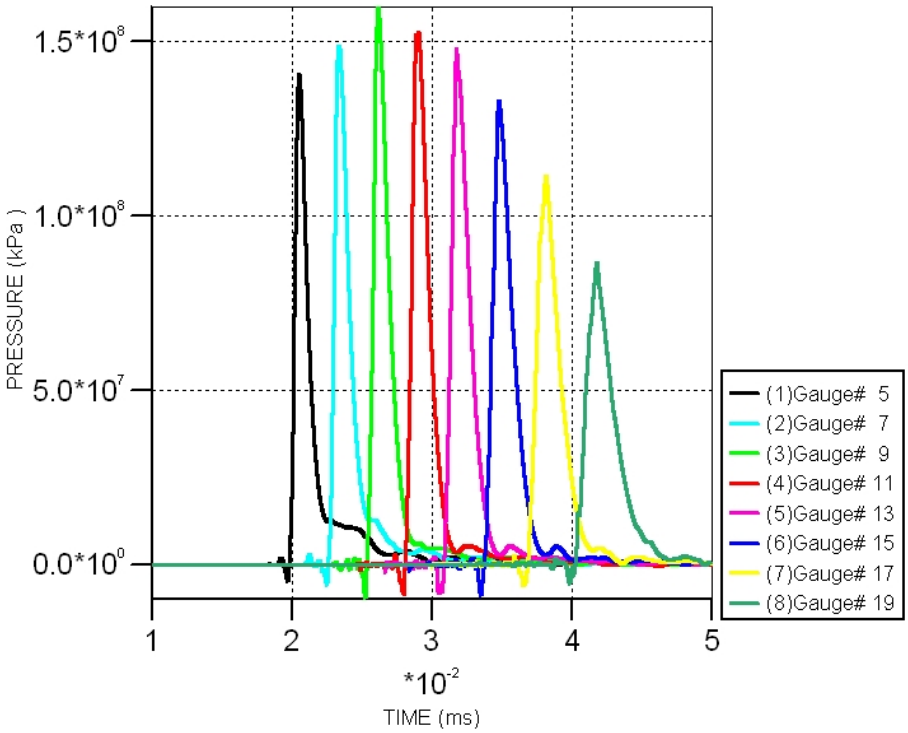

Figure 31: Pressure vs. time plot of fixed gauges, placed along the axis.

a function of time. The velocity at the inflection point was assumed as the flow velocity (Fig. 32), because after this (collapse) point a gauge is going into jet or slug (q. v. Fig 27). The inflection point of adjacent gauge rows is used to extract time data. Position data of corresponding moving gauges is used to calculate the changing of x and y position in this time period. Then the stagnation velocity v_{stag**} can be calculated with

$$v_{stag**} = \frac{\sqrt{\Delta\, x^2 + \Delta\, y^2}}{t_2 - t_1} = \frac{\Delta\,(x+y)}{\Delta\, t}. \tag{25}$$

The reproducibility and validation of each mentioned technique is examined and later used to evaluate theoretical statements.

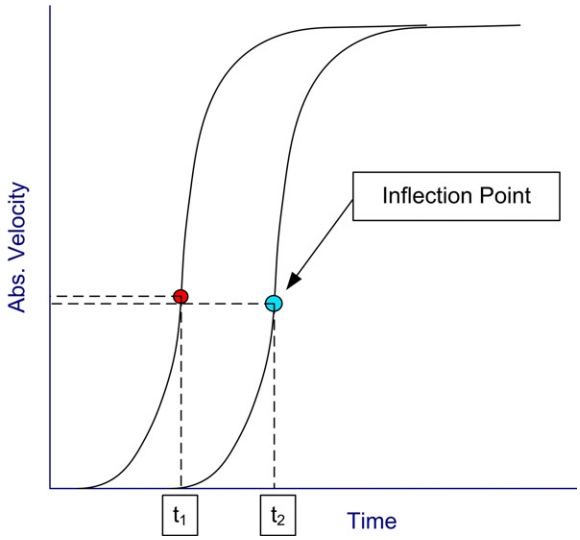

Figure 32: Inflection point method to estimate stagnation velocity

2. Flow velocity

The flow velocity is important for jet coherency theory, as previously mentioned. To investigate the value of the flow velocity, two approaches to estimate the flow velocity were performed.

From the absolute velocity plot one can see that after a certain point, called collision point, the particle, represented as a moving gauge, is going into jet or slug. Figure 33 shows the principle of gauge movement during the collapse process. An example for the absolute[14] velocity plot of the colored gauges is shown in Fig. 34. In this first approach, the velocity at the infection point is referred to the flow velocity. This flow velocity, combined with the time at the inflection point allows to generate the graph of the flow velocity.

Gauges at the air interface (blue) reach a slower jet velocity than gauges at the partition interface (green) because they experience less pressure in the stagnation region. The red gauge arrives earlier at the stagnation front and experiences a higher axial acceleration caused by higher pressure. The gray colored gauge flows into the slug.

[14] absolute or residual velocity combined from x and y-velocity

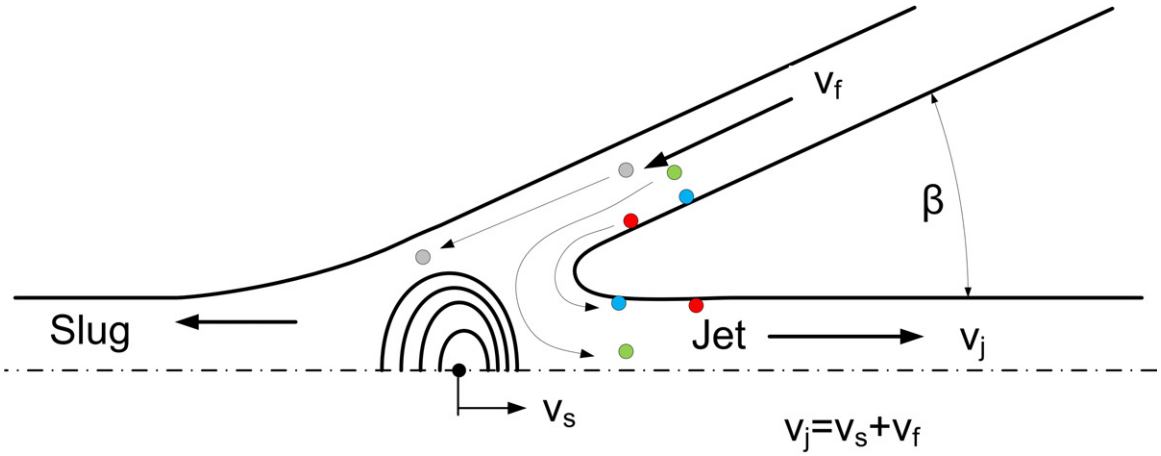

Figure 33: An illustration of the use of moving gauges in AUTODYN to monitor the motion of liner flow during and immediately after passing through the high pressure stagnation region.

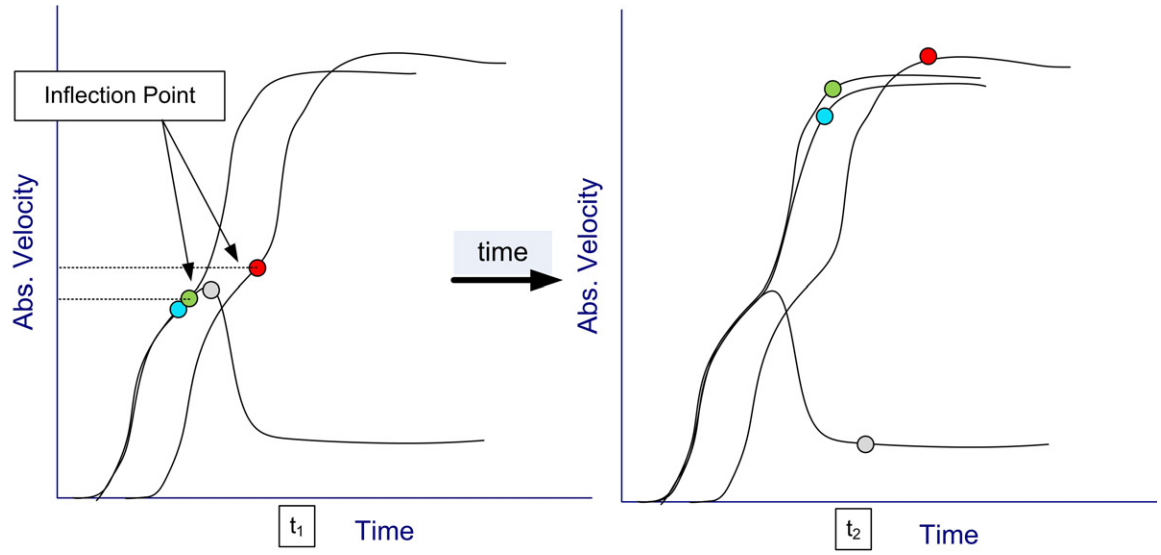

Figure 34: An example of gauge velocity paths in the mass flow, the respective velocity inflections that are assumed indications of stagnation motion and final jet and slug velocities are sketched above.

The second approach relies on tracking the motion of the stagnation front, based on the time arrival of peak pressures along fixed gauges at and parallel to the axis of symmetry.

$$v_f = v_j - v_s. \tag{26}$$

Herewith, both approaches can be compared and their results contributed to developing improved approximation methods for jet coherency.

F. EFFECT OF COAXIAL ROD ON PENETRATION

Jets formed by shaped charges can be substituted with rods due to comparable shape. This means that the general information from material behavior and penetration performance can be adapted to a shaped charge jet. The goal of these simulations was to select materials and liner orientations that would at least affect penetration and if necessary to understand potential penalties of less than optimal material configurations. The expected results were more qualitatively than quantitatively, but they were essential for design configurations.

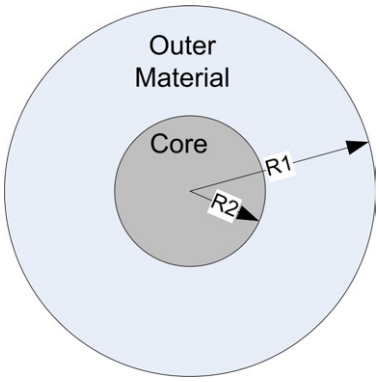

Figure 35: Rod cross-section

Simulations of bimetallic rods against armored steel were conducted with copper and tungsten rods. The rod diameter was in all cases 6 mm and had a length of 120 mm, so the L/D-ratio was 20. The simulations were conducted with different ratios, and additionally with pure liners of copper and tungsten. Important for the design, was to leave

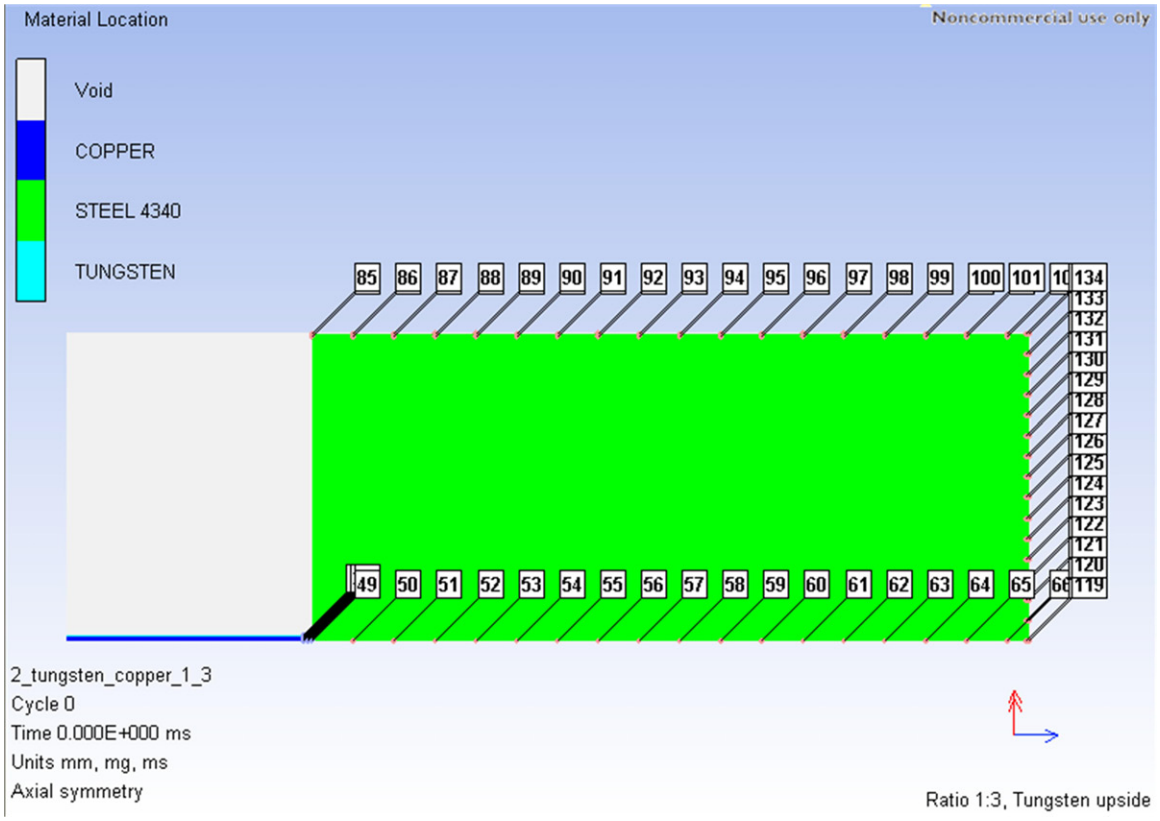

Figure 36: General simulation setup (incl. gauge locations)

sufficient lateral space to allow the target to expand, and not to touch the grid limits (shown in Fig. 36).

The gauges placed along the the penetration axis measured the penetration depth and velocity. Other gauges placed on top and left of the steel target were used to examine traveling waves and target expansion. Fixed gauges in the front of the rod were used (three rows with each 16 gauges) were used to correlate penetration velocity times with fixed gauges along the axis.

G. MULTIMATERIAL DESIGN CONCEPTS

There are presented in this section design strategies for increasing the performance and cost and performance effectiveness of shaped charge by the use of multi-material liners. The merits of two basic design approaches, referred to AB and ABA, are introduced and discussed. Included in the discussions are some of the unique opportunities that can be afforded for enhancing penetration performance and minimizing concomitant investment for incorporating materials that are in short supply and that are relatively more costly than copper, which is the most used liner material. Potential implications of fabrication are addressed at the conclusion of the section.

1. Basic considerations

Of the many possible reasons and potential applications for multi-material, the consequences to resultant penetration are a primary issue. As previously discussed, material density, the sound or shock velocity under the dynamic conditions during the history of liner collapse and jet formation are prominent issues affecting penetration. The extremely high velocities and thermal conditions along the effective portion of jets result in negligible contribution of material strength and the extremely high shock pressures during target impact are generally more than an order of magnitude greater than target strength. Thus, penetration potential of shaped charge jets at short standoff can be reasonably estimated by the aforementioned hydrodynamic square root density law. Most important to this study this law can be used to accurately assess the relative effect of material (i. e., density) changes.

The remaining factor of the density law is jet length, which is dependent on host of previously discussed parameters. However, using an argument of "all other things equal', sound propagating properties are also a factor in material selection since it is this property that governs the maximum jet velocity attainable and therefore elongation. Density, longitudinal velocity and Hugoniot values for some of the most likely liner material candidates are reported in Table 2.

The combined effect of density and sound (or shock) velocity on penetration is illustrated in the following equations:

$$P = l\left(\frac{\rho_j}{\rho_t}\right)^{\frac{1}{2}} \tag{27}$$

$$l = \int (v_{\text{jet tip}} - v_{\text{jet tail}})dt \tag{28}$$

$$v_{\text{j}} = v_f + v_s \tag{29}$$

$$v_s = f(\text{Detonation velocity } U_D) \tag{30}$$

$$v_{\text{flow max}} = f(\text{sound velocity}) \tag{31}$$

Table 7 presents the selected material combinations for both designs, ordered in the preferred resultant jet. One material is denoted as liner part A, the second as liner part B.

Core	Sleeve
Ta	Al
Al	Ta
Hf	Cu
Cu	Hf

Table 7: AB/ ABA material selection

2. Jet/ Slug Partitioning

As previously discussed, designs that insure good jet quality rely on an understanding and accurate predictability of jet formation dynamics; including the ability to estimate

the consequences of material substitutions and mass partitioning. Specific issues are discussed earlier in this text and reported results from a previous series of copper and copper/zirconium lined charges highlight the importance of these factors.

3. Liner Material Configurations

Two types of configurations, referred to as AB and ABA (and ABC), are considered in this research. Conic configurations with constant thickness are assumed in all cases, however, the approaches can be used for any geometry.

a. AB design

The first design is a called AB. The liner in this case is composed of two material layers over the entire length or alternatively over only a portion of the entire liner. In both cases jet/slug partitioning can be an essential feature or not.

A full bimetallic liner cladding, as illustrated in Figure 37, could be an approach for (a) minimizing the amount of a costly material component, (b) generating coaxial jets, and (c) protecting one of the components from chemical reaction along the explosive interface or the exposed surface and/or galvanic action. High density materials like tungsten and tantalum, in particular, are effective penetrators but are more costly than copper. The smallest amount required of either would be that included within the partition and liner-air surfaces. One of the materials of a liner in a coaxial jetting charge would have to occupy, at a minimum the remaining volume between the outer liner materials and the partition surface, as shown in Figure 37. Partial cladding configurations include those providing means for adding special jetting characteristics at either the jet tip and along the terminus of the jet. For example, the addition of a high sound velocity material along the apex region can be used to produce a rapidly elongating precursor jet in front of the main jet or low-density and/or incendiary materials inserted along the basal regions for purposes of increasing terminal hole size and spallation or enhancing beyond-the-target damage by rapid combustive reaction.

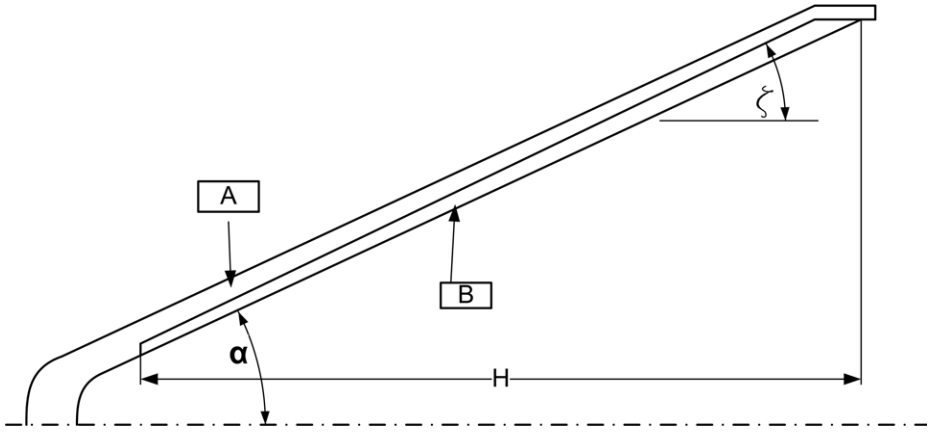

Figure 37: AB design

The material substitution is in relationship with the partition interface of the main material liner. This is obtained by a simulation of the main material of the liner with identical liner parameters.

α denotes the liner angle, ξ the insert angle, respectively. If $\alpha = \xi$, the insert has a constant thickness, and therefore the resultant jet contains of material A and B, with increasing proportion of material A. Using $\alpha < \xi$ allows to substitute material along the partition interface. Moreover, different angles allow to control the liner material flowing into jet and secondary, to control the ratio of jet material thickness.

A variety of jets can be formed with the AB configuration. First, a **single material jet** can be formed by placing the desired materials solely between the partition and liner-air surfaces (or for that matter the liner can contain an excess of jetting material).

Positioning two layers of materials within the partition and/liner- air interfaces provides means for generating a **bi-material coaxial jet**; provided that the materials cohere. Multi-layered jets can also be formed, however, liner fabrication would be extremely challenging and the performance value questionable.

Using high density material as the jet core, results in a small amount of high performance material flowing into the jet, the major amount flowing into the slug. The low density material clads the jet core and is fully used in the jet, no mass going into slug. Consequently, one may avoid this kind of configuration due to high costs and a

low efficiency of high performance material. If the materials are applied vice versa, a jet with a low density core and a high density clad will form. Under this circumstances the high-performance material is used efficiently and the low density material flowing into the slug is acceptable, anyway not avoidable. A lower penetration depth is expected, but with reference to conducted rod penetration studies, the high-density clad contributes to a larger hole diameter.

The AB design offers several applications, however, efficient, coaxial bimetallic jets with high penetration performance (depth) can not be achieved with this design.

b. ABA design

The ABA design originated during the development of the AB design. As aforementioned, the AB design does not allow to form a bimetallic coaxial jet with high-density core at low cost. The ABA design merges the advantages of a coaxial bimetallic jet with a material cost efficient application. Monolithic jets can not be be formed with this design, but both jet types, coaxial and following (q.v. section IV.F), can be achieved by varying the insert position and amount of material. Heretofore, no experiments or simulations are known examining such liner design.

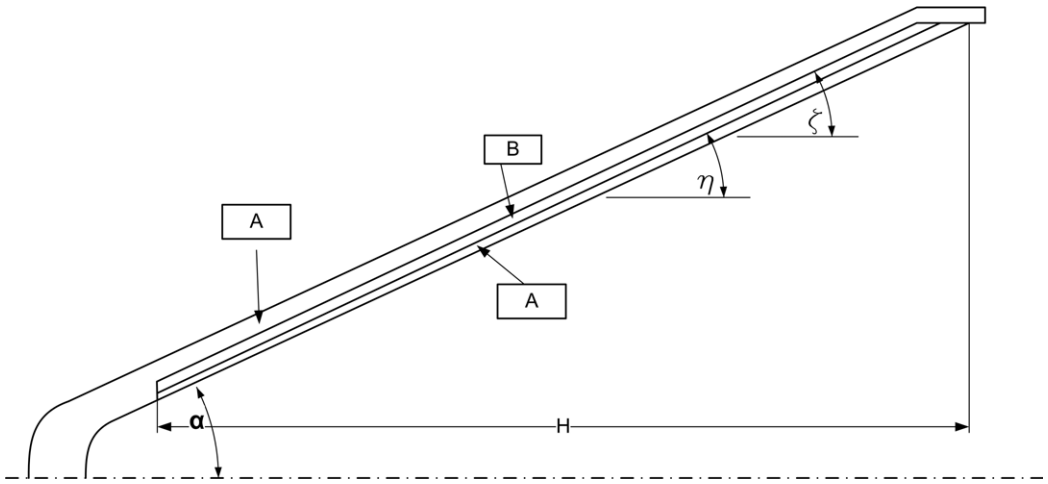

Figure 38: ABA design

Fig. 38 provides a general geometrical setup for the ABA design. It shows a conical liner with constant thickness and two laminates. An additional angle η is introduced, representing the angle of the second laminate. η and ξ can be equal, keeping the ratio between both materials identical within the insert; or the inserts can be designed with different angles, affecting the resultant material distribution in the formed jet. If $\eta < \xi$, then a jet with more material A at the tip will form. Along the liner, the material ratio in the jet will change in aid of material B, which will have the highest amount in the jet tail. The effect will be vice versa, if $\eta > \xi$.

The first laminate creates the later jet core material (material B), the second laminate shrouds the jet core (material A), and protects it from the environment during storage and after liner collapse. Using two laminates instead of one insert, results in (i) a decrease of each insert thickness, and (ii) higher requirements on liner material and assembly quality. Keep in mind, that more than two materials can be used. Then the design would turn into a ABC design, respectively.

In typical shaped charge jets the core is moving fastest, with decreasing velocity to the outside. This is caused by the high pressure distribution in the collapse region. With modification in the insert height, it might be possible to balance the velocity distribution with materials of lower density as second laminate.

The insert height H must not be equal for both laminates. $H_{\text{insert B}} > H_{\text{insert A}}$ can be applied, especially if the density of material B is lower. In this case, the resulting higher velocity of material B, due to lower density, can be compensated with the usually slower part of the jet formed by high density material. As consequence, it should be possible to form a coaxial bimetallic jet that has an approximately equal velocity gradient from inside to outside.

4. Fabrication and Cost Issue

The developed and described design concepts address liners with at least two layers. This requires higher accuracy and advanced manufacturing techniques than a solid material liner. Especially the interfaces of liner parts need to match to avoid disruptions.

On the other hand, the AB and ABA designs provide potential for using high density and expensive liner materials by optimizing the effectiveness. The costs of applying high valuable materials are much lower than for solid material liners, however, the investigation on the effect of (total) costs was not an issue of this research.

VI. RESULTS

The results of the research are presented in this section and interpreted in the following one with additional plots and visual results presented in appendices E and G. Initial work focused on simulating the Dragon experiments and comparing with observation for purposes of adding to the NPS validation base and studying the structural integrity of the copper/zirconium jets produced by the modified liners used in the experiment. Comprehensive study of results reported by Chanteret were completed for the purpose of resolving issues related to coherent jetting. A series of computations were performed for purposes of developing general understanding of the effect of coaxial jet impact on target penetration. The final work brings these results together for demonstrating examples of AB and ABA design solutions and recommended designs for a possible UIUC experiment.

Some definitions for the following statements: (i) In the subsequent sections some of the results refer to partition or air interface gauges. Partition gauges are denoted as last gauge in a row of moving gauges, flowing into the jet. Air interface gauges represent the gauges in a row of moving gauges which are closest to the air interface or on the edge between liner and air. Note, that for each row only one gauge is called air interface gauge and one gauge is called the partition gauge. (ii) The notation for liner angles in the plots is denoted as combination of material and angle, e. g. Cu 20 for a copper lined charge with liner angle 20°.

A. DRAGON

The DRAGON simulations were conducted to study jet formation, elongation, and mass partitioning within the liner. The results of these simulations where used to validate the simulation setup and to provide a foundation for subsequent simulations. The description of the layout, placing of gauges and used materials are presented in section V.D and in appendix A.

1. DRAGON Baseline

The DRAGON baseline simulation showed a smooth run without termination due to ANSYS problems. A coherent jet, with jet tip velocity at 2 CD standoff with 9.11 km/s after 54.7 μs was measured; the jet velocity obtained from experimental results was 9.09 km/s. Calculations for the jet length and position correspond well with radiograph positions, measured from apex. Results are presented for the basal insert simulations, because both calculations are almost identical.

Fig. 39 provides the cumulative mass vs. velocity distribution after 2 CD standoff. It shows the amount of mass traveling with corresponding velocity and is an indication how much mass is in the jet tip. Unfortunately, no experimental data was provided for the velocity and mass distribution.

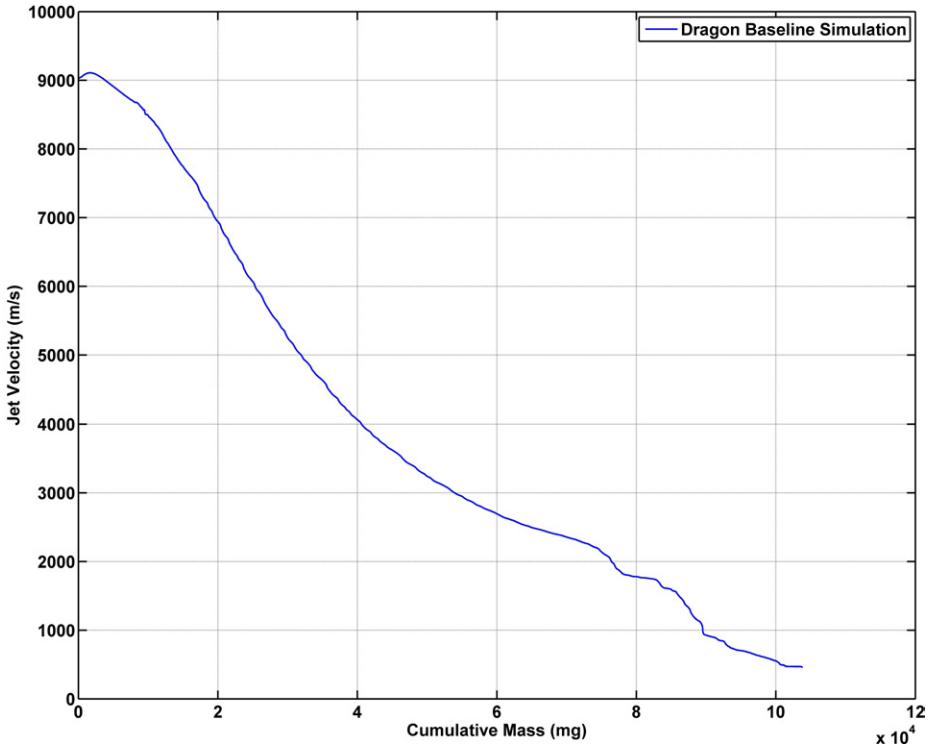

Figure 39: DRAGON baseline: cumulative mass vs. jet velocity at standoff 2 CD

The liner partition was detected with moving gauges, provided by appendix E.A. The mass flowing into jet starts at an apex distance of 3 mm and increases to a maximum

of 67% of liner thickness towards the base. The values of the the last set of gauges (No. 175-189) do not show explicit results for mass flowing into jet or slug due to disturbances and overall low velocities, and could not be evaluated. Fig. 40 shows the distribution of liner mass flowing into jet vs. distance from apex. To compare the detection accuracy for moving gauges, an identical simulation, where moving gauges were placed with a gap of 0.05 mm (instead 0.1 mm), was conducted. The analysis showed an identical mass partition line and the performance could not be increased by this approach.

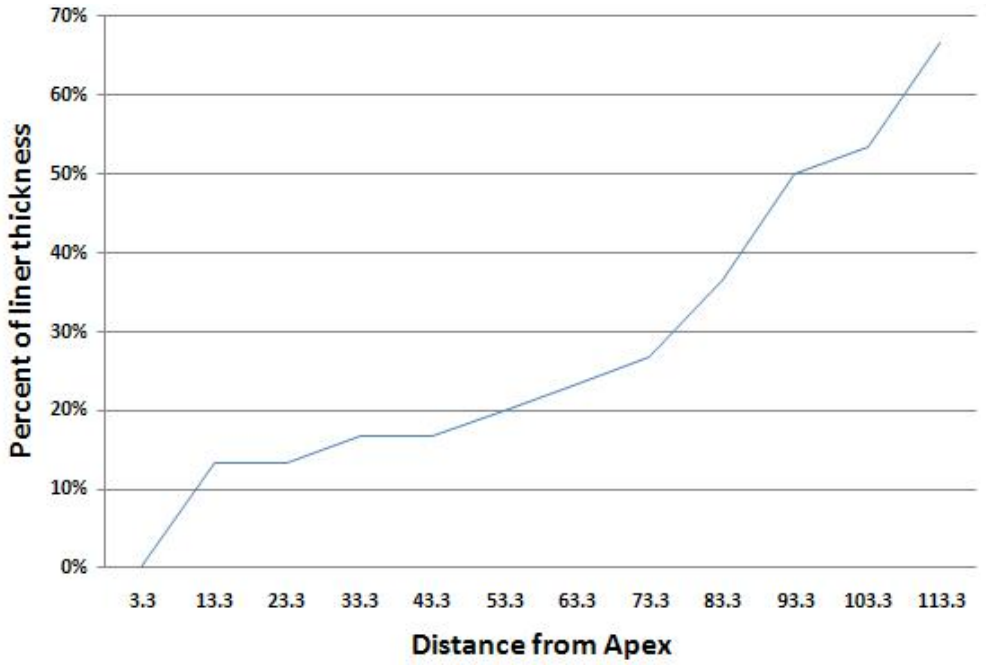

Figure 40: DRAGON baseline: percentage of liner flowing into jet mass vs. distance form apex (mm)

Calculations for the radial velocity gradient were not performed for this simulation because available radiographs did not allow for this kind of analysis. The analysis for the DRAGON base insert covers radial velocity gradients.

2. DRAGON Base insert

The jet formation and resultant jet shape is identical to the DRAGON baseline setup. Hence, this is not surprising, since both simulations have the same basic geometrical setup.

Radial velocity gradients from simulation were compared with depicted jet particles from radiograph FTD13. The average maximum velocity gradient in the radiograph was estimated with 33 m/s, maxima reached values of 69 m/s. Computation results show, that the average radial velocity (y-velocity) in or after the collapse region is about 20 m/s with maxima of 110 m/s. However, material near the centerline tends to have less bouncing effect than material on the jet outside. Radiograph FTD13, showing frames at 170.0, 183.2, and 389.3 μs, is provided by appendix D.

With obtained data after 54 μs, the jet tip position was calculated and compared with results from radiograph FTD13 (Fig. 41). The calculation over-predicted the jet tip position with 3.2 % at 183.2 μs (1375.7 mm vs. 1333 mm) and under-predicted the jet tail velocity with 7.4 % (183.2 μs; 482 mm vs. 520.6 mm).

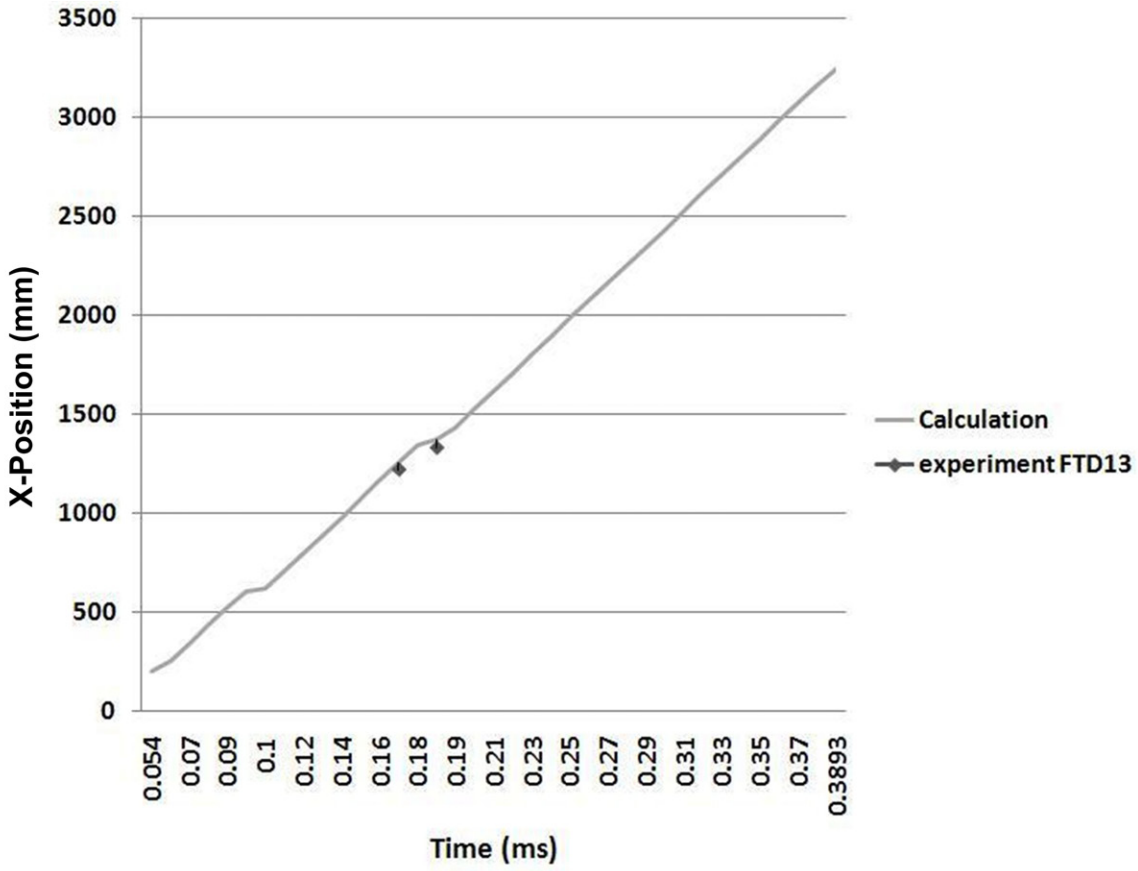

Figure 41: Jet tip position (mm) in calculation vs. radiograph

The jet and slug partition of the base insert simulation was almost identical to the DRAGON baseline simulation. Small differences have been detected in the base region, were zirconium was inserted. As one can see in Fig. 42, the jet tail is formed by copper and zirconium with zirconium on the outside. Fig. 43 (radiograph) provides the copper/

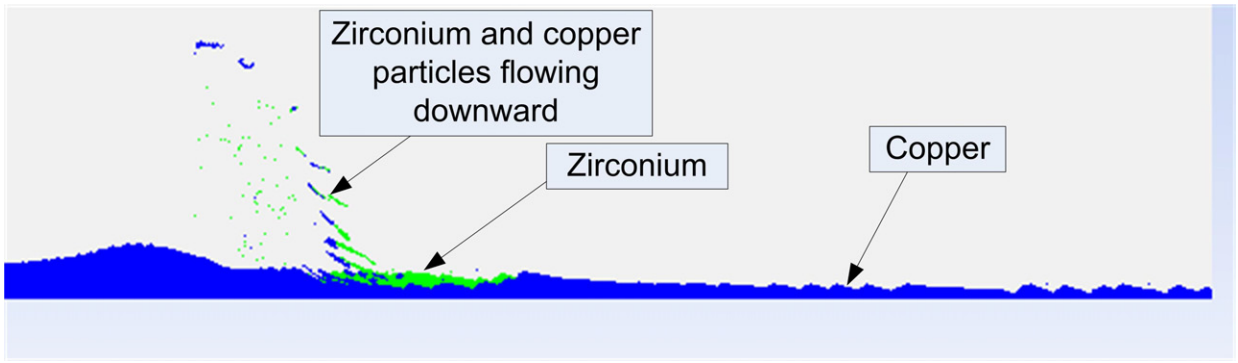

Figure 42: Copper/ zirconium jet in a late stage of jet formation (after 62 μs)

zirconium jet after 170 μs. A simulation result can not be shown due to termination after 90 μs.

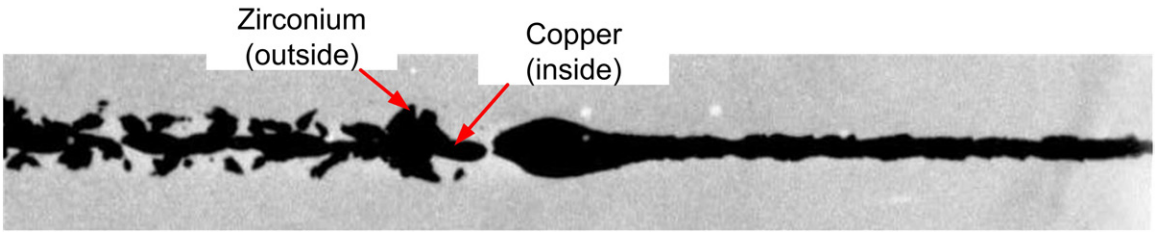

Figure 43: Jet Tail after 170 μs (FTD13)

B. ESTIMATION OF FLOW AND STAGNATION VELOCITIES

The following results are based on simulations with the DRAGON design as basis, and liner angle series with copper (20°, 25°, 42° liner) and nickel (20°, 25° liner). The jets were compared with copper and nickel jets from experiments by Chanteret [Cha92, CL95]. Although, Chanteret varied explosive, liner thickness, and initiation type, the values can be used to support the findings qualitatively. Table 8 provides jet quality for the results.

exp/sim	material	angle	coherent	bifurcation
exp	Cu	20		✓
sim	Cu	20		
exp	Ni	20	✓	
sim	Ni	20	✓	
sim	Cu	25	✓	
sim	Ni	25	✓	
exp	Cu	28	✓	
exp	Cu	42	✓	
sim	Cu	42	✓	

Table 8: Jet quality comparison of simulation and Chanteret (experiment)

1. Stagnation velocity approach results

The stagnation velocity was estimated with two approaches. The method, using times of peak pressure along the centerline was found to be the most accurate way to estimate the stagnation velocity. The pressure data were compared with the Hugoniot P-ν-plane. This was derived from the U-u Hugoniot with equations for conservation of mass and momentum ($\nu = \rho^{-1}$ is denoted as specific volume, P as pressure, and s as Hugoniot slope in the U-u-plane):

$$P = c_0^2 \left(\nu_0 - \nu\right) \left[\nu_0 - s \left(\nu_0 - \nu\right)\right]^{-2} \tag{32}$$

Fig. 44 shows that Hugoniot values are lower than obtained pressure values, but the curvature is mostly identical. This was expected as the moving gauges are not at the centerline, but have a vertical offset. Given that the pressure value is less important than the timing and curvature, the data can be used for calculations. The pressure values from AUTODYN were calculated with peak pressures at the centerline. Hugoniot data was calculated with density date from partition gauges. Partition gauges were used because they are closest to the centerline, instead of air interface gauges. The pressures reach maxima of ca. 187 GPa for copper and nickel with liner angle 20°. Pressure, compression and the rising of density decrease with radial distance from the centerline. Further details are covered by the next section.

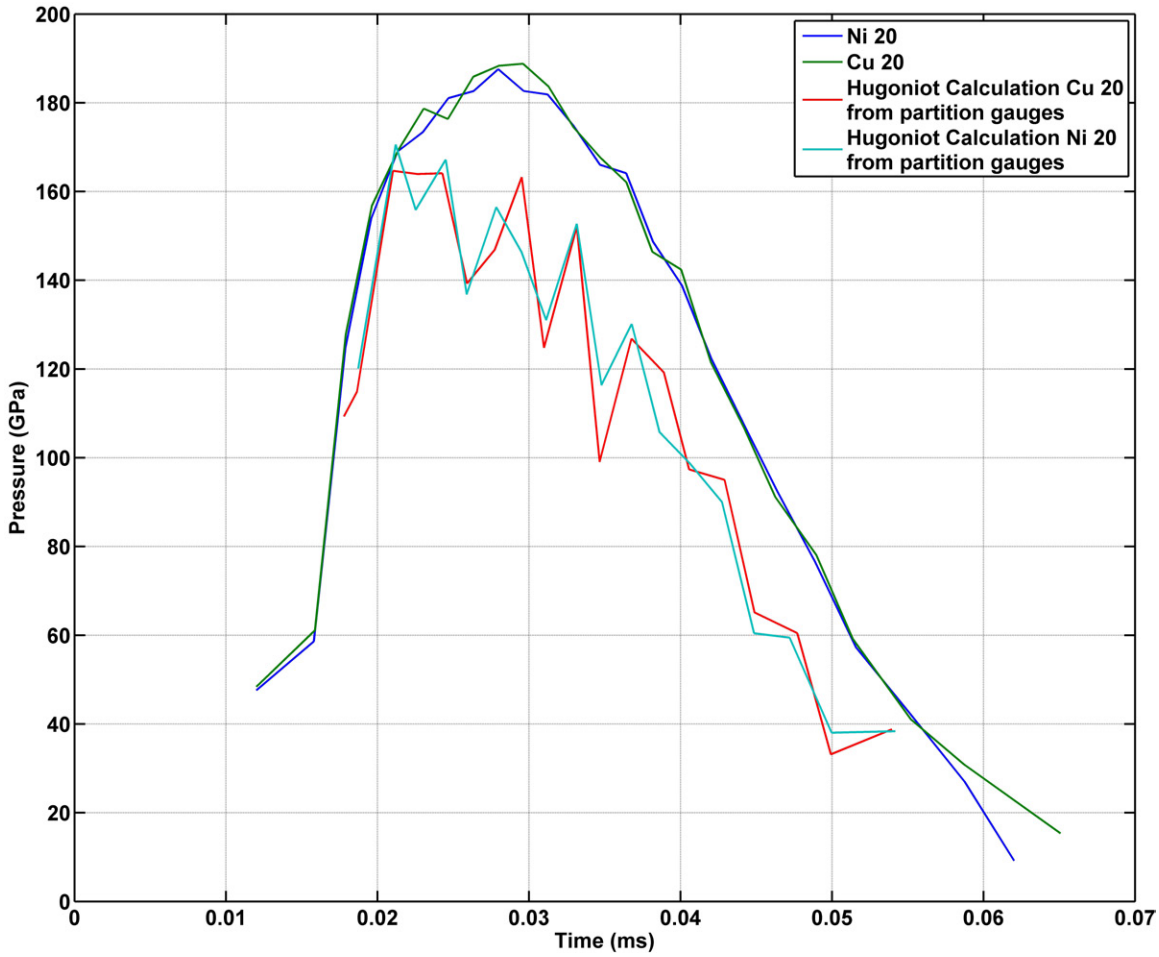

Figure 44: Pressure vs. time comparison of AUTODYN data and Hugoniot calculations for copper and nickel jets from 20° liner

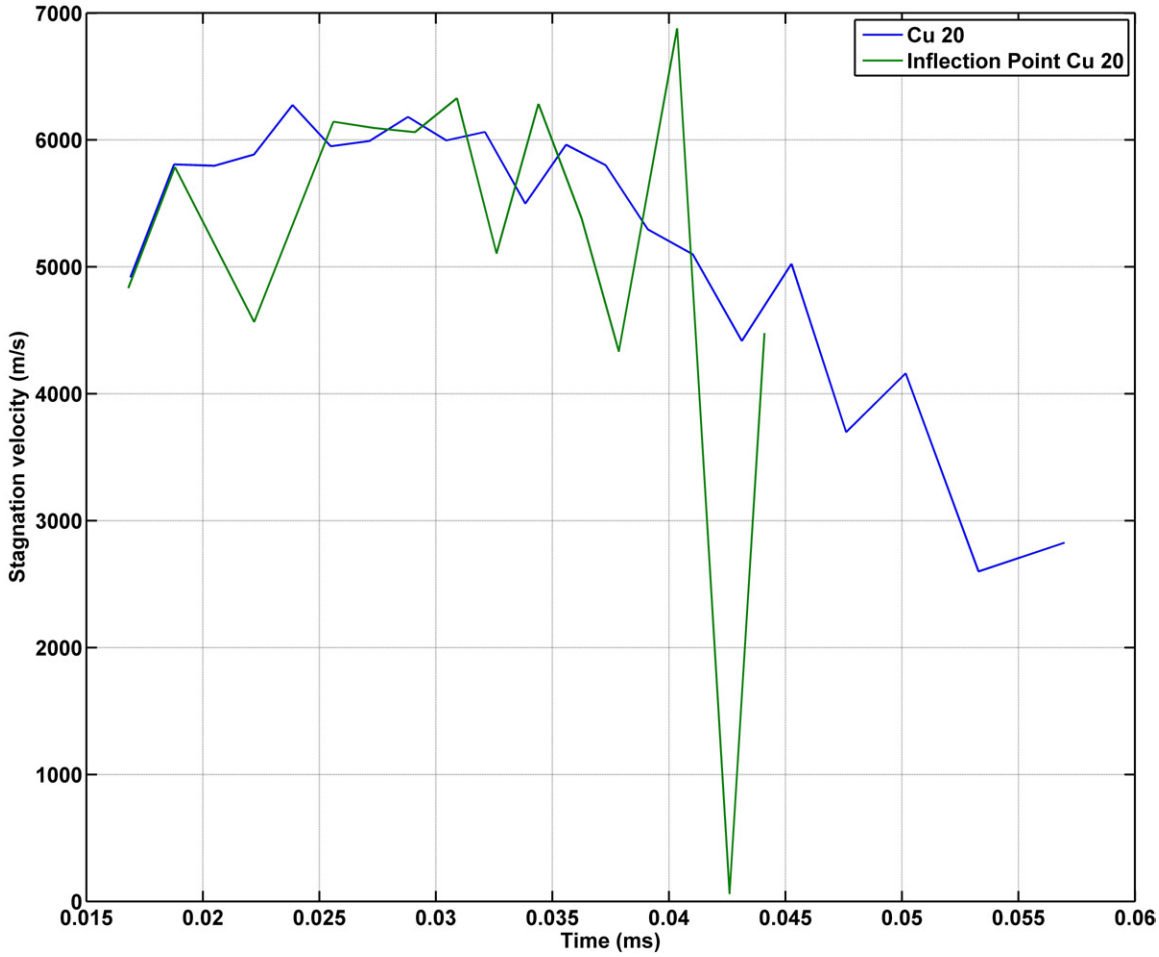

Figure 45: Stagnation velocity comparison for pressure and inflection method with 20° copper lined shaped charge; pressures at the centerline and partition gauges were used

The second approach to calculate stagnation velocity was conducted by the inflection point method. The results show reasonable match with the first method, although the variance is greater. Fig. 45 presents a comparison of both methods for the conical copper lined shaped charge with liner angle 20°.

2. Flow velocity approach results

The first approach for the estimation of flow velocity used the inflection point method. The search for the ”right” inflection point was done by hand because a technique, to fit a curve into the absolute velocity plot was not established. This lowers the accuracy

of this approach. Fig. 46 provides the flow velocity from inflection points for a copper 20°, 25°, 42° liner, all with basic DRAGON design and adapted head height. That means, that the head height was held constant, the shaped charge was longer with decreasing liner angle (q. v. appendix F). The values do not change drastically, moreover, they do not exceed

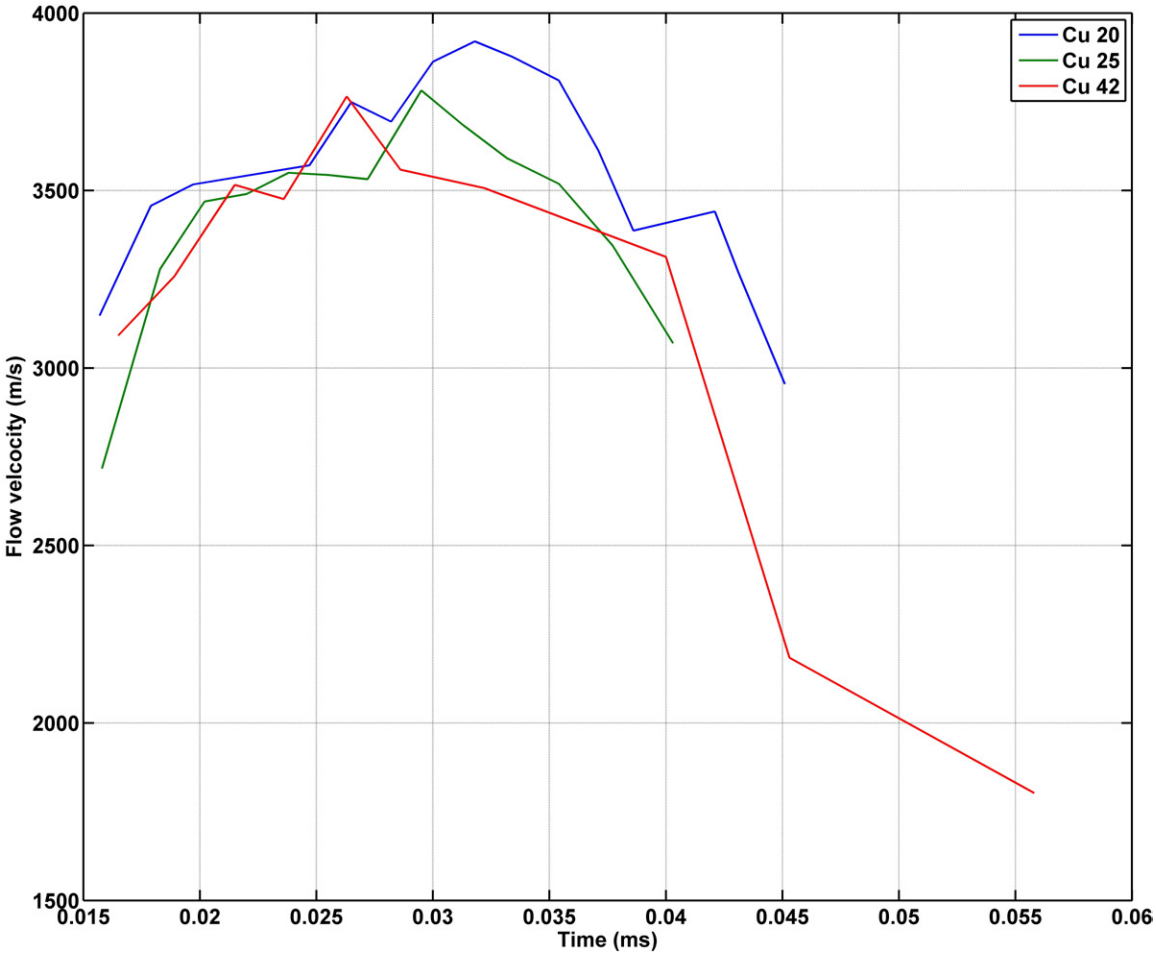

Figure 46: Flow velocities for a copper lined shaped charge by inflection point method

4 km/s. A similar result was obtained for nickel simulations using this method.

The second method to estimate flow velocity, as difference of jet and stagnation velocity, was performed with copper and nickel setups. Fig. 47 provides the flow velocity for copper, Fig. 48 the results for nickel. The plots show the flow velocities of the copper and nickel series and compare the values with the Harrison criterion. With this approach, flow velocity values increase with decreasing liner angle, which is consistent with theory.

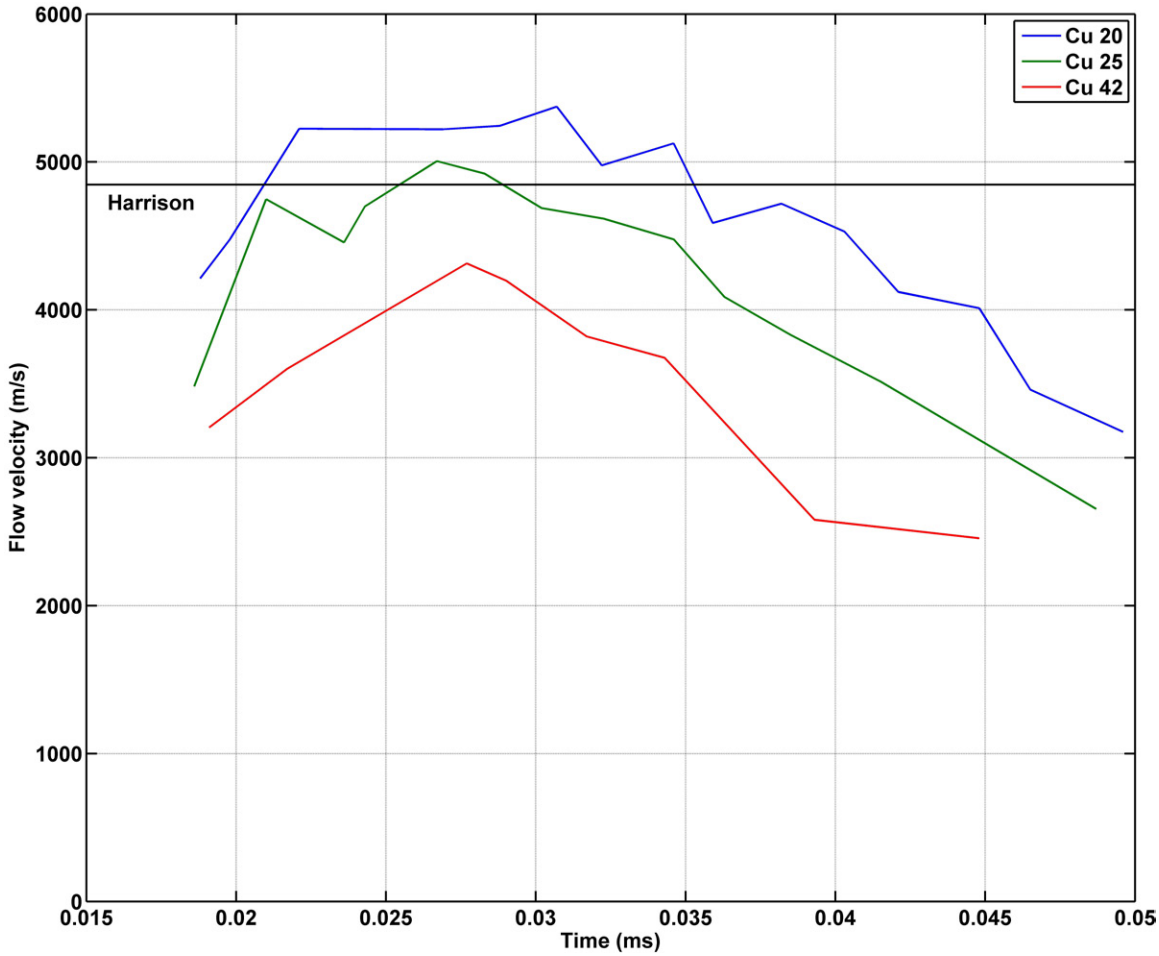

Figure 47: Flow velocities for a copper lined shaped charge by difference method. The Harrison coherency limit at $v_f = 1.23c_0 = c*$ is shown; $c*$ = 4846 m/s

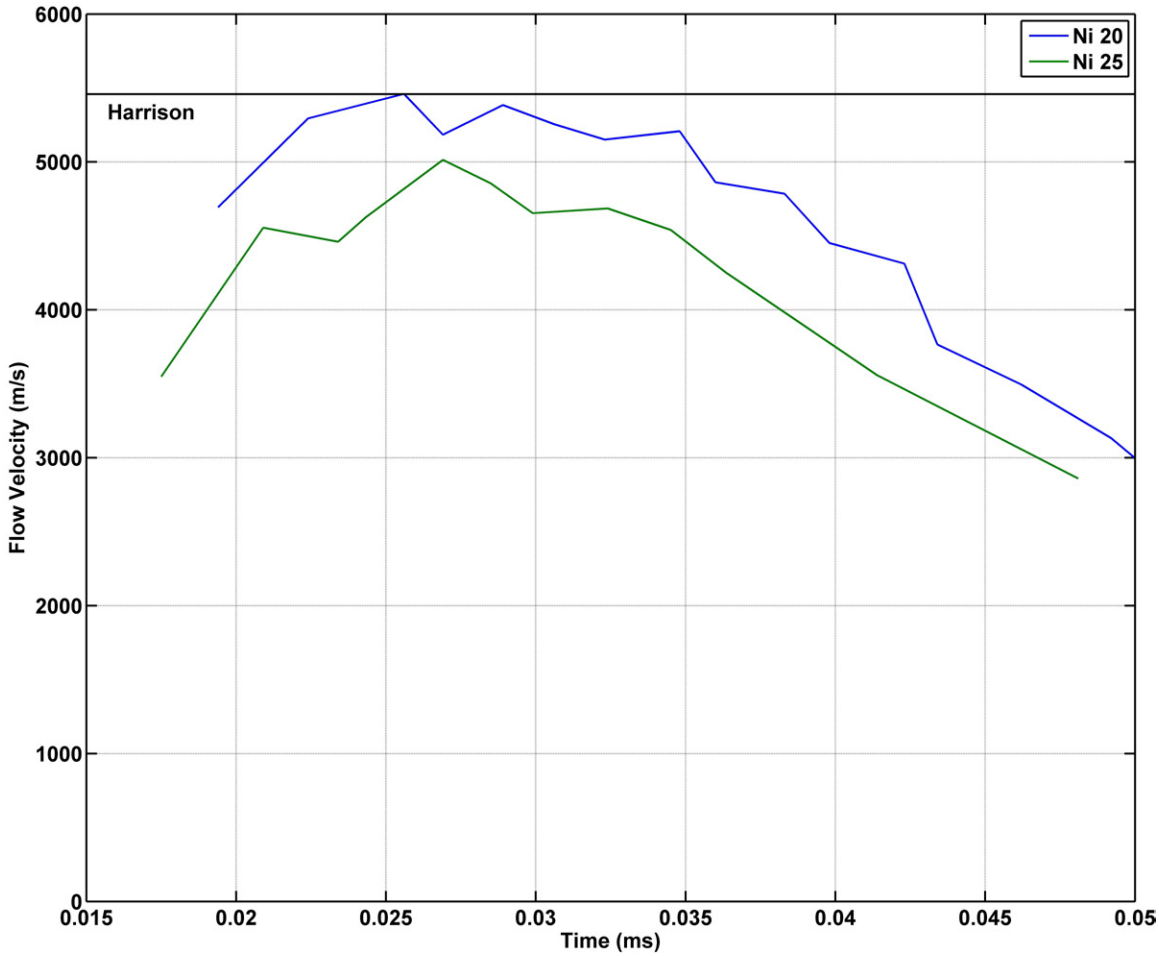

Figure 48: Flow velocities for a nickel lined shaped charge by difference method. The Harrison coherency limit at $v_f = 1.23c_0 = c*$ is shown; $c*$ = 5459 m/s

Obtained jets show good agreement for expected flow velocities and the Harrison criterion. The copper jet with 20° liner was incoherent in simulation and experiment. The 25° and 42° liner were coherent in the simulation, although the flow velocity was touching the Harrison criterion. There are no experimental results for a 25° liner, but Chanteret conducted an experiment with a 28° liner which was coherent. The 42° liner was coherent like in the DRAGON baseline experiment.

Nickel jets from 20° and 25° liner showed also good agreement with experimental results. Both jets were coherent, and the flow velocities did not exceed the Harrison criterion.

The jet velocities from the copper angle series are provided by Fig. 49. With simulation results it should be possible to obtain a coherent jet velocity of 10-10.2 km/s.

C. EFFECT OF PRESSURE AND COMPRESSION ON JET COHERENCY

This section provides results for pressure, compression and density with the above mentioned copper and nickel series.

The pressure values for the same y-position, e. g. at the x-axis or 2.5 mm parallel to the x-axis, do not differ between copper and nickel. Hugoniot data for pressures was estimated with Eqs. (32) and was also found to be almost identical for copper and nickel jets (q. v. previous section). The pressure values (i) decrease with radial distance to the centerline, and (ii) decrease with increasing liner angle. This is provided by Fig. 50 and 51.

The results for density and compression had no significant difference for copper and nickel simulations. Although, both materials have almost identical initial densities but differ in coherency, both, the densities and compression showed an identical behavior during liner collapse (q. v. Fig. 52 and 53).

The dependence of coherent jets was also considered under the assumption, that the coherence does depend on the shock velocity, not the bulk sound speed. Therefore Hugoniot calculations to estimate the shock and particle velocity were performed using the

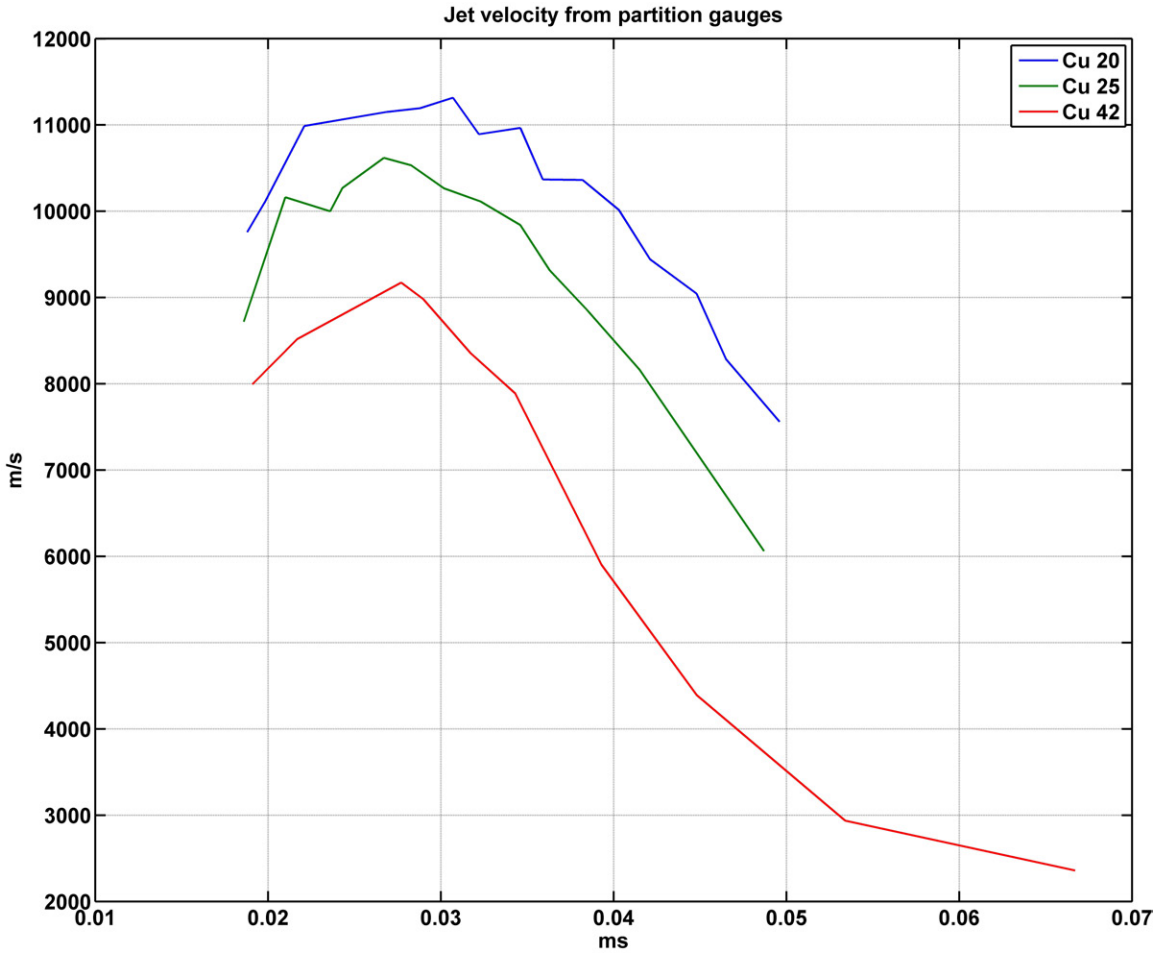

Figure 49: Predicted final velocities of liner materials originating near the jet/slug boundaries as function of liner angle.

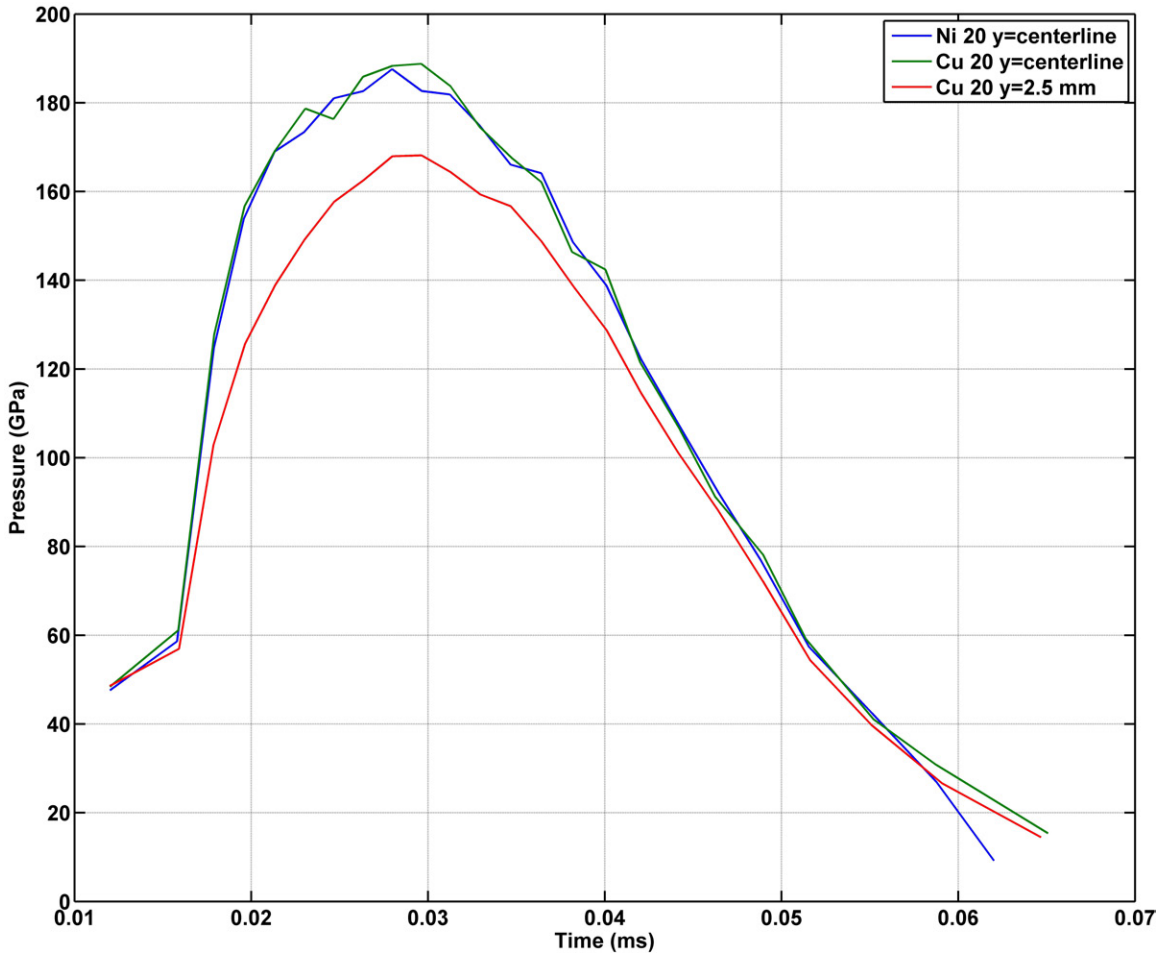

Figure 50: Pressure vs. time for nickel and copper; values from fixed gauges along the centerline and 2.5 mm above

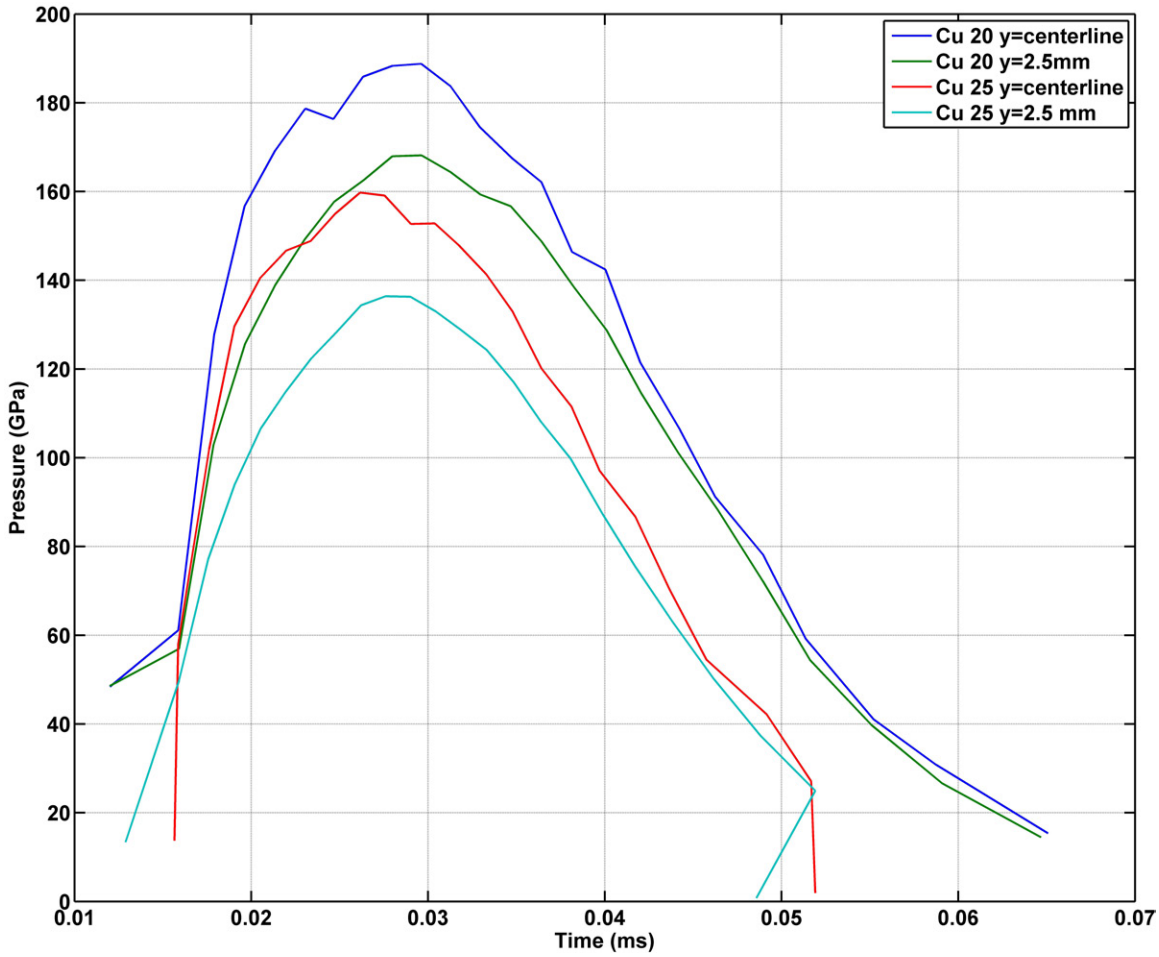

Figure 51: Pressure vs. time for copper; values from fixed gauges along the centerline and 2.5 mm above with 20° and 25° liner

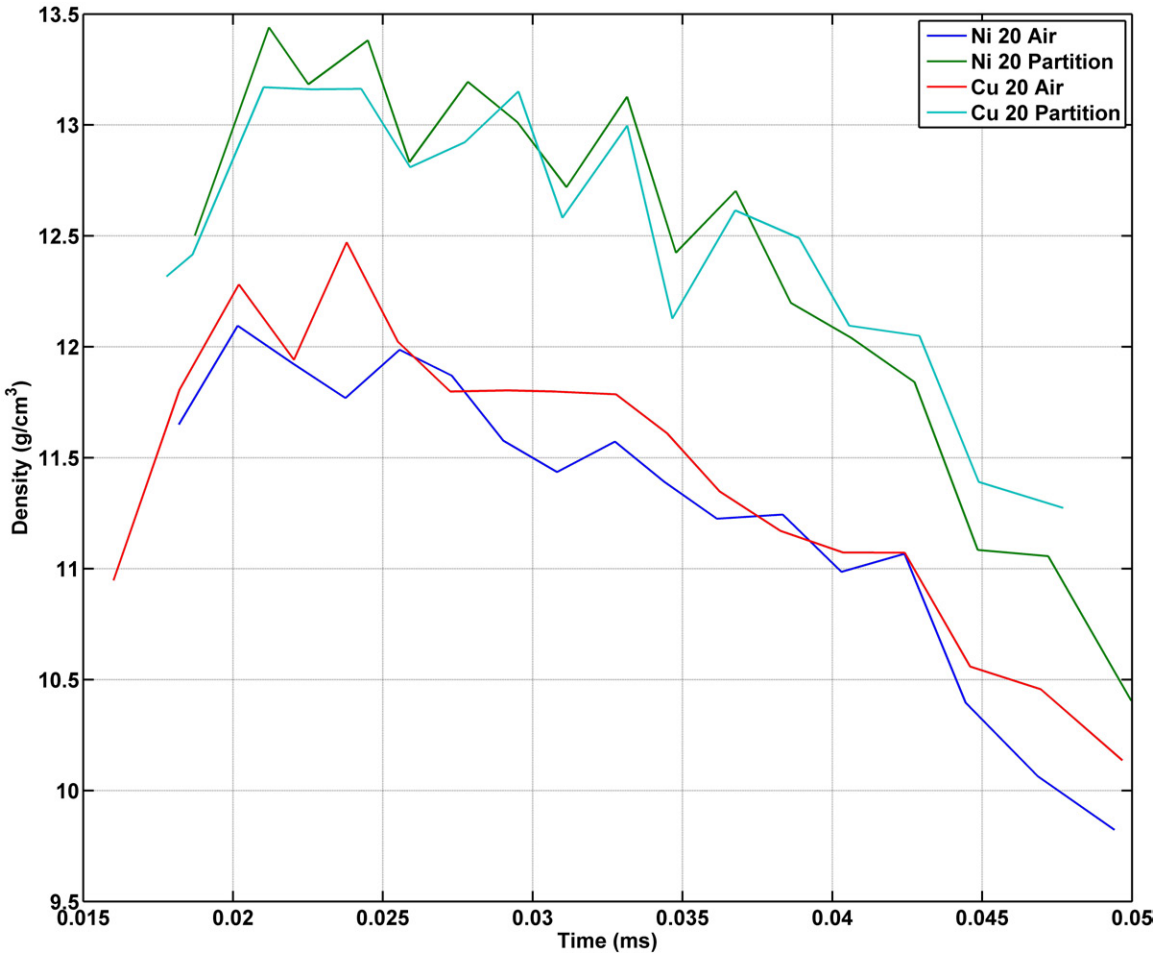

Figure 52: Density vs. time for copper and nickel jets from a 20° liner; measured with partition gauges

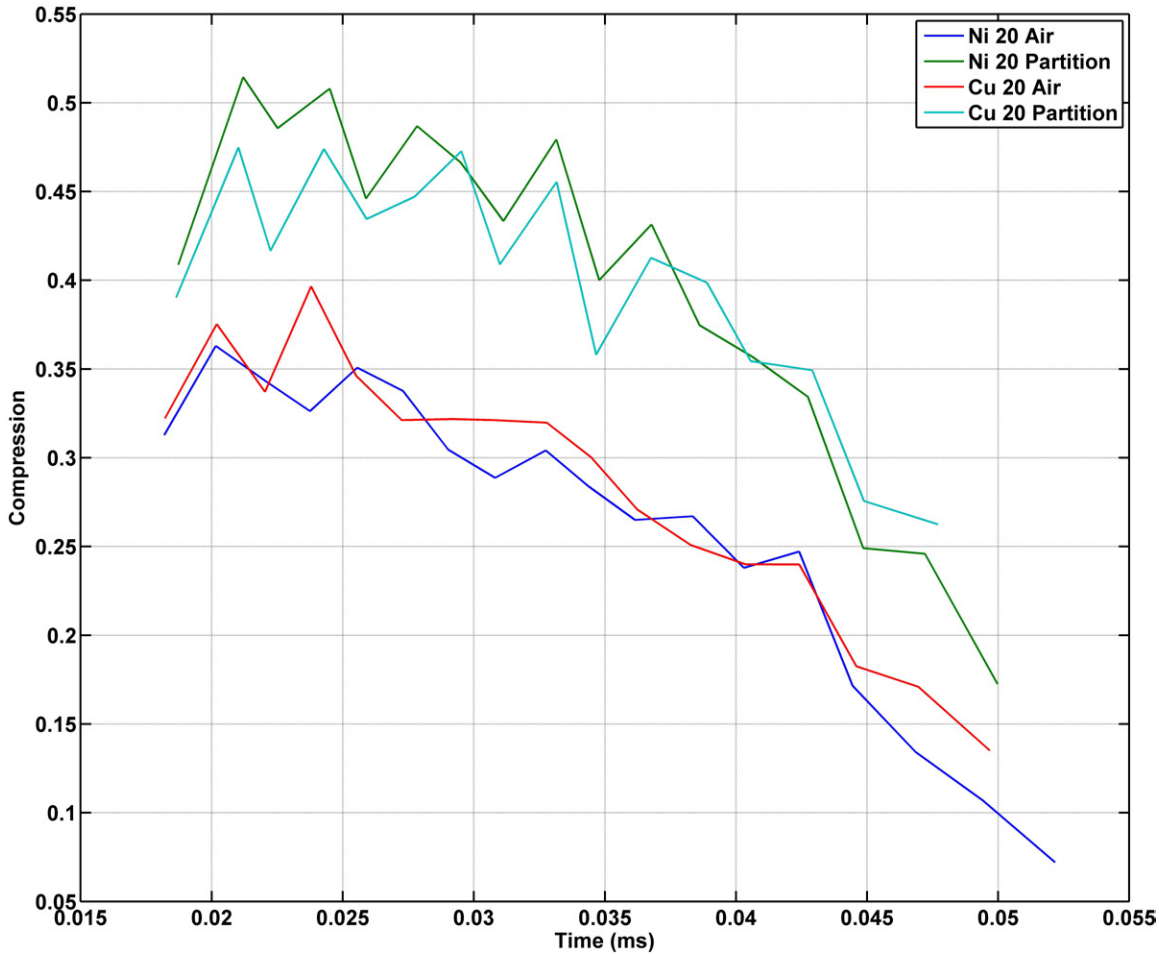

Figure 53: Compression vs. time for copper and nickel jets from a 20° liner; measured with partition gauges

density and pressure data. At pressures of ca. 150 GPa, the shock velocity was calculated to be about 7.4 km/s. The pressure in this research reaches maxima of approximately 190 GPa, this would lead to even higher shock velocities. The values are much higher than obtained flow velocities. Thus, the shock velocity has not been found to be the key factor to review coherent jets, which is in contradiction to Murphy's theory statements.

Walker's theory on jet coherency was also reviewed. He states, that the flow velocity should not exceed the longitudinal sound speed for a coherent jet. The longitudinal sound speed for copper and nickel is presented in Tab. 9, together with the Harrison criterion for comparison. Values were calculated by Eqs. (22) and material properties from the AUTODYN library. The threshold values for copper and nickel are very close for both theories.

material	$1.23c_0$ [m/s]	c_l [m/s]
copper	4846	4807
nickel	5459	5548

Table 9: Harrison and Walker value comparison

D. EFFECT OF COAXIAL ROD ON PENETRATION

This paragraph covers the results obtained from initial rod penetration simulations. The simulation layout is provided by section V.F.

The following results are based on a 4 cell/mm Simulation. The ratio means the amount of inner radius to outer radius. If the ratio is 1/1, then the first 1.5 mm of the radius are filled with core material and the residual 1.5 mm are filled with outer material which has a strong effect on the volume. With a ratio of 3/1, the first 2.25 mm is core material and the rest is outer material (see Fig. 35). Fig. 54 shows the effect of clad material on mass and penetration perfomance.

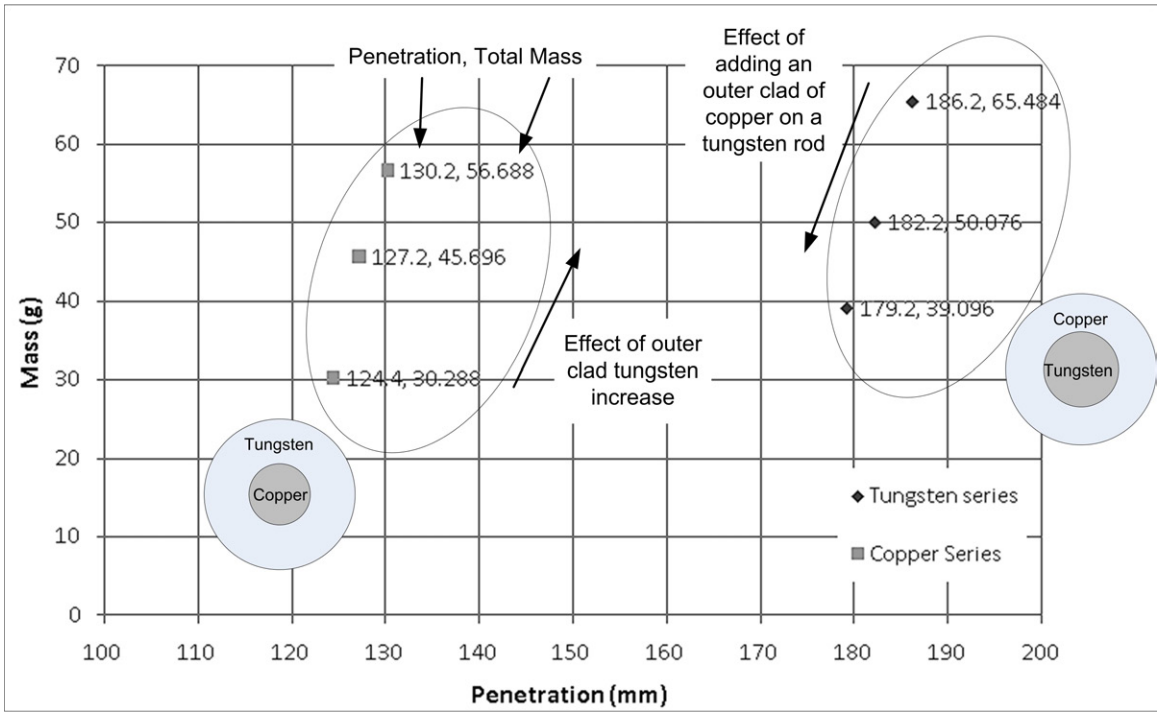

Figure 54: Effects of adding outer clad material to a copper or tungsten core

Core	Outer Material	Ratio	$\frac{Mass}{Length}$	Calc. Time (ms)	Depth (mm)	Diameter (mm)
Copper	Tungsten	1/1	4.724	9.948e-2	130.2	37
Copper	Tungsten	3/1	3.808	1.092e-1	127.2	34
Tungsten	Copper	1/1	3.258	1.389e-1	179.2	24
Tungsten	Copper	3/1	4.173	1.241e-1	182.2	27
Copper	None	-	2.524	1.908e-1	124.4	27
Tungsten	None	-	5.457	2.063e-1	186.2	32

Table 10: Predicted effects of material replacements in coaxial rods on penetration

E. AB DESIGN

Simulations, using liner materials tantalum/ aluminum, copper/hafnium, and vice versa, respectively, were conducted to see the visual material behavior of multi-material lined shaped charge configurations. Liner collapse, jet formation, separation, and jet tip velocities were studied. Most of the results for AB and ABA simulations were reviewed by visual results as analytical methods are not known to rate the quality.

The **tantalum/aluminum** liner produced a coaxial, bimetallic jet with tantalum as core material and aluminum as clad. The liner collapse process was smooth and without disturbances, although it seemed that aluminum was ”overtaking” tantalum. In the jet, aluminum had a higher velocity due to its low density and traveled faster than tantalum. This resulted in a hollow jet tip, but a coaxial jet without breakup behind the jet tip (q.v. Fig. 55). The jet tip velocity of tantalum, obtained from the calculation was about 8.42 km/s.

Necking was detected for the shrouding material, however, it seemed to protect the core material from necking and breakup. This phenomena might contribute to penetration performance.

The jet did not show indication for material separation, even though aluminum moved faster.

The **aluminum/tantalum** liner formed a jet with a small amount of aluminum at the tip and a monolithic main jet of tantalum. The jet tip velocity for copper was 9.2 km/s, for tantalum 8.6 km/s, accordingly. The total amount of tantalum flowing into slug could be decreased by reducing the insert height of tantalum. The penetration depth should be

better than in the vice versa setup, having the high-density material as core. Anyhow, the simulation predicts early necking and incoherence of the jet (q. v. Fig. 57), probably because the bulk sound speed of tantalum is about 1.9 km/s lower than of aluminum.

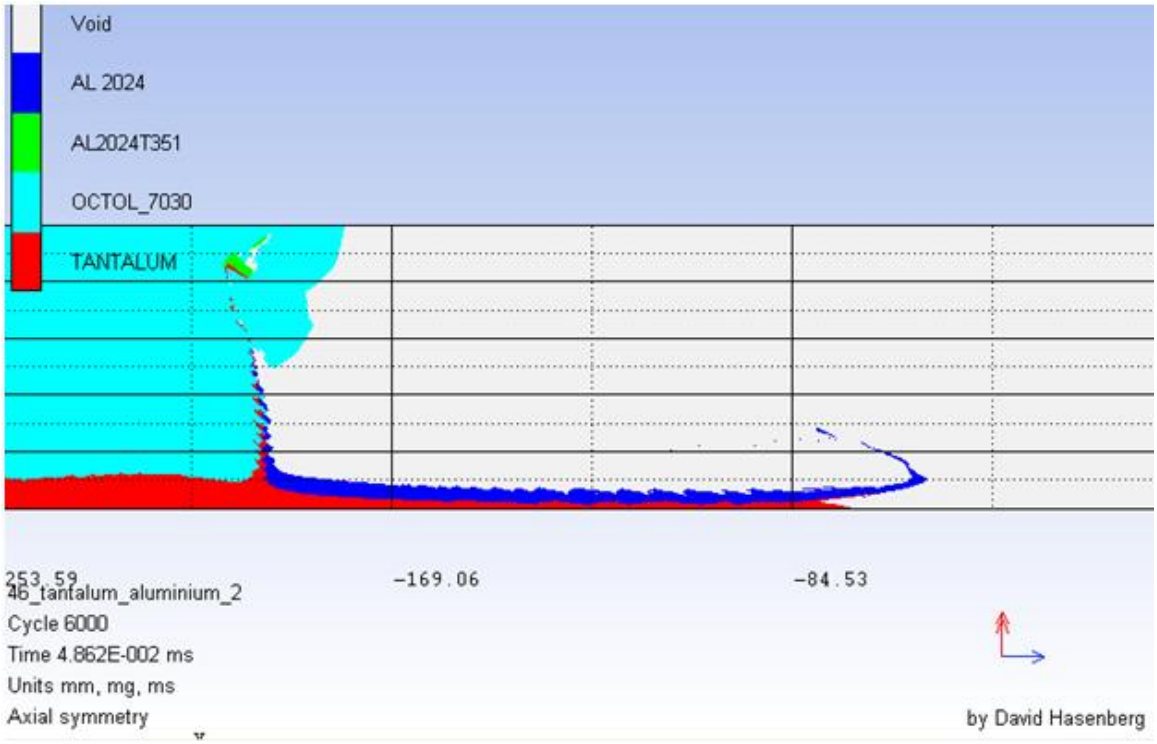

Figure 55: Tantalum/ aluminum jet after 48 μs

Another simulation with copper/hafnium was conducted. The goal was to form a high-density hafnium jet with high amount of hafnium flowing into jet, least hafnium flowing into slug. The substitution was applied along the partition line, starting at about 13 mm distance from the apex to ensure a minimal insert thickness of 0.3 mm. The setup is shown in Fig. 58.

The simulation showed almost all hafnium flowing into jet, as it was intended. Copper formed the jet tip because of zoning/ memory limits. These limit the ability to place hafnium along the liner apex. The low bulk sound speed of hafnium, c_0 = 2954 m/s, caused early necking of the jet. The formed jet is shown in Fig. 59 after 53 μs. A possible solution

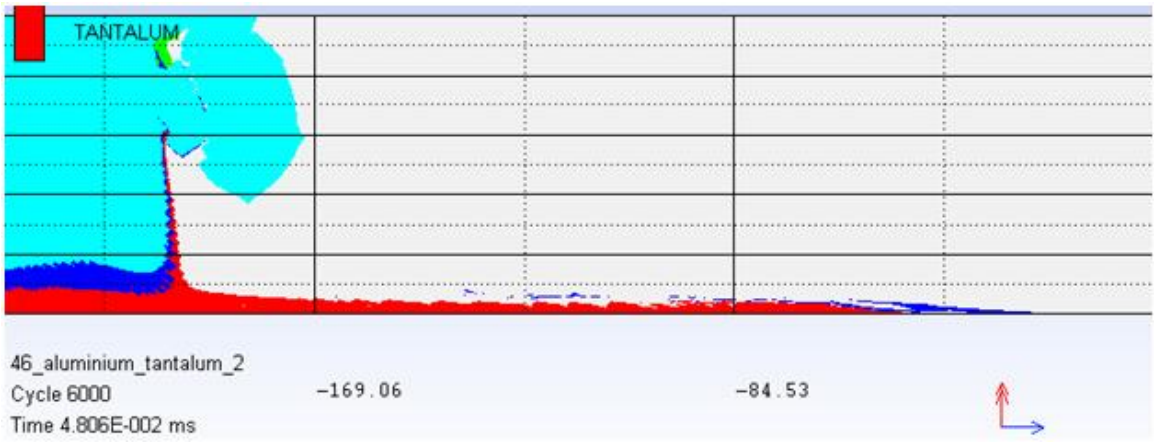

Figure 56: Aluminum/ tantalum jet after 48 μs

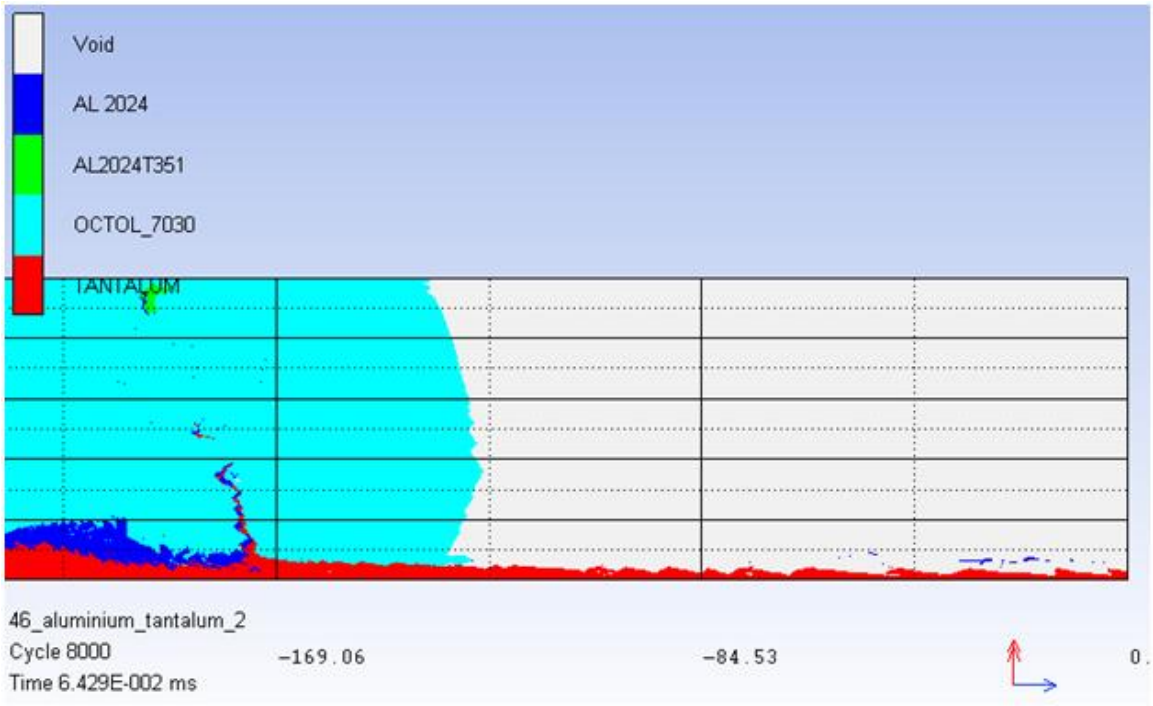

Figure 57: Necking of aluminum/ tantalum jet after 64 μs

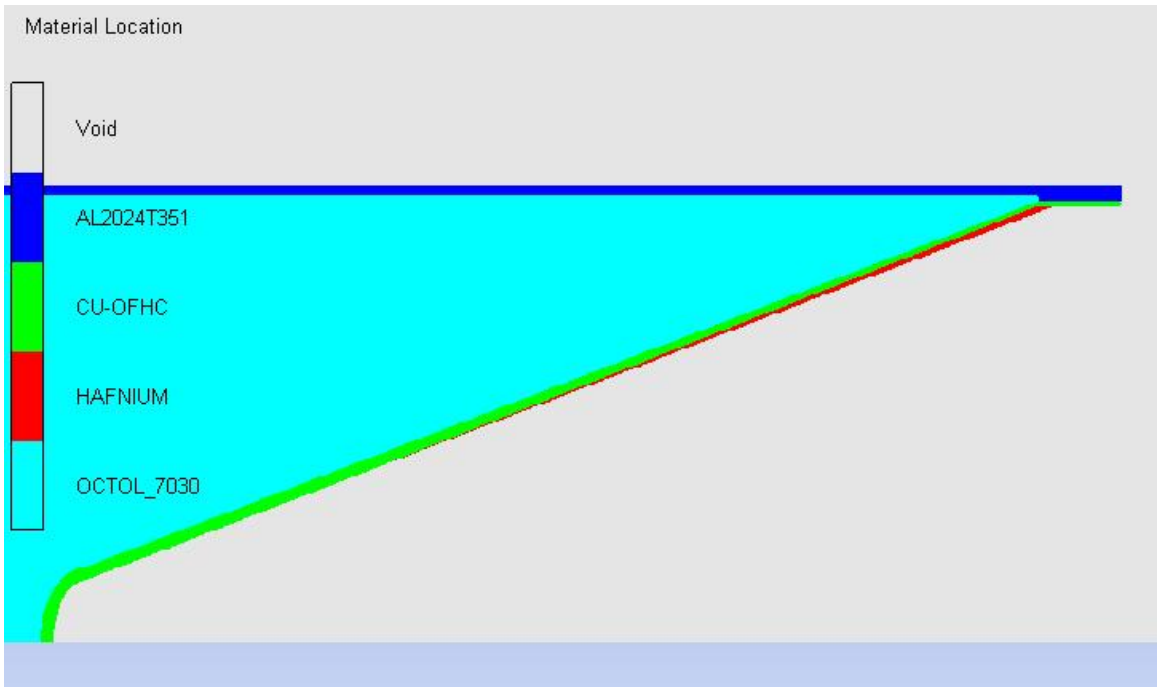

Figure 58: AB design: copper liner with hafnium base insert

for this issue will be presented in the discussion. Further simulation frames, showing stages of jet formation are presented in appendix G.

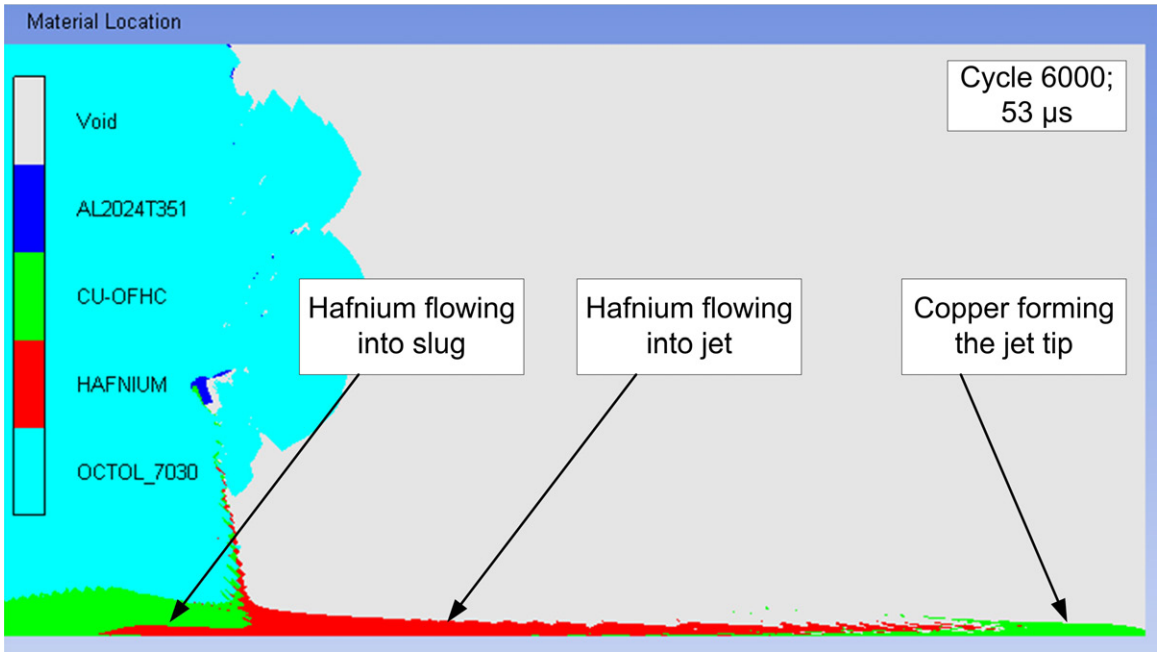

Figure 59: Resulting copper/ hafnium jet after 53 μs

F. ABA DESIGN

The ABA design was applied to simulations where at least two materials are jetting, for example, where a high-density core is used improve penetration, or where core materials needs to be protected from the environment. Therefore, exemplary computations with aluminum as material A and tantalum as material B (AlTaAl) were conducted. For means of jet/ slug partition line estimation a copper/ copper liner was tested at the beginning.

The liner had a total thickness of 1.5 mm in all cases but presented results can also be transfered to thicker or thinner liner designs, as long as the M/C-ratio is held on a constant level. All other geometrical parameters were equal in these simulations. Fig. 60 provides the geometrical setup to obtain a bimaterial coaxial jet, here as an example with a copper/copper liner. Other material combinations had the same layout.

The copper/ copper simulation, performed, to see the effect of liner partition estimation, showed a non optimal result. The amount of laminate 1 flowing into jet was greater

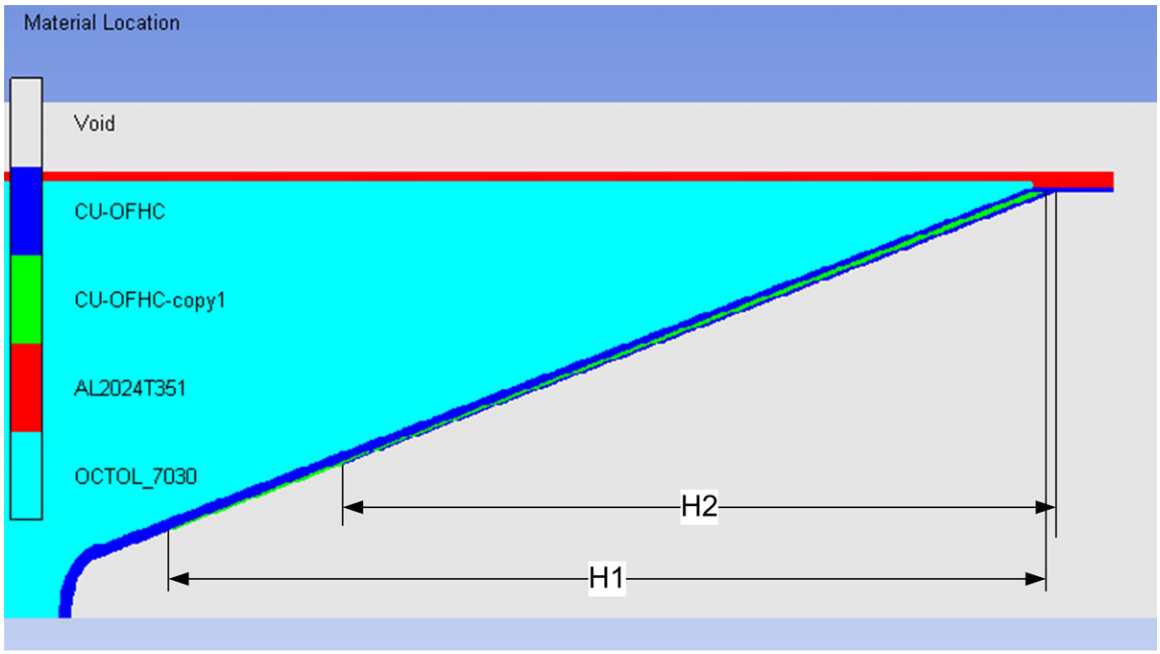

Figure 60: ABA design layout illustrating the insert height for a copper/ copper simulation

than intended; the full amount of liner material 2 was flowing into jet. Simulation pictures after selected times are presented in appendix G.

The simulation for AlTaAl showed a liner breakup after ca. 20 % of liner collapse, with resulting disturbances in the first part of the jet (q. v. Fig. 61). The resulting jet with tantalum as core and aluminum as clad material was formed surprisingly good. However, the value of this result should not be over-estimated. It shows, that aluminum and tantalum, having a big difference in densities, are not as easy to pair as material combinations with less density difference.

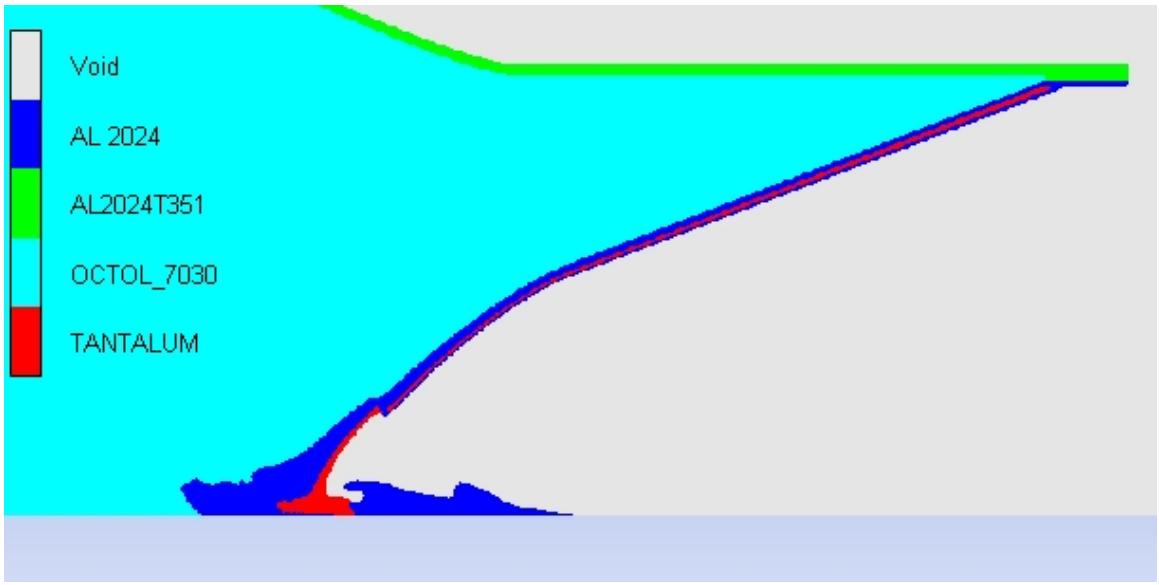

Figure 61: Aluminum/ tantalum jet with liner disruption after 19 μs

G. UIUC DESIGN RESULT

The geometrical design of the 50 mm NM charge for the UIUC was modeled as shown in Fig. 62. The body is relatively thick, compared to the DRAGON design, in order to increase the detonation pressure and to support higher velocities especially in the jet tail. Mechanical drawings are attached in appendix C.C, appendix F provides the simulation layout.

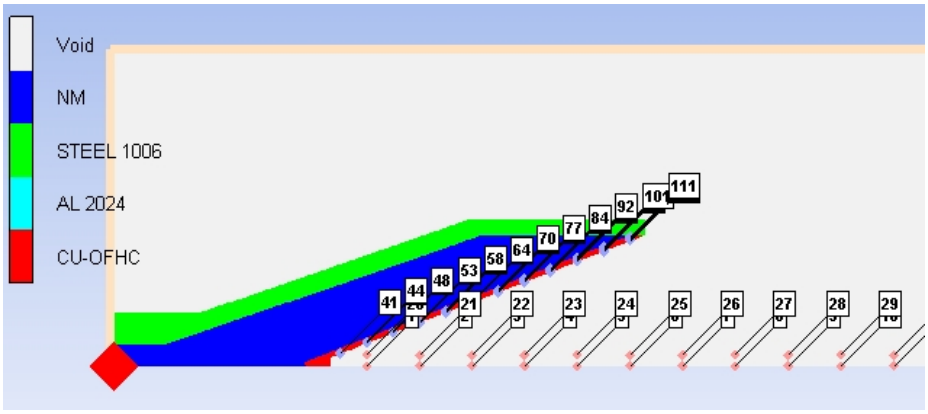

Figure 62: UIUC simulation layout with a 1 mm liner illustrating boundaries and gauge placement

The initial simulation was performed to estimate the jet/ slug partition interface in the liner. The initial liner used by the UIUC was 1.61 mm thick; the zoning in this initial simulation was chosen with 6 mm/cell with a fast running simulation. Obtained data was used to define timing to halt subsequent simulations. Informations from moving gauges could not be used successfully because the resolution was too coarse.

A second simulation was conducted with a graded 12/8 mm zoning and a vertical gauge distance of 0.1 mm in order to increase the resolution for moving gauges. The results did not match expectations, as only a small percentage (about 0-15 %) was flowing into the jet and the jet tip velocity was slow (5.46 km/s). However, gauge results were consistent with visual results.

Since very little mass flowed into jet and the jet tip was slow, and the liner appeared to be thicker than it should be based on other experiences, a series of computations to esti-

mate the effect of liner thickness reduction was performed. An overview of liner reduction effects is provided by Tab. 11.

As consequence, a setup with a thiner liner (1 mm) was conducted. This simulation produced a faster jet (6.3 km/s at the tip) and it also allowed for an analysis of the partition line. The jetting partition was increasing up to 35 % of the liner thickness (absolute velocity plots and gauge positions are presented in appendix E). Anyway, the applied explosive, NM, has a lower detonation velocity and pressure causing a worse performance than octol 70/30 in the DRAGON simulations. Additionaly, the liner is relatively thicker than in the DRAGON simulations. However, the simulation formed a good jet with less decreasing axial velocity gradient.

To improve the performance, a thiner liner with 0.75 mm thickness, about 1.5 % of the charge diameter, was studied. This lead to lower a M/C ratio and higher velocities, with 40 % of liner mass flowing into the jet and jet tip velocities of 6.7 km/s.

Liner Thickness (mm)	Jet Mass per Total Liner Mass (%)	Jet Tip Velocity (km/s)
1.65	15-20	5.46
1	35	6.31
0.75	40	6.72

Table 11: Effect of liner thickness on jet tip velocity and relative mass flowing into jet

The basic result of the UIUC simulation is the estimation of the jet/slug interface. The partition line starts at a distance of 15 mm from the apex with 0.1 mm thickness and increases almost linearly to the base with a thickness of 0.4 mm. This is a guide for further possible material insertion designs; a first example is shown as follows.

After successful simulations with solid copper liners, an approximated base insert simulation with aluminum as insert was conducted. In the solid copper simulation the amount of a 1 mm liner flowing into the jet was about 40 %. Aluminum has a much lower density than copper, so that the partition line changes in a base insert simulation. In general, every change of liner materials or design affects the partition line. Therefore, a

series of simulations would be required to fully optimize the application. The simulations, performed in this research, focus on initial qualitative effects and guidelines.

A base insert simulation was conducted with a 1 mm liner and increasing insert thickness along the partition line. The liner volume is constant, however, the mass along the liner is decreasing because of an increasing amount of aluminum (q. v. design layout in appendix F). The visual result is showed by Fig. 63, showing the aluminum insert with H=48 mm and an initial thickness of 0.1 mm. This design showed a good jet formation quality and equal jet tip velocities, compared to the solid copper liner (q. v. Fig. 64). It also performed much better than an insert simulation based on the initial UIUC design (1.61 mm thick liner with equally thick base insert; H=10.1 mm), where material separation occurred in early stages.

For the base insert simulation, it was recognized that the liner turning was faster than for the solid copper liner. This is a result from less liner mass towards the tail and thus a changing M/C-ratio. Additionally, the velocities of copper and aluminum differentiated along the jet radius, even at the interface. The copper core was a lot slower than the aluminum clad (q. v. Fig. 65). Although the materials stay together in the simulation, where aluminum is moving faster than copper, the real effect is not known. The simulation predicted a coaxial jet with a hollow jet tip of aluminum, provided by Fig. 117. In the DRAGON base insert, where zirconium was jetting together with copper at the jet tail, the effect of differentiating velocity was negligible (the velocity difference between copper and zirconium was about 0.03km/s). Anyway, the base insert simulation represents a first result on material behavior and on the effect of liner turning and jet formation of an copper/ aluminum liner.

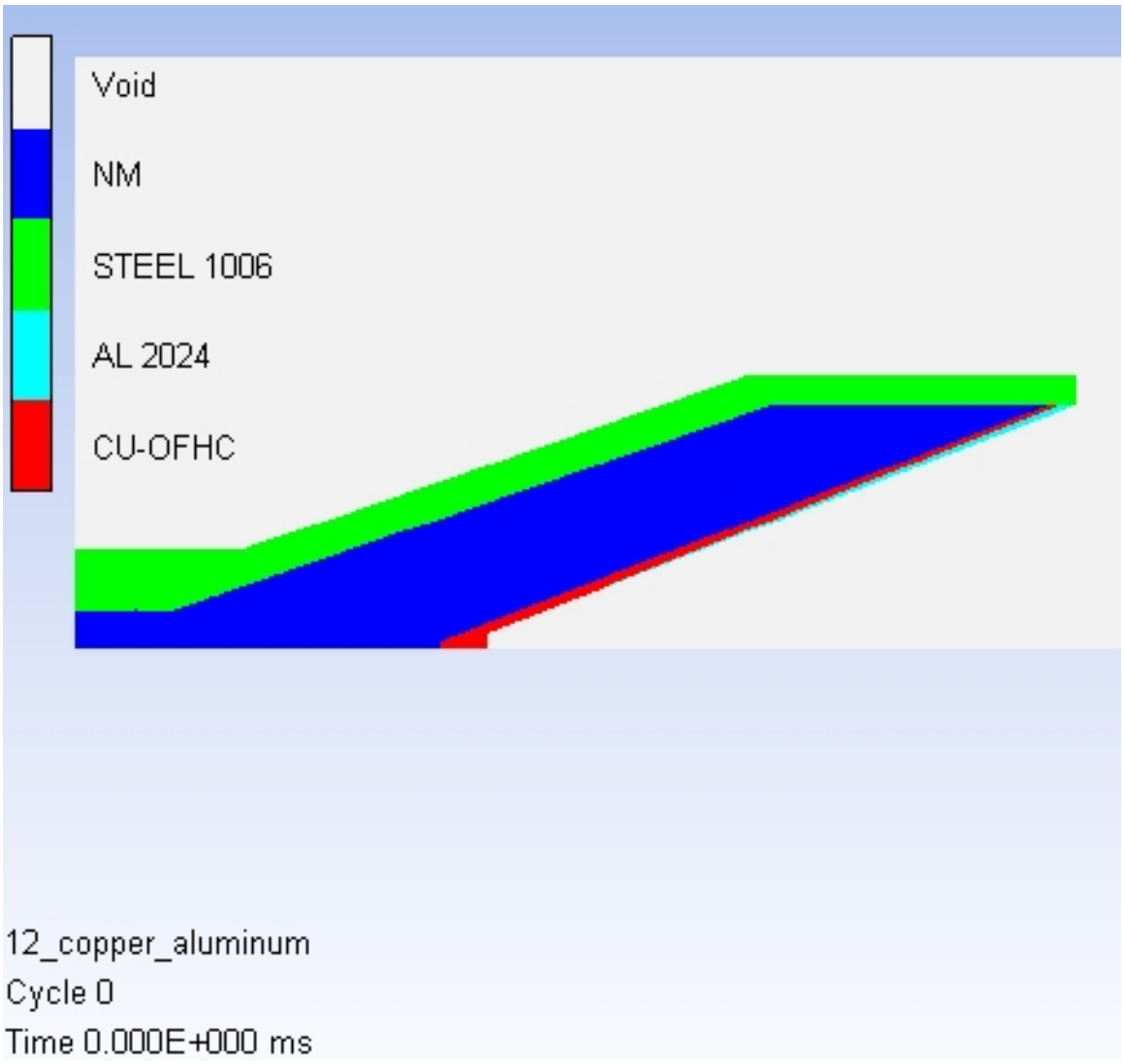

Figure 63: UIUC design with 1 mm liner thickness and basal insert

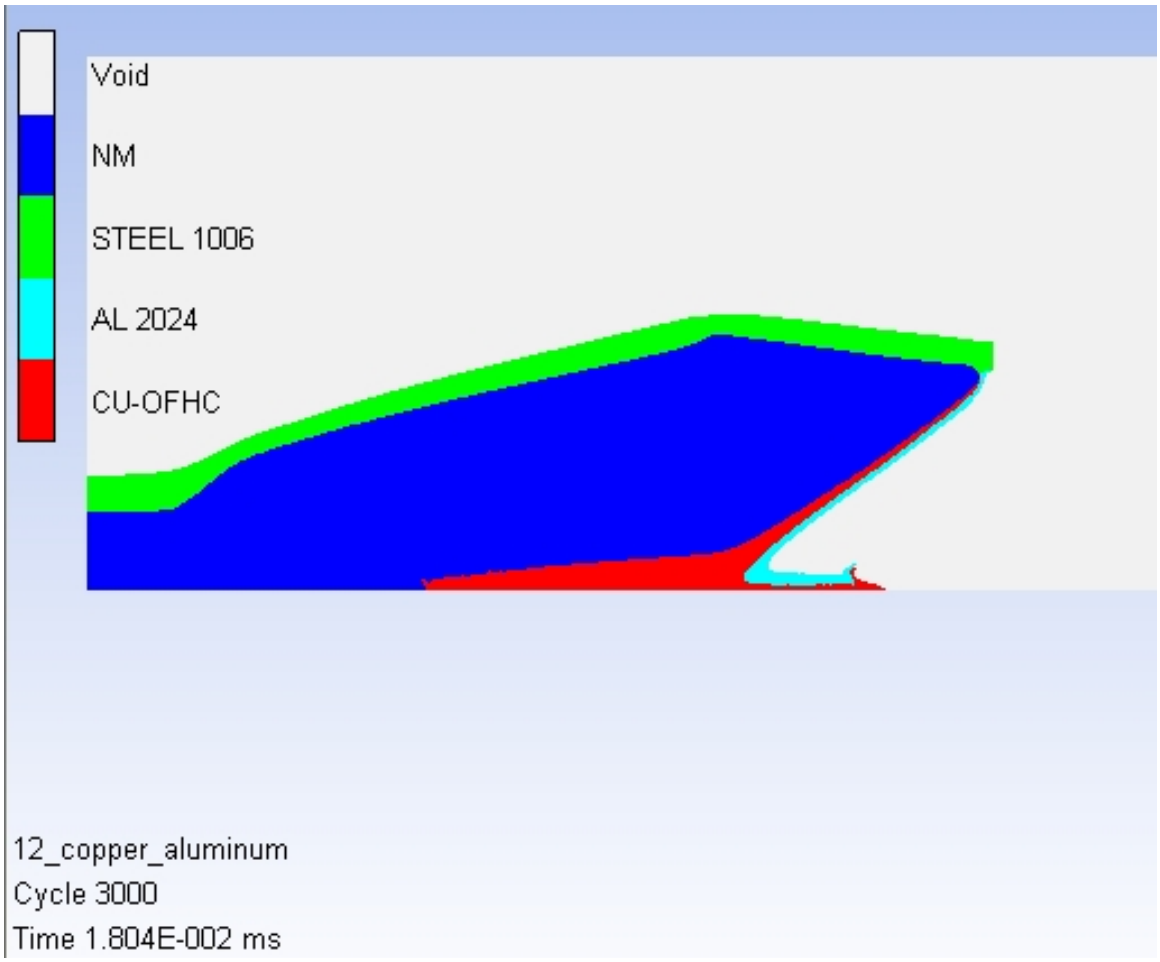

Figure 64: UIUC design: 1 mm liner thickness with basal insert after 18 μs

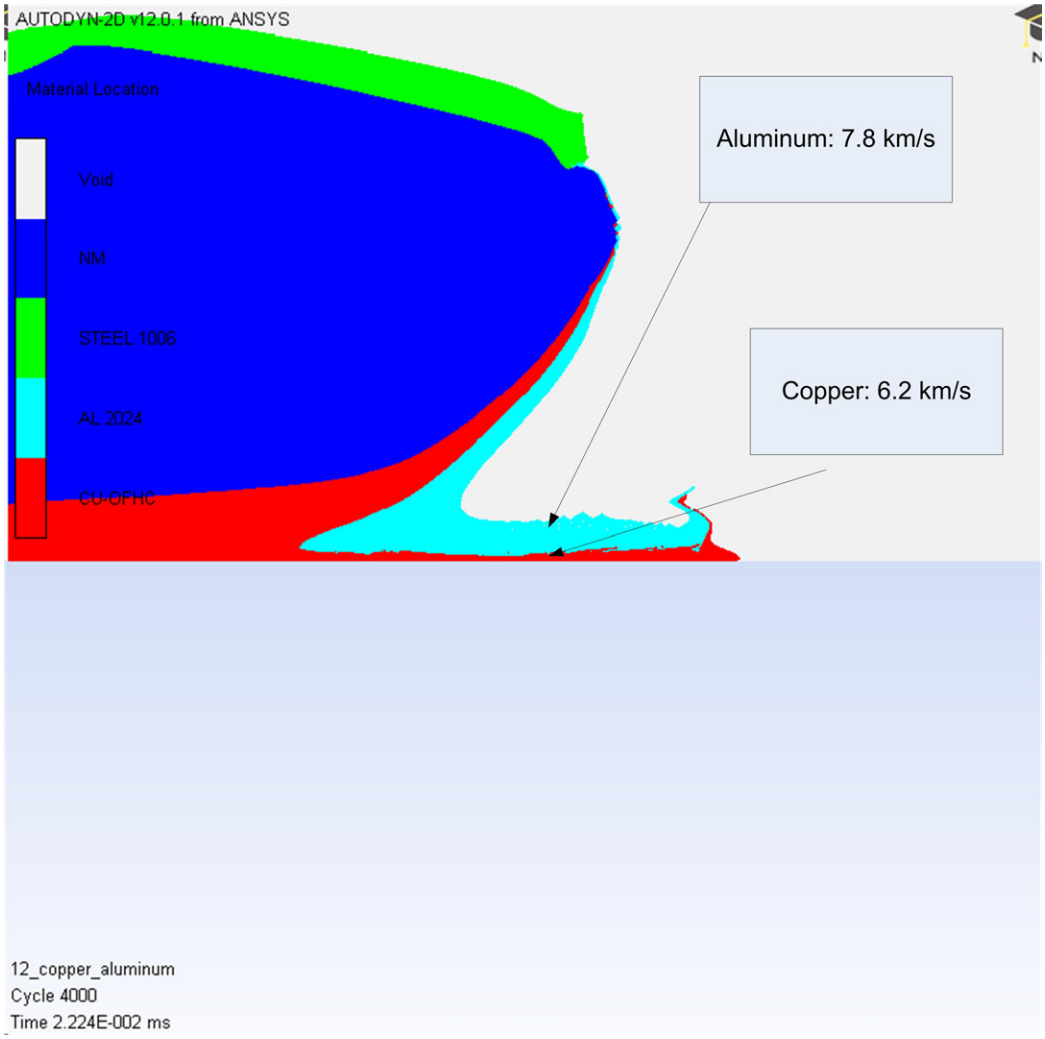

Figure 65: Velocity of aluminum and copper along the jet radius at the same x-position

VII. DISCUSSION OF RESULTS, AND NECESSARY ASSUMPTIONS AND POTENTIAL IMPLICATIONS

The results presented in the previous chapter are discussed in this chapter. If available, experimental and simulation results will be compared and deviations explained. Moreover, made assumptions and potential implication will be presented.

It is important to note that the contours of the components of each charge are not continuous because of zoning limitations (and memory allocation limitations). Therefore, resultant jets are likewise relatively rough (or coarse). Also, the boundaries between liner components are by necessity inserted as step functions, which also artificially skew computational results. In the real world of precision machine programming and machining, these problems are eliminated.

The used material properties in AUTODYN are presented in appendix A[15].

A. DRAGON

The DRAGON results provide an experimental validation forming a foundation for this research (i. e. jet formation, jet elongation, basal insert jetting, detection of the partition line). The simulation setup was used for further simulation studies as basis to support findings.

Overall, presented results for the DRAGON baseline and DRAGON base insert simulation match good with experimental results. Computations for jet velocity, jet elongation and length, and jet coherency were within acceptable tolerances and were in good agreement with experimental data. This supports the used materials (and material models) as well as the simulation setup, including zoning and other simulation softeware options.

[15]Material properties in the AUTODYN library differ partially from values provided by [Coo96, Isb05, Lyn74]. For instance, the sources provide different speed of sound and slope values that affect the calculation. Anyway, these differences might change the results slightly, but not significantly. Keep in mind this being a source of error when comparing simulation results with experiments. Presented results were reviewed by additional spot-check calculations to verify values.

Due to studies of the liner mass partition, the liner partition flowing into jet is increasing almost linearly from apex to base with a maximum of 67 %, or ca. 1 mm. Kennedy's basal insert had a thickness of 0.76 mm (about 51 % of the liner thickness), consequently zirconium and copper were jetting in this part of the liner. This is also shown by the DRAGON base insert simulation frame after 62 μs (Fig. 42).

The simulation result shows, that the insert would need to be greater than 0.76 mm to form a zirconium only jet tail. This design would contribute to the effect of zirconium within the target. Jet tail velocities were in agreement in both simulations; the formation of the jet tail showed few differences in simulation and experiment.

B. APPROACH FOR FLOW AND STAGNATION VELOCITIES

The two approaches used to estimate stagnation velocity were found to be in agreement (peak pressure motion and velocity inflection). The values of both are reproducible, but the approach using the time of peak pressure along the x-axis calculated stagnation velocity values with less variation between points. Moreover, this technique is easier to apply, as it requires only the time of peak pressures and the distance between fixed gauges. Additionally, the search for the inflection point is less accurate (q. v. the following discussion of the flow velocity), and this technique can be arduous with increasing number of gauge points.

The two approaches used to estimate flow velocity produced very different findings. Results obtained for the flow velocity with inflection point method showed that the absolute velocity at the inflection point is not consistent with PER theory. The estimated jet velocity, as sum of flow and stagnation velocity, was in a range of 1-1.4 km/s (for copper) lower than the independently measured jet velocity. Further, the flow velocity did not respond in an expected way on the variation of liner angles. Therefore this method is not applicable to estimate the flow velocity and it should also not be used to estimate the stagnation velocity by inflection point.

An additional attempt to check, if the flow velocity is reached at the time of maximal pressure in moving gauges, showed that this would over-predict flow velocity values by 1-2 km/s. Accordingly, the flow velocity is reached at a time, after the inflection point but before the peak pressure in the moving gauges.

Calculations of flow velocity with the second method showed an increasing flow velocity with decreasing liner angle. The values did meet expected values and were in agreement with results from Harrison and Chanteret. This result points out, that the coherency criterion, proposed by Harrison, is valid for conical shaped charges in this research. At least, simulation and experimental results for copper and nickel jets were consistent with this theory. Other researchers showed, that the criterion is also applicable for other materials, except for aluminum.

The process to reach the flow velocity can be explained as follows. The high pressure stagnation region moves behind the collision point with v_s in the direction of detonation, and continues to exert a force on the material flow in both directions, i. e. forward jet flow and backward slug flow. At the onset of collapse material partitions, the pressure stagnation region encounters first with the material partitions. The final flow velocity occurs at the point where the high pressure region catches up with the collision.

In general, the established values have been found to be consistent with theory, as the stagnation pressure increase with decreasing angle. The values have been validated with calculations, looking at the conservation of mass and momentum and at the Hugoniot.

This is the first successful approach to estimate stagnation and flow velocities from hydrocode simulations without applying geometrical relationships or calculating liner collapse angles. The basis for this technique is the vector triangle $v_j = v_s + v_f$ and knowledge about the liner collapse process.

C. EFFECT OF FLOW VELOCITY AND PRESSURE ON JET COHERENCY

Results from experiments conducted by [Cha92], [Har81] and others have shown, that the limit for coherent jets equates to the Harrison criteria. Also, results of an approach

to estimate flow and stagnation velocities, compared to jet velocities showed that the Harrison criterion can be applied to predict the coherency of shaped charges. The flow velocity in conducted copper and nickel simulations with different liner angle α provided that the flow velocity seems to be the key factor for jet coherency, but the provided criterion by Walker, that the longitudinal sound speed is the factor for coherent jets, was also applicable. In most cases, the longitudinal sound speed does not vary much from Harrison's values. For copper, the Harrison criterion allows a flow velocity of 4846 m/s, with Walker, the flow velocity would be limited to 4807 m/s.

Analysis of densities and compression show comparable compression and density values for copper and nickel. As both have similar densities, the bulk sound speed of nickel is ca. 12 % higher than for copper. This indicates a higher maximal allowable flow velocity for coherent nickel jets and is in agreement with simulation and experimental results.

The dependence of coherent jet was also considered under the assumptions made by Murphy. Murphy's theory could not be validated at all. It is found in this case that the flow coherency limit is not affected by the shock velocity (or at least not above 1.23 times the bulk sound velocity and/or the longitudinal velocity limit prescribed by Walker).

Again, Walker's theory, that the jet velocity depends on the longitudinal sound speed was applicable. However, there is only a small difference between the Walker and Harrison guided predictions for the copper and nickel results, thus it is not possible to claim that either is absolutely correct.

D. COAXIAL ROD PENETRATION

The rod penetration study was performed to examine the effect of material arrangement in coaxial multi-material jets. The results had a major influence on the AB and ABA design and show benefits and penalties of material substitution in a coaxial bimetallic rod or shaped charge jet.

The generic findings are that a coaxial penetrator containing the denser material in the core will penetrate much better than the opposite material orientation. However, for the

case where a lower dense material is preferred in the core for other reasons, a denser sleeve will increase penetration slightly.

This is supported the following findings:

- Tungsten with its higher density penetrates more than copper (here about 50%); this is consistent with the hydrodynamic theory.
- Placing the high density material on the inside of a bimetallic rod increases the penetration depth.
- Increasing the ratio between the high and low density material increases the hole diameter, independent on the material positioning.
- Decreasing the portion of the higher density material leads to a higher weight decrease but a slow penetration decrease, if the high-density material is on the inside. [e.g. comparing a pure tungsten rod with a 3/1 tungsten/copper rod, which means, that copper is with 0.75 mm on the outside and tungsten is with 2.25 mm on the inside of the rod (core); the resulting weight reduction is 24 %, but the penetration is reduced by only 3 %]
- Increasing the portion of the high density material on the outside leads to a higher increase of mass, and a small increase of penetration depth [e.g. comparing pure copper to a copper/tungsten with ratio 3/1; mass increase of 50 % with penetration increase of 2.5 %]

As one can see, a benefit in penetration depth would be achieved, if a coaxial multi-material jet with the high-density material as core could be designed. On the other hand, the penetration diameter increases, if a low-density core is shrouded by a high-density clad. There are applications utilizing either configurations.

Note, that the amount of core material can be decreases (as long as the jet stays stable and does not bend) with low penalties of penetration performance but significantly lower jet mass. This means, that a jet from a thinner liner could perform almost as good as

heavily lined shaped charges or that a thicker liner does not increase the penetration very much. This is also consistent with hydrodynamic theory.

This result was used as major input for the AB and ABA design. The challenge was to design a shaped charge that produces a coaxial, not separating multi-material jet with a high velocity gradient.

E. AB RESULT

The obtained results from tantalum/ aluminum showed that it is possible to form a bimetallic jet with the high-density material on the inside and a low-density material on the outside. Although both materials have a big difference in their density and bulk sound speed, the jet stayed together and should have a good penetration efficiency, if the disturbances are small from the hollow jet in the front. In the vice-versa setup, it was possible to achieve a solid tantalum jet with a small amount of aluminum in the front. Both simulations performed successfully in terms of expectations.

The copper/ hafnium simulation showed almost all hafnium flowing into the jet. However, the jet started necking in a early phase which might affect the penetration performance. Overall, this second material combination, with less difference in densities, showed better jet formation then aluminum and tantalum. The effect of density differences should be reviewed in further research by simulations and experiments.

Anyway, the AB results supported design considerations and assumptions made on jet formation. Findings also pointed out to examine material behavior for ABA design, as the AB design was effective, showing that a jet of high valuable material can be formed by reduced material cost. The next paragraph describes a possible design to overcome early necking of the hafnium jet.

To reply to early necking, a second type of jet could be formed in the following configuration. Here, the first part within the partition should be copper. The height of the first material should be chosen as long as high flow velocities occur. Hafnium with c_0 = 2954 m/s (copper: c_0 = 3940 m/s), should go into the jet after the flow velocity de-

creases to $c*$ = 3633.42 m/s (Harrison criterion for hafnium) to ensure a coherent jet. To analyze the position where hafnium should be placed, would require to search for the x-position in the liner, at which the flow velocity falls below the maximum coherent flow velocity for hafnium.

F. ABA RESULT

Results from ABA studies show more challenges with a three-layered liner than designs with a two-layered liner. For instance, the liner broke in the aluminum/ tantalum simulation during the collapse process, nevertheless, it seemed to form a coherent jet afterwards; disturbances near the jet tip were caused by the early disruption and computational limitations.

In the test simulation with copper and copper[16], no disturbances (e. g. liner break) could be detected. It was noted that the estimated partition line did not match 100 % in the test simulation. Although, both copper materials were identical, different results might be an issue of the material interface in the simulation software. This should be understood as a warning that the partition interface can change in simulations, even if equal materials are used.

Although problems occurred, the ABA simulations performed better as expected. Yet, they do not provide sufficient results to design an experiment, so that additional simulations are required.

Finally, AB and ABA simulations contributed to the understanding of multi-material liner design. The intention of both designs is new, although there have been attempts for bimetallic liners in the past, as it wants to form a cost and material effective jet, especially with high-performance insert materials or laminates.

[16]The same copper was used; just two names in the simulation.

G. UIUC

To give an qualitative recommendation for the UIUC experiments, simulations with the initial UIUC design, in addition with different liner thickness, were conducted. In general, the initial UIUC design with a 1.6 mm liner showed a worse jet formation than thinner liner designs. For each case, the amount of mass and the jet tip velocity increased relatively, by decreasing the liner thickness (q. v. Tab. 11).

The variation of liner thickness lead overall to an equal or slightly higher total jet mass because the liner volume decreases less than 50 %, but the relative amount of jet mass is about the double (comparison of 1.61 mm versus 0.75 mm liner). Assuming that the change in total mass is not crucial, the thinner liner will perform at least as good as the 1.61 mm liner, considering the penetration. Since the quality of jet formation is better with a thin liner, the general recommendation for the UIUC is to use a thinner liner (about 2% of the charge diameter).

The base insert simulation with the 1 mm liner showed good material attachment and a smooth jet formation process. The result is better than a base insert simulation with the 1.6 mm liner, where aluminum separated in an early stage from the copper jet.

In general, it is recommended for the UIUC experiment that the liner thickness should be decreased to obtain a better explosive to charge mass ratio (M/C-ratio). This will result in less total liner mass and reduce material cost, without crucial penalties for the total jet mass. The jet stretching (elongation), especially at low standoff, will benefit from higher jet tip velocities leading to an increasing jet length. Note, that this can also lead to early jet breakup due to higher jet tip velocity. Therefore, experiments need to be performed because exact jet breakup can not be calculated with simulations (it is only a mathematical jet breakup).

In order to avoid disturbances and to use the full amount of insert material, the basal insert needs to be adapted to the partition interface, starting out as thin as possible and increasing to the appropriate thickness. This results in an jet area, where both materials are present along the radius, and a jet tail with solid insert material, here aluminum.

Although, the jet formation of this initial insert simulation performed well, the liner turning is affected by the a decreasing mass along the liner. Since aluminum has a much lower density than copper, it might also be beneficial to design an insert with gradually increasing insert thickness, towards the axis of symmetry, to balance the M/C-ratio. This would not change the copper-aluminum interface, but the total liner mass could be held equal, resulting in a constant explosive to inert mass ratio. Otherwise, the partition interface changes because of a large change in the liner mass towards the base.

The UIUC could only provide penetration results, so the jet formation data and velocities could not be compared with simulation results. Anyway, simulation results provide qualitative and quantitative recommendations and form a reasonable baseline for further designs.

THIS PAGE INTENTIONALLY LEFT BLANK

VIII. CONLUSIONS

It is shown in this research the possibilities of generating stable bi-material coaxial jets, potentially useful for a wide range of applications, e. g. overcoming coherent flow limitations or enhancing behind the target effects. Several bi-material designs are proposed based on examinations of the following candidate materials: aluminum, tantalum, zirconium, copper, nickel, hafnium and tungsten.

The proposed applications of this research are based on finite difference computations using the ANSYS AUTODYN code. Comparisons between experimental results from a 100 mm octol copper lined shaped charge with code prediction are reported. These comparisons include jet tip velocities, jet velocity/cumulative mass distributions, jet elongation, and the identification of specific disruptive characteristics during jet formation.

An approach for improving the geometrical input in AUTODYN with MATLAB code was established.

Furthermore, approaches for estimating flow and stagnation velocities were developed and verified with experimental results. Results have been found to be consistent with jet coherence theory provided by Harrison or Walker, however, none of both theories could be validated because both predict close maximum coherent flow velocities.

Using penetration capability as a performance objective, it is predicted that a representative material pair can replicate the performance of a baseline copper charge. In this case the second material shrouding the copper core might reduce chemical and/or electrical interactions.

Moreover, multi-material design concepts with at least two material layers within the liner were developed, discussed and tested with depicted material pairs. For example, it is shown that a bi-metallic tantalum/aluminum or inlay of tantalum in an aluminum liner can be designed to form a coaxial (or primary tantalum) jet that has superior penetration capability relative to copper at small material cost penalty. It is also possible to form a copper/hafnium combination, where hafnium is the primary interest for penetration.

A simulation study for a running UIUC experiment was conducted. It has been shown that a thinner liner should be used to increase the explosive to liner mass ratio. It was estimated that the jet velocity, jet stretching, and thus penetration will benefit.

Relevant experimental data, material response models, and computational approaches and set ups are reported.

IX. RECOMMENDATIONS

There are three major research fields that should be part of further investigations. First, several experiments have to be conducted. The designed and simulated multi-material shaped charges are based on bi-metallic experiments, however, none of these designs was focus of previous experimental setups. Especially the material attachment of multi-material designs should be focused on. Penetration simulations could not be conducted due to time restrictions of this work. In order to compare with experimental results, penetration simulations should be part of further investigation directed towards multi-material shaped charge studies.

In all simulations the charge diameter was 25 or 100 mm with constant liner thickness. Additional simulations with biconic liners or different liner thickness should be run to investigate the effect on mass partition and jet formation.

Also, impact experiments with bi-material rods should be conducted to validate effects on penetration.

Second, the coherency criteria provided by Walker and Harrison need to be investigated in more detail with other materials than copper and nickel, where the maximum coherent flow velocities are less close. This might validate one theory and add information for approaches to exceed current maximum flow coherency limitations.

Finally, results from stagnation and flow velocities show that the flow velocity is the key factor for jet coherency. Higher coherent jet velocities should be reached if the stagnation velocity can be increased without affecting the flow velocity. Also, penetration performance would benefit from this attempt.

THIS PAGE INTENTIONALLY LEFT BLANK

APPENDIX A: MATERIAL PROPERTIES

Material Name	**CU-OFHC**	**Nickel**	**Zirconium**
Equation of State	Shock	Shock	Shock
Reference density (g/cm3)	8.93	8.874	6.505
Gruneisen coefficient	2.02	1.93	1.09
Parameter C1 (m/s)	$3.94\text{x}10^3$	$4.602\text{x}10^3$	$3.757\text{x}10^3$
Parameter S1	1.489	1.437	1.018
Parameter Quadratic S2 (s/m)	0.0	0.0	0.0
Relative volume, VE/V0	0.0	0.0	0.0
Relative volume, VB/V0	0.0	0.0	0.0
Parameter C2 (m/s)	0.0	0.0	0.0
Parameter S2	0.0	0.0	0.0
Reference Temperature (K)	$3.0\text{x}10^2$	$3.0\text{x}10^2$	0.0
Specific Heat (J/kgK)	$3.83\text{x}10^2$	$4.01\text{x}10^2$	0.0
Thermal Conductivity (J/mKs)	0.0	0.0	0.0
Strength	None	None	None
Failure	None	None	None
Erosion	None	None	None
Material Cutoffs	-	-	-
Maximum Expansion	$1.0\text{x}10^-1$	$1.0\text{x}10^-1$	$1.0\text{x}10^-1$
Minimum Density Factor	$1.0\text{x}10^-6$	$1.0\text{x}10^{-6}$	$1.0\text{x}10^{-6}$
Minimum Density Factor (SPH)	$2.0\text{x}10^{-1}$	$2.0\text{x}10^{-1}$	$2.0\text{x}10^{-1}$
Maximum Density Factor (SPH)	3.0	3.0	3.0
Minimum Soundspeed (m/s)	$1.0\text{x}10^{-6}$	$1.0\text{x}10^{-6}$	$1.0\text{x}10^{-6}$
Maximum Soundspeed (m/s)	$1.01\text{x}10^{20}$	$1.01\text{x}10^{20}$	$1.01\text{x}10^{20}$
Maximum Temperature (K)	$1.01\text{x}10^{20}$	$1.01\text{x}10^{20}$	$1.01\text{x}10^{20}$

Table 12: Liner Materials in AUTODYN

Material Name	**Tantalum**	**Aluminum 2024**	**Hafnium**
Equation of State	Shock	Shock	Shock
Reference density (g/cm3)	16.654	2.785	12.885
Gruneisen coefficient	1.6	2	0.98
Parameter C1 (m/s)	3.414x10^3	5.328x10^3	2.954x10^3
Parameter S1	1.201	1.338	1.121
Parameter Quadratic S2 (s/m)	0.0	0.0	0.0
Relative volume, VE/V0	0.0	0.0	0.0
Relative volume, VB/V0	0.0	0.0	0.0
Parameter C2 (m/s)	0.0	0.0	0.0
Parameter S2	0.0	0.0	0.0
Reference Temperature (K)	3.0x10^2	00.	0.0
Specific Heat (J/kgK)	3.83x10^2	0.0	0.0
Thermal Conductivity (J/mKs)	0.0	0.0	0.0
Strength	None	None	None
Failure	None	None	None
Erosion	None	None	None
Material Cutoffs	-	-	-
Maximum Expansion	1.0x10^-1	1.0x10^-1	1.0x10^-1
Minimum Density Factor	1.0x10^-6	1.0x10^{-6}	1.0x10^{-6}
Minimum Density Factor (SPH)	2.0x10^{-1}	2.0x10^{-1}	2.0x10^{-1}
Maximum Density Factor (SPH)	3.0	3.0	3.0
Minimum Soundspeed (m/s)	1.0x10^{-6}	1.0x10^{-6}	1.0x10^{-6}
Maximum Soundspeed (m/s)	1.01x10^{20}	1.01x10^{20}	1.01x10^{20}
Maximum Temperature (K)	1.01x10^{20}	1.01x10^{20}	1.01x10^{20}

Table 13: Liner Materials in AUTODYN (continuation)

Material Name	**LX14**	**Nitromethane**	**Octol 70/30**
Equation of State	JWL	JWL	JWL
Reference Density (g/cm^3)	1.835	1.128	1.804
Parameter A (kPa)	8.261x10^8	2.0925x10^8	7.1395x10^8
Parameter B (kPa)	1.724x10^7	5.689x10^6	1.289x10^7
Parameter R1	4.55	4.40	4.50
Parameter R2	1.32	1.2	1.2
Parameter W	3.8x10^{-1}	3.0x10^{-1}	3.8x10^{-1}
C-J Detonation Velocity (m/s)	8,800	6,280	8,330
C-J Energy/ Volume (kJ/m^3)	1.02x10^7	5.1x10^6	9.18x10^6
C-J-Pressure (kPa)	3.7x10^7	1.25x10^7	3.20x10^7
Burn on Compression Fraction	0	0	0
Pre-Burn Bulk Modulus (kPa)	0	0	0
Adiabatic Constant (kPa)	0	0	0
Auto convert to Ideal Gas	Yes	Yes	Yes
Strenght	None	None	None
Failure	None	None	None
Erosion	None	None	None
Material Cutoffs	-	-	-
Maximum Expansion	1.0x10^{-1}	1.0x10^{-1}	1.0x10^{-1}
Minimum Density Factor	1.0x10^{-6}	1.0x10^{-6}	1.0x10^{-6}
Minimum Density Factor (SPH)	2.0x10^{-1}	2.0x10^{-1}	2.0x10^{-1}
Maximum Density Factor (SPH)	3.0	3.0	3.0
Minimum Soundspeed (m/s)	1.0x10^{-6}	1.0x10^{-6}	1.0x10^{-6}
Maximum Soundspeed (m/s)	1.0x10^{20}	1.0x10^{20}	1.0x10^{20}
Maximum Temperature (K)	1.01x10^{20}	1.01x10^{20}1.01x10^{20}	

Table 14: Explosives Properties in AUTODYN

Material Name	**AL2024T351**	**Steel 1006**
Equation of State	Shock	Shock
Reference density (g/cm3)	2.785	7.896
Gruneisen coefficient	2.00	2.17
Parameter C1 (m/s)	5.328x10^3	4.569x10^3
Parameter S1	1.338	1.49
Parameter Quadratic S2 (s/m)	0.0	0.0
Relative volume, VE/V0	0.0	0.0
Relative volume, VB/V0	0.0	0.0
Parameter C2 (m/s)	0.0	0.0
Parameter S2	0.0	0.0
Reference Temperature (K)	3.0x10^2	3.0x10^2
Specific Heat (J/kgK)	8.75x10^2	4.51x10^2
Thermal Conductivity (J/mKs)	0.0	0.0
Strength	Johnson Cook	Johnson Cook
Shear Modulus (kPa)	2.76x10^7	8.18x10^7
Yield Stress (kPa)	2.65x10^5	3.5x10^5
Hardening Constant (kPa)	4.26x10^5	2.75x10^5
Hardening Exponent	3.4x10^{-1}	3.6x10^{-1}
Strain Rate Constant	1.5x10^{-2}	2.2x10^{-2}
Thermal Softening Exponent	1.00	1.00
Melting Temperature (K)	7.75x10^2	1.811x10^3
Failure	None	None
Erosion	None	None
Material Cutoffs	-	-
Maximum Expansion	1.0x10^-1	1.0x10^-1
Minimum Density Factor	1.0x10^-6	1.0x10^{-6}
Minimum Density Factor (SPH)	2.0x10^{-1}	2.0x10^{-1}
Maximum Density Factor (SPH)	3.0	3.0
Minimum Soundspeed (m/s)	1.0x10^{-6}	1.0x10^{-6}
Maximum Soundspeed (m/s)	1.01x10^{20}	1.01x10^{20}
Maximum Temperature (K)	1.01x10^{20}	1.01x10^{20}

Table 15: Confinement Materials in AUTODYN

Material Name	**4340 Steel**
Equation of State	Linear
Reference Density (g/cm^3)	7.83
Bulk Modulus (kPa)	1.59x10^8
Reference Temperature (K)	3.0x10^2
Specific Heat (J/kgK)	4.77x10^2
Thermal Conductivity (J/mKs)	0.0
Strength	Johnson Cook
Shear Modulus (kPa)	8.18x10^7
Yield Stress (kPa)	7.92x10^5
Hardening Constant (kPa)	5.1x10^5
Hardening Exponent	2.6x10^{-1}
Strain Rate Constant	1.4x10^{-2}
Thermal Softening Exponent	1.03
Melting Temperature (K)	1.793x10^3
Ref. Strain Rate ($/s$)	1.0
Strain Rate Correction	1st Order
Failure	None
Erosion	None
Material Cutoffs	-
Maximum Expansion	1.0x10^{-1}
Minimum Density Factor	1.0x10^{-4}
Minimum Density Factor (SPH)	2.x10^{-1}
Maximum Density Factor (SPH)	3.0
Minimum Soundspeed (m/s)	1.0x10^{-6}
Maximum Soundspeed (m/s)	1.01x10^{20}
Maximum Temperature (K)	1.01x10^{20}

Table 16: Target Properties

THIS PAGE INTENTIONALLY LEFT BLANK

APPENDIX B: SIMULATION SETUP WITH AUTODYN

Key features of the menu-driven setup and specific details that have to be considered for setting up an axi-symmetric shaped charge and penetration computations are discussed below. It is important to note that it is only necessary to construct half of the problem geometry because of the cylindrical symmetry.

As mentioned above, the user has to consider different techniques to improve the computational time. For relatively simple problems, the simulations run fairly fast, but for more detailed and realistic problems, which need a higher accuracy, the computations can run for several weeks or even months. Accordingly, techniques like graded, i.e. variable, zoning, removal of used materials, and using subgrids were integrated into the design of the simulation layouts, resulting in the reduction of the total run time of typical simulation setups in this research.

A. GENERAL SETUP AND BOUNDARY CONDITIONS

The ANSYS AUTODYN material library contains a good selection with several strength models of materials, including explosive materials. The choice of materials is the first step in setting up a simulation. If the internal material library does not contain the needed material, the user can add manually defined materials to the library. Used materials are shown in appendix A.

Next, boundary conditions have to be initialized. Transmit boundaries are used on the left and upper side of the used grid (Fig. 66). They let materials transmit which are perpendicular to the surface; however, the bouncing of angular material is not significant for the results and thus unattended. An outflow boundary is setup on the right side of the grid for purposes of allowing unhindered flow-out of the jet. An array of fixed gauges is positioned along this boundary to sense the velocities of the jet and the respective radial dependence (q.v. Fig. 120). The centerline of the problem is the axis of symmetry. The

outflow boundary is selected to consist of the same material as the void in the computational grid.

In these simulations void space instead of air is used due to:

- The outflow velocities of jet and air can not be differentiated (main reason)
- Less memory allocation
- Small fractions of compressed air in a cell resulting from detonation product gas expansion can cause a reduction in time setup.

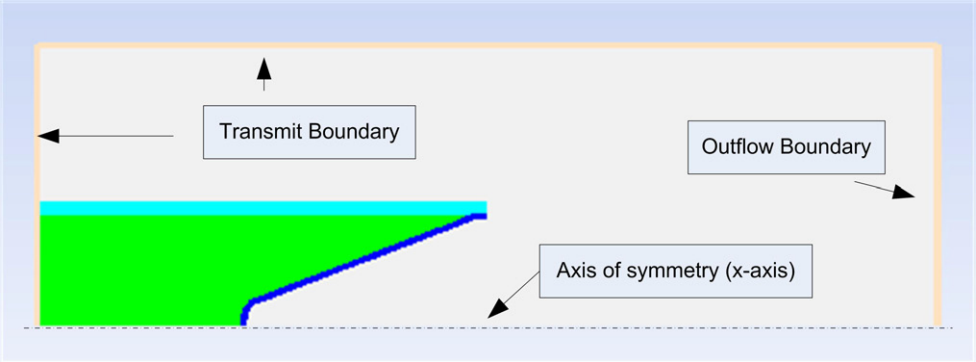

Figure 66: Boundary conditions of the charge grid

B. SUBGRID

One can model the problem in one huge grid, which contains the shaped charge and the target. This approach results in a gigantic number of cells and a relatively long computation time. An optimized option is to divide the grid in several subgrids, so that the simulation starts with no more than one subgrid. The first subgrid is called the ”charge” subgrid, because it represents the detonation and jet formation process. The next subgrid, which is called ”target” subgrid, is then joined to the charge subgrid (v.q. Fig. 67). To enable a successful joining, the adjacent subgrids need to have exactly the same zoning. To employ the advantage, the simulation is halted before the jet reaches the right end of the first subgrid. Then, the next subgrid is joined to the first one, gauges are placed, boundary conditions are allocated, and the simulation resumed.

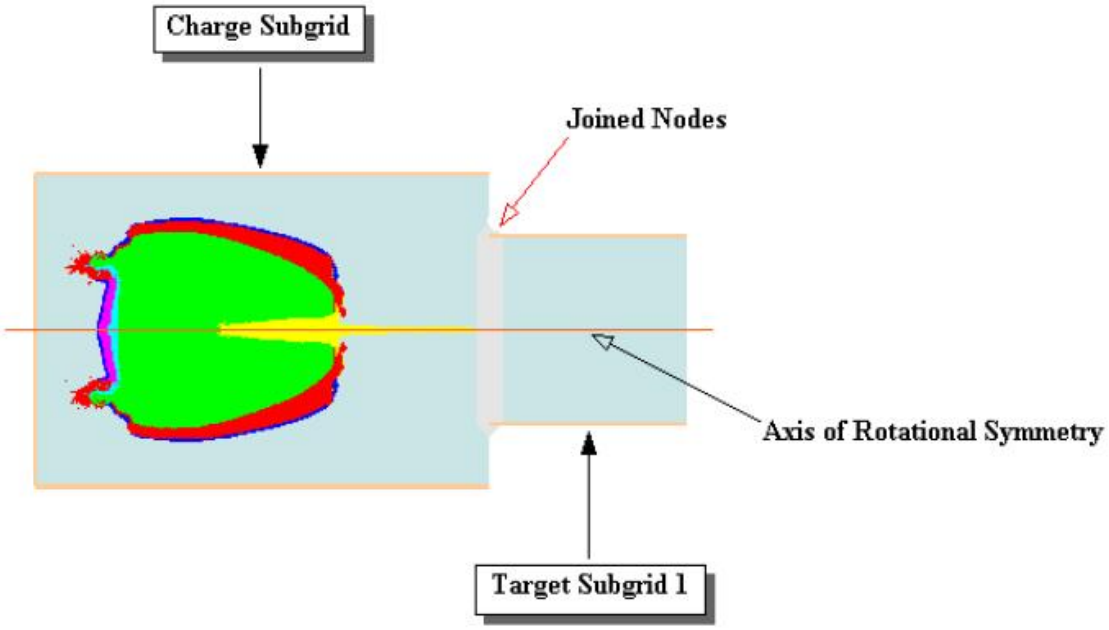

Figure 67: Example for subgrid joining (from Doung)

C. ZONING

The main step in the simulation setup is the geometrical definition of the part(s). The initial mesh is defined as a rectilinear mesh in an I and J range. The number of cells depends, first, on the dimensions of the grid or subgrid, and second, on the cells per mm. It is in common that a high resolution and a huge grid lead to high number of cells and consequently to a very long computational time. There is also a hardware boundary that limits the number of cells by the memory. To avoid these problems and to sustain the required accuracy graded, i.e. variable, zoning is used. It combines the advantage of fine zoning and a high accuracy in the area of interest and coarse zoning in less important regions. Graded zoning can be applied for I and/ or J-direction and the user can choose whether it is an upper, middle, or lower grade zoning. In the chosen area the user then sets the size and number of fine cells for the specific direction. In the shaped charge simulation, since axial symmetry is used, a lower zoning is applied. The size and number of the cells is

dependent on the overall dimensions of the setup. An example of a zoning plan is illustrated in Figure 68 and in the paragraph below.

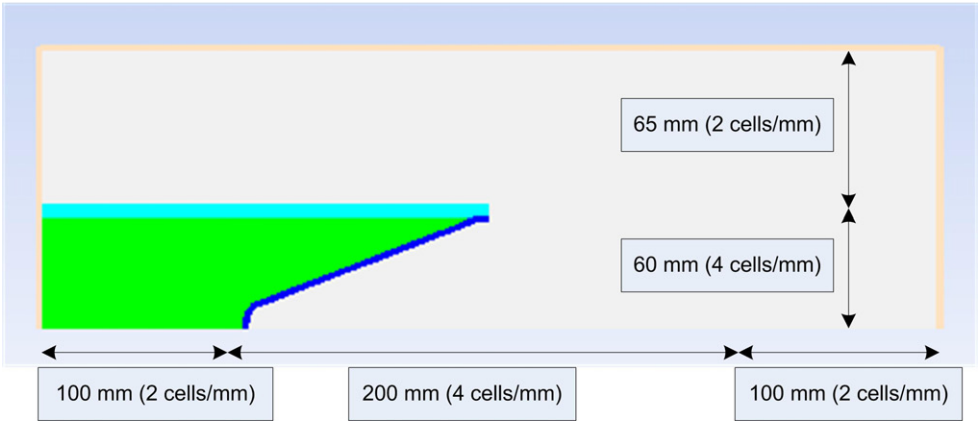

Figure 68: Example for graded zoning of a 100mm charge

Example Illustration of zoning architecture for a 100 mm charge shown in Fig. 68 with dimensions of the charge subgrid: 400 mm $\times$ 125 mm. The zones per mm in the I and J dimensions are varied as shown.
Zoning with 4 cells/mm results in a number of cells:

$$(400\ mm \times 4) \times (125\ mm \times 4) = 800,000 \text{ cells}$$

$$(200\ mm \times 4 + 100\ mm \times 2 \times 2) \times (60\ mm \times 4 + 65\ mm \times 2) = 444,000 \text{ cells}$$

The graded zoning significantly reduces memory while minimizing the consequences on quantitative resolution. For example, the percentage decrease between a constant 4 cells/mm zoning and the graded zoning shown in Figure 68 is 45 % percent.

D. FILLING

Initially, the entire mesh is filled as void. The geometry of the shaped charge has to be translated in x-y spatial coordinates and added to the simulation. This step is referred to as Filling. The process of filling is started by using the Fill command. The user can

utilize Quad, Rectangle and Ellipse Fill commands to shape the final geometry. The fill commands also include the filling with a material, velocity, or initial condition that can be also a previously chosen velocity. The definition of velocities as initial conditions increases the flexibility of the simulation.

E. DETONATION

After filling the initial mesh with different material of different shape, the detonation point needs to be set. For the problems of interest in this investigation, direct point initiation is used. The initiation time is set to 0.00 ms in all simulations. The point is located on the left side of the explosive filler at the longitudinal axis (x-axis). Other options, e.g. time delays or the type of the path, are optional and not used here.

F. GAUGES

Using gauges is essential for the successful simulation study. If no gauges are applied, the simulation would mainly serve the purpose of visual results. In order to estimate material displacements, velocities, changes in density, momentum, internal and kinetic energy, fixed and moving gauges are placed at positions of interest. Fixed gauges are used to monitor changes in material flowing pass them and moving gauges are used to track the changes in extrinsic material characteristics and respective displacement with respect to time.

For instance, moving gauges are used to study the mass partitioning during the liner collapse process. Further details on mass partitioning are provided in section V.C. The monitored gauge data is available for analysis or post processing in the History tab. Selected information can also be plotted therein. For further analyzing methods, it is possible to export the gauge data into a UHS, HTML, or CVS file and to use it with other software tools[17].

[17]This feature is important for simulations that have to be halted for any purpose and then resumed on a computer cluster. The cluster only starts simulations from the zero-cycle file, consequently the history has to be merged after the simulation

G. REMOVAL OF USED MATERIAL

During the simulation it is possible to remove used material. This option is also used to decrease the computation time and to avoid measurement errors of reflected material which do not pass the transmit boundary. To identify the point in time to remove material, without affecting the overall result, the simulation has to be halted and the plot of the kinetic energy (KE) of the liner material examined. Once the KE of the liner material plateaus (reaches or approaches an asymptote) other materials in the problem can be removed. At this point the liner material has conserved the maximum energy it could gain from the detonation. This reduces memory allocation required for completing a computation. The other materials can be removed from the materials list; color assignments can change with material removal.

H. SPECIFICATIONS FOR COUPLED JET FORMATION AND PENETRATION STUDIES

The standoff[18] distance is used quite often for the distance between the shaped charge and the right end of the space. Figure 69 shows a general layout with the target in the same grid. But in most cases a target is added at a multiple charge diameter distance to the warhead as a new subgrid as mentioned in apendix B.B. Then the simulation layout is comparable to Fig. 67, which contains transmit boundaries on the upper side of the subgrid.

In order to avoid reflections of the traveling waves inside of the target material, which occur from the right side, an outflow boundary should be applied to the right side of every simulation.

There a two possible approaches. (i) If the target is fully displayed within one (target)-subgrid, then the target should not be placed against any boundary in order to avoid destructive reflections unless it is very long. (ii) If the target is very long, one might model it with several subgrids. In this case the material needs to be placed against the outflow boundary on the right side between the target subgrids. It is important to mention

[18] Standoff refers to the distance of the liner base form the target.

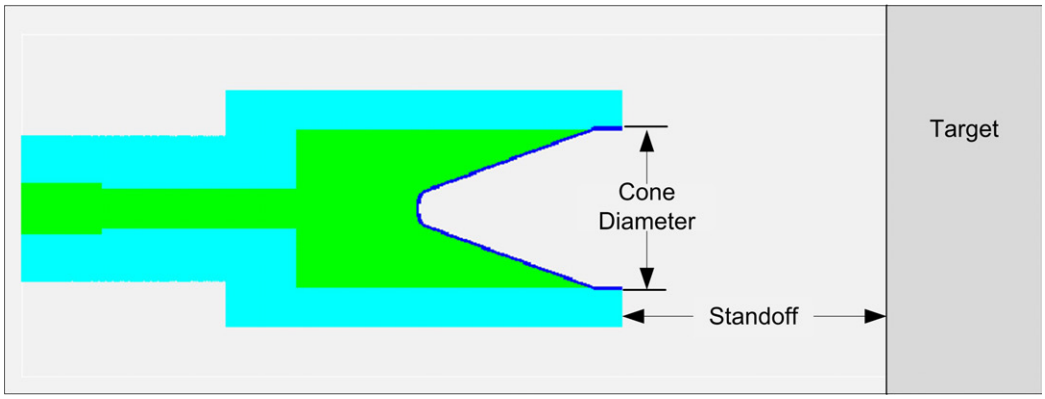

Figure 69: Standoff from the target

that the outflow boundary should contain the target material as preferred material. In the ”last” target subgrid one should let enough space and proceed as in approach (i). The target material has to be filled until the right side of the grid without a gap and the same material has to be applied for the boundary condition on that side. Before joining a further subgrid, the boundary condition has to be cleared, the next subgrid joined and the same boundary condition applied to the ”new” right end.

I. CONTROLS

In the controls tab the runtime parameters are set for the simulation. These are the wrap-up criteria:

- cycle limit (maximum number of cycles)
- time limit (maximum runtime)
- energy fraction (percentage of maximum energy error; default 5 %)
- energy reference cycle (start cycle to apply the energy fraction to the calculation)

The cycle and time limit as well as the energy reference cycle are set to high values (e.g. 100,000) to assure a uninterrupted simulation. Next, the time-step options are set. To ensure a continual run of the simulation, the minimum time-step should be reduced to

1.0×10^{-20} ms, because during the simulation particles with varying sized will be produced. The maximum time-step of 1.0×10^{20} ms needs no adjustment.

The transport option relates to the transport of mass, momentum and energy from cell to cell. The following change is only related to the energy transport. One can choose between the conservation of total energy (kinetic + internal energy) or internal energy during the transport. Using the ”internal energy” transport in Euler shaped charge calculations achieves better results, where the detonation products escape into void at high speed (high kinetic energy). This configuration leads to a more precisely determination of the internal energy in a cell instead of the default setting ”total energy”.

During the simulation very small particles can result with unrealistically high velocities and therefore produce calculation errors. Setting the maximum velocity cutoff to 15000 m/s in the global velocity cutoff limits the problem.

J. OUTPUT

In the output tab the save options need to be set up to be able to restart a simulation from a specific point or to create an animation in the post-processing. It can be chosen between save by cycle or by time. The saving by cycle is more appropriate for shaped charges, the small time-steps result in an increase of cycles and in more detailed save points. The saving by time results in decreasing the number of saved points, and as a consequence reduces quantitative detail especially during the penetration process.

The monitoring of x and y position as well as the temperature are turned off for the history, by default. This xy-function is useful to monitor the position in space of moving gauges and to gain date for radial radial velocities. The monitoring of temperatures might be useful for study of thermal expansion.

K. OTHER SETTINGS

First, all simulations need to be setup on a PC. Then, the computations can be conducted either on a PC or on a cluster. In this research, the main advantage using a cluster is

not the higher performance but the outsourcing of processes from the workstation. Parallel computing can not be applied to AUTODYN-2D problems and does not offer additional performance enhancement. Conducting the computations on the workstation instead of the cluster, the display frequency refreshing should be increased to at least 50 cycles in order to reduce slow-down occurrences.

Time-step problems can also occur as a result of the diffusion of small packets of low density detonation products. In this case, it is found that the material density cutoff should be set to 1.0×10^{-6} instead of the default 1.0×10^{-4}. This option can be changed in the materials tab with the modify option (Cutoffs $\rightarrow$ Minimum Density Factor).

THIS PAGE INTENTIONALLY LEFT BLANK

APPENDIX C: MECHANICAL DRAWINGS

A. 25 MM MECHANICAL DRAWING

The 25 mm simulations are based on the following Figures 70 (units: mm) and 71 (units: in). The 0.500 in part (here: bottom Fig. 71) was not implemented into the simulation, because it is not relevant for the shaped charge analysis.

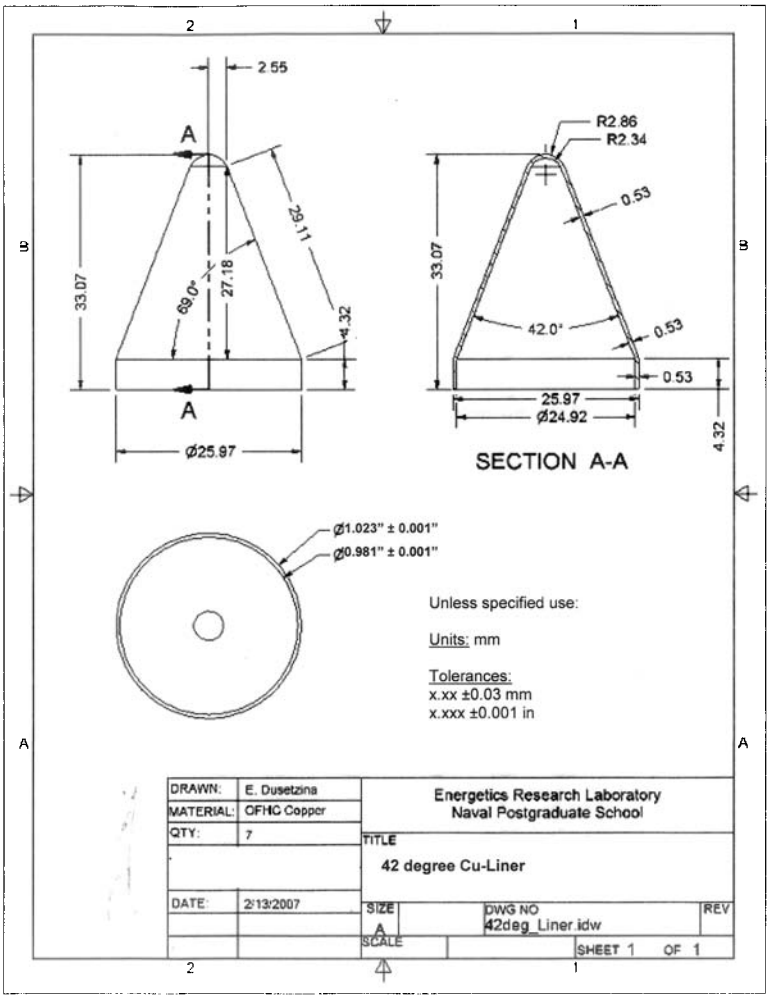

Figure 70: Liner (Copper)

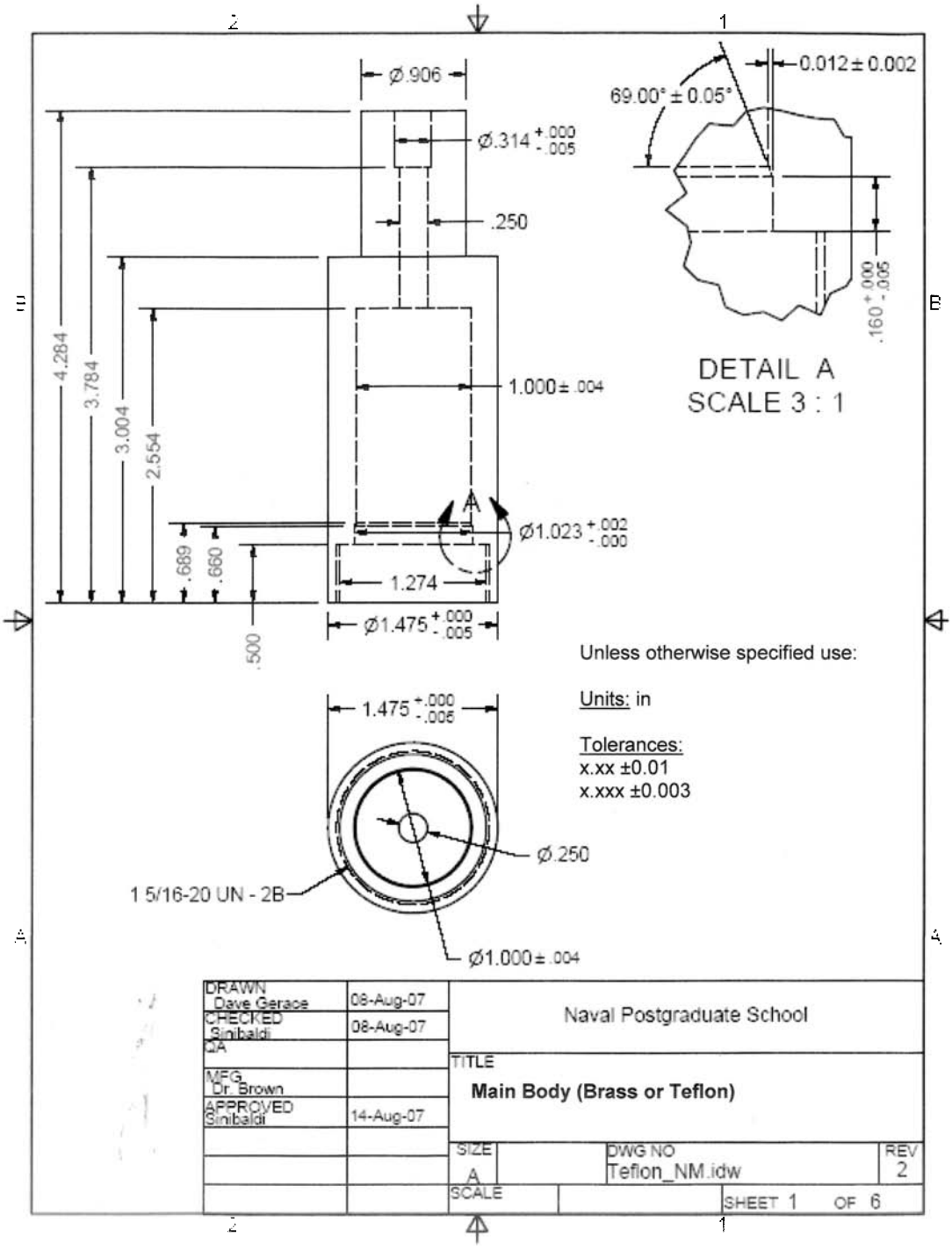

Figure 71: Main Body (PTFE)

B. DRAGON

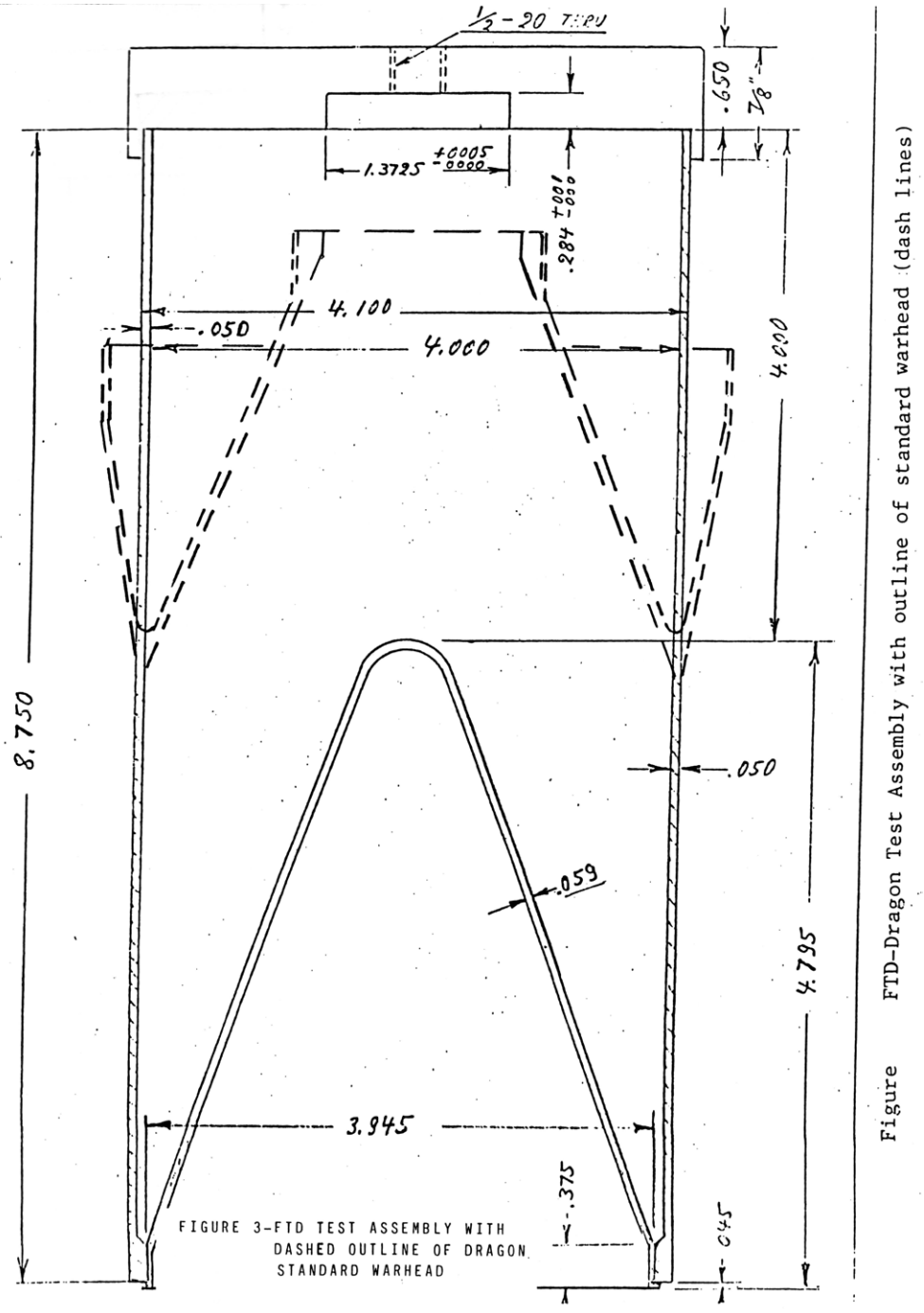

Figure FTD-Dragon Test Assembly with outline of standard warhead (dash lines)

Figure 72: DRAGON baseline geometrical setup (original from report; units: in) [KB81]

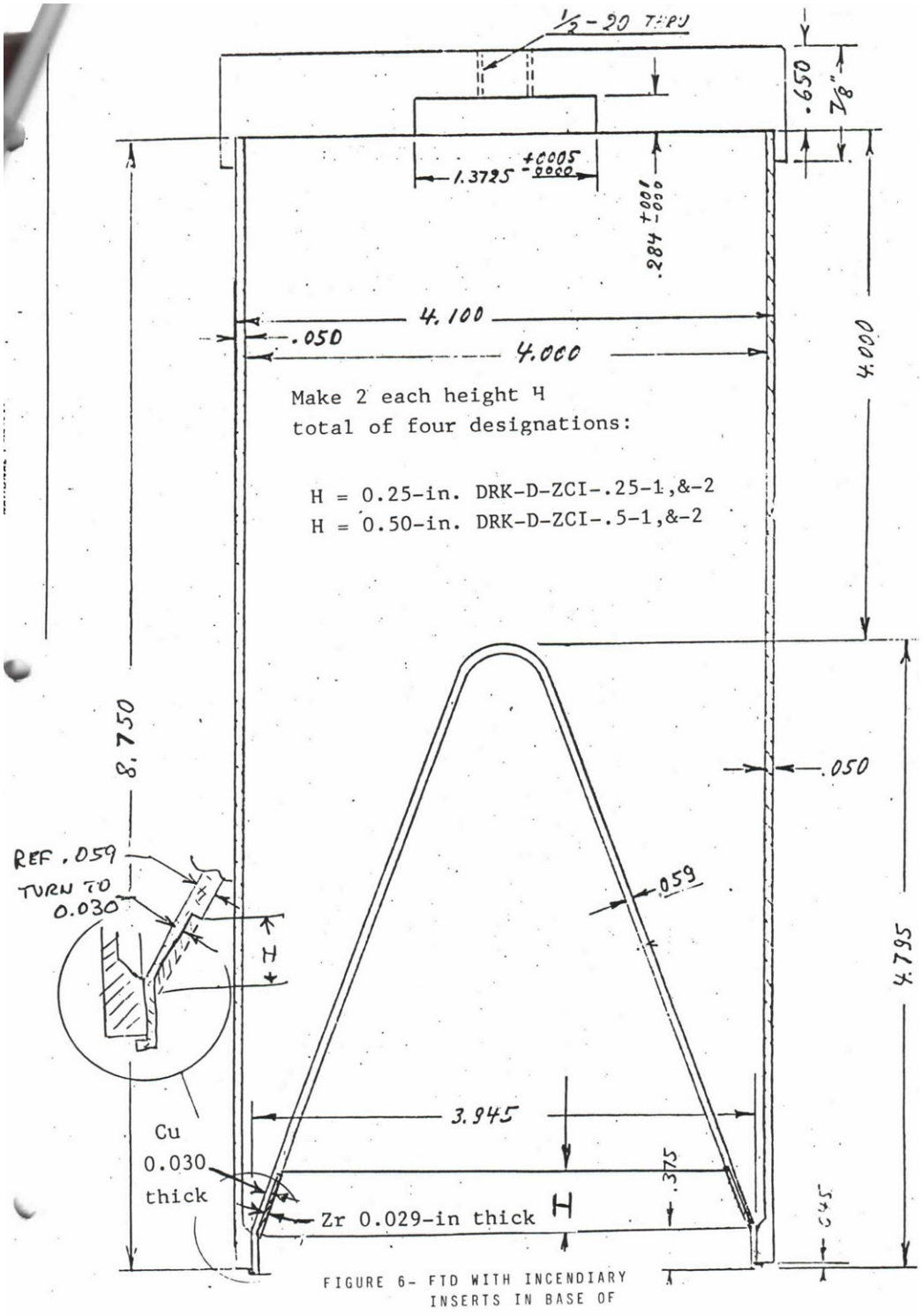

Figure 73: DRAGON base insert. H denoted as the insert height (units: in) [KB81]

C. UIUC

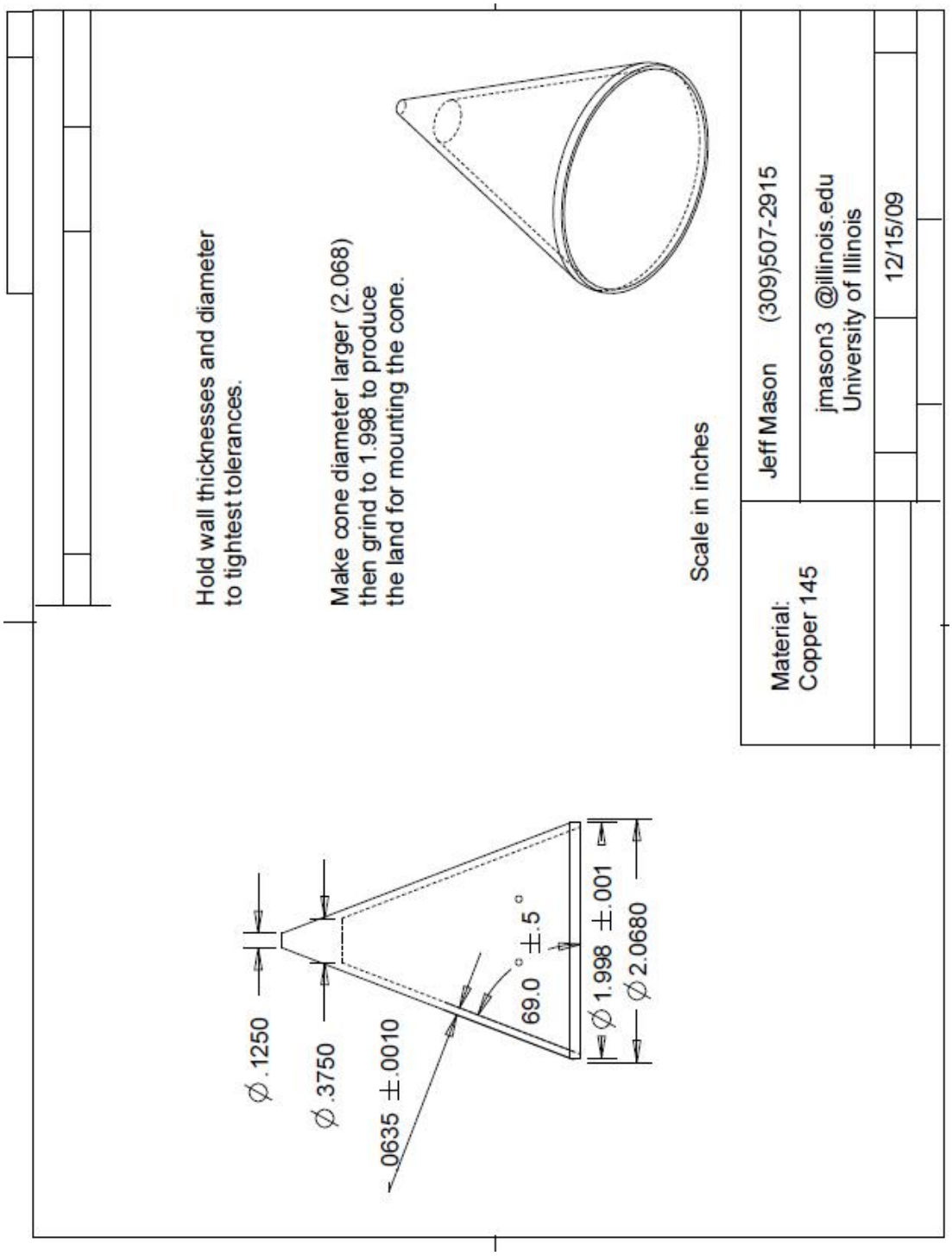

Figure 74: UIUC solid copper liner with 1.61 mm liner thickness [Mas10]

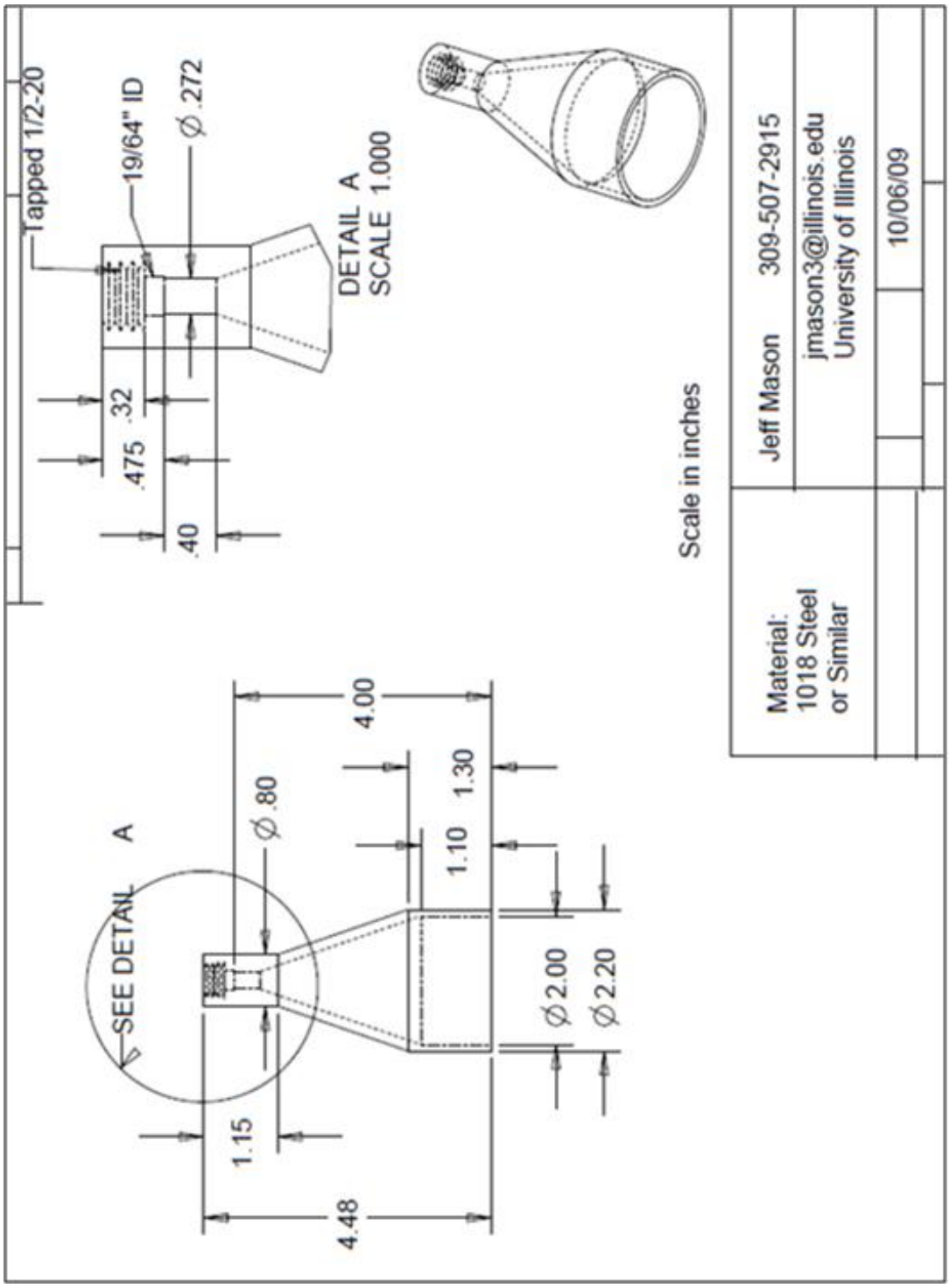

Figure 75: UIUC shaped charge body [Mas10]

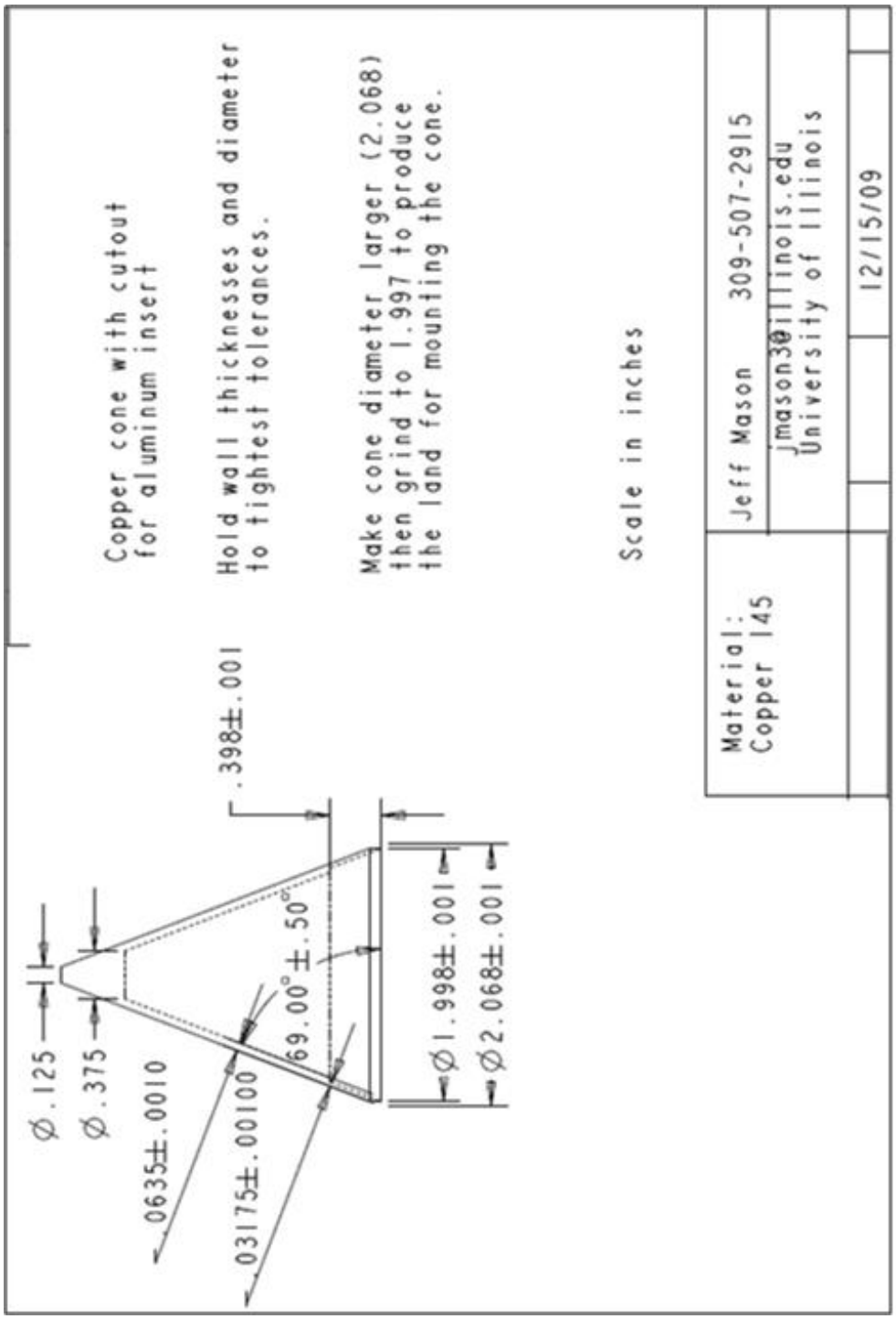

Figure 76: UIUC liner design for aluminum insert [Mas10]

THIS PAGE INTENTIONALLY LEFT BLANK

APPENDIX D: RADIOGRAPHS KENNEDY

Figure 77: FTD 13 Front [KB81]

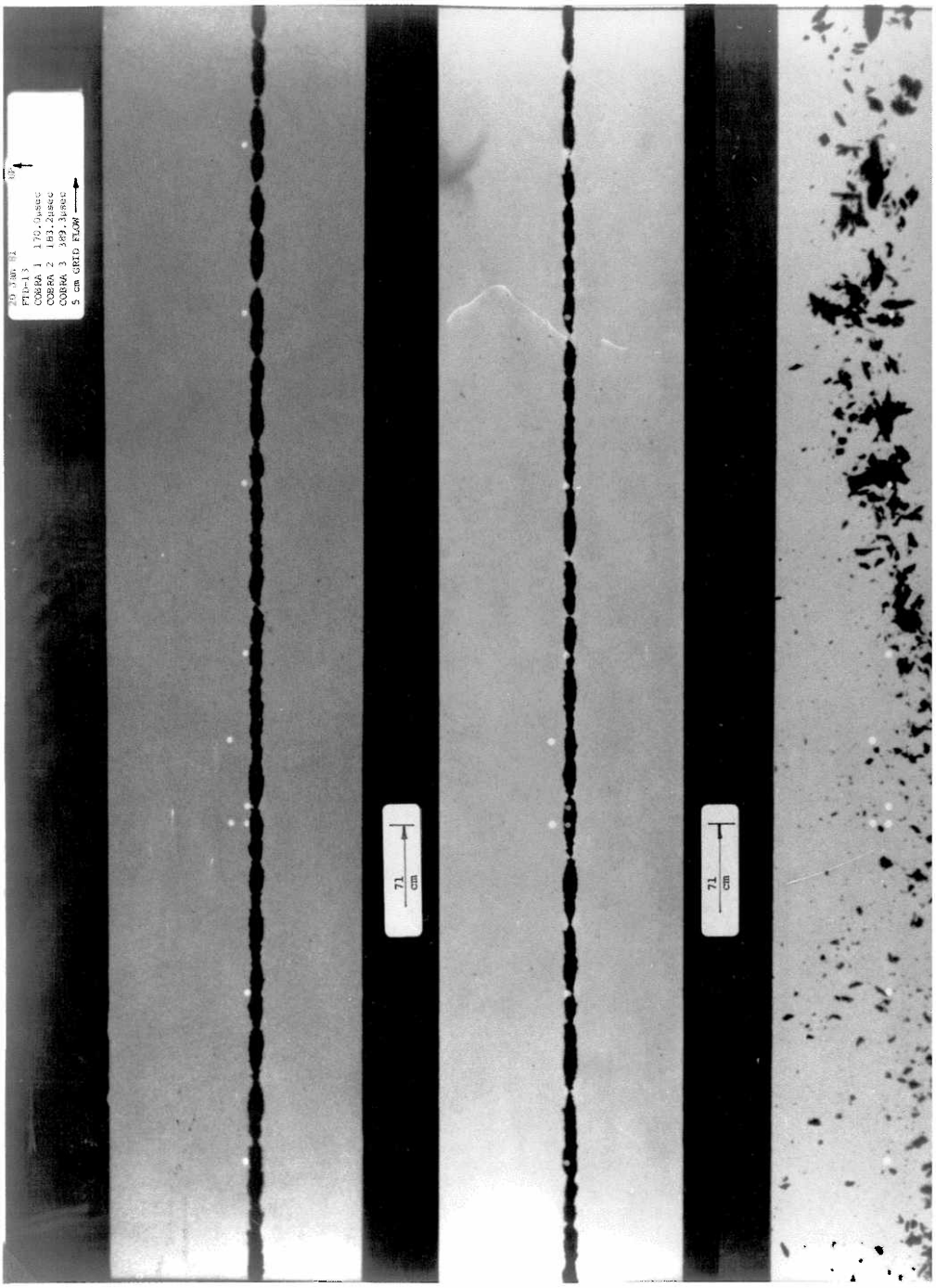

Figure 78: FTD 13 middle [KB81]

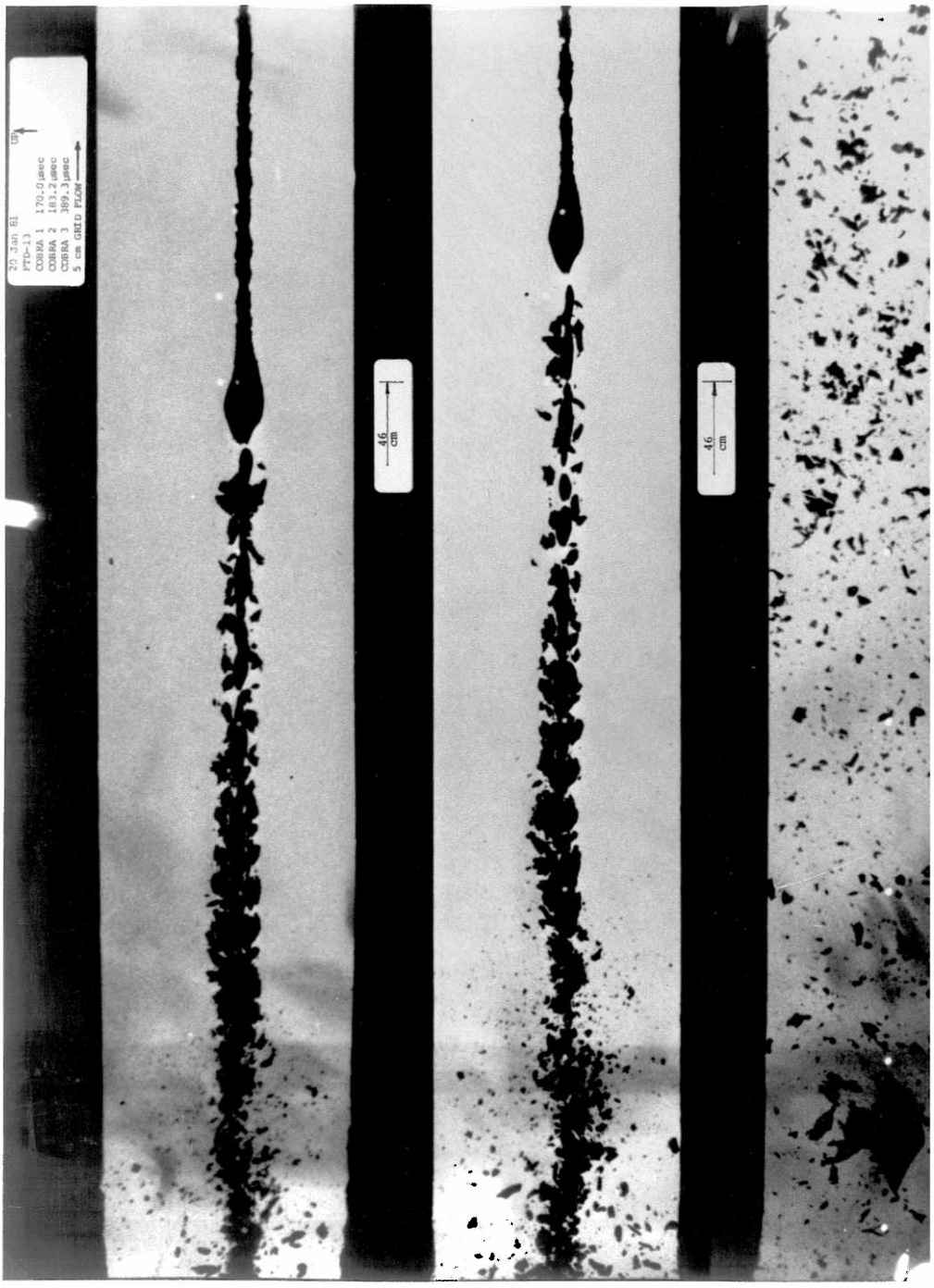

Figure 79: FTD13 tail [KB81]

THIS PAGE INTENTIONALLY LEFT BLANK

APPENDIX E: DATA PLOTS

A. ABSOLUTE VELOCITY VS. TIME PLOTS

1. DRAGON Baseline

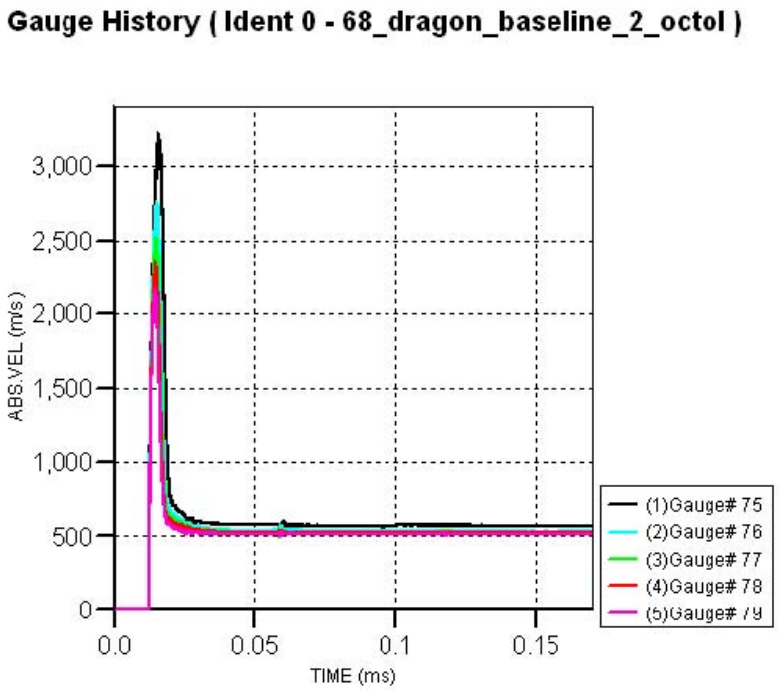

Figure 80: DRAGON baseline gauge 75-79

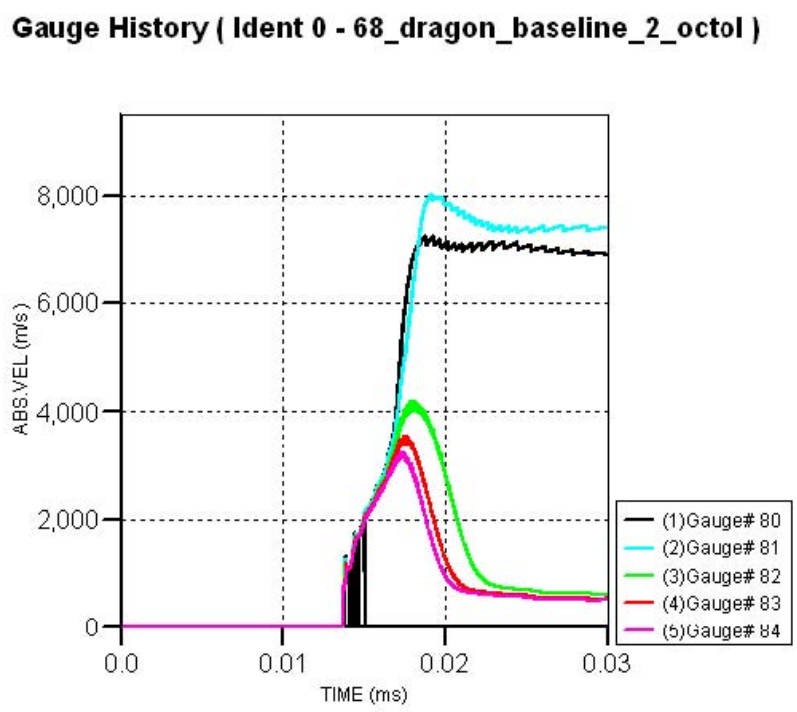

Figure 81: DRAGON baseline gauge 80-84

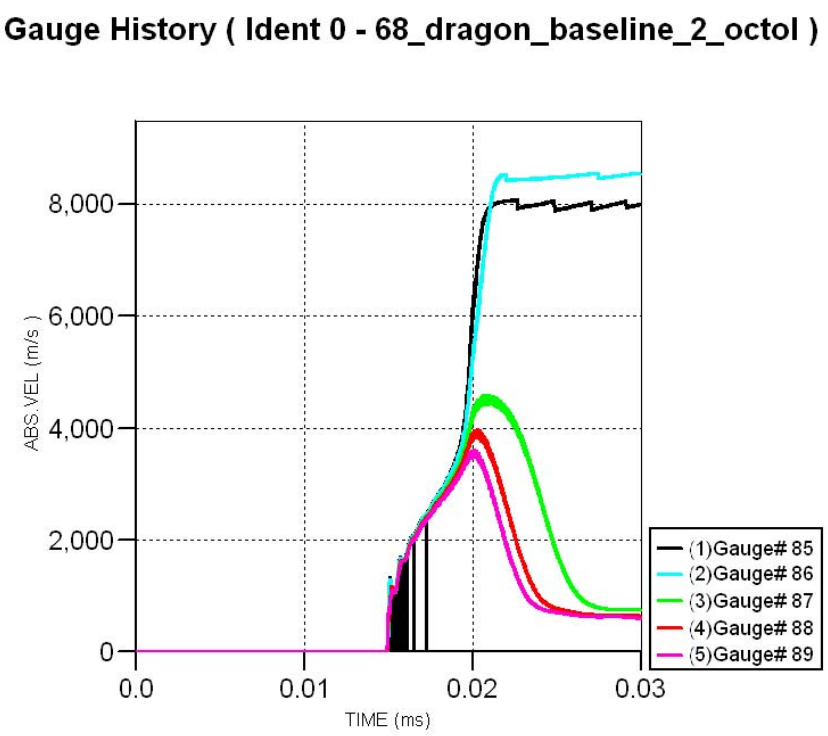

Figure 82: DRAGON baseline gauge 85-89

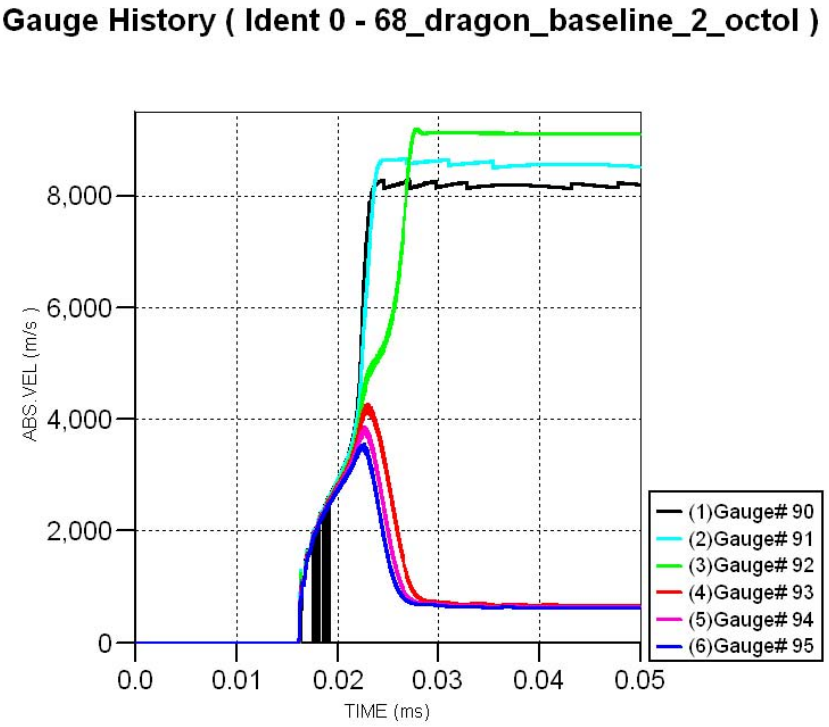

Figure 83: DRAGON baseline gauge 90-95

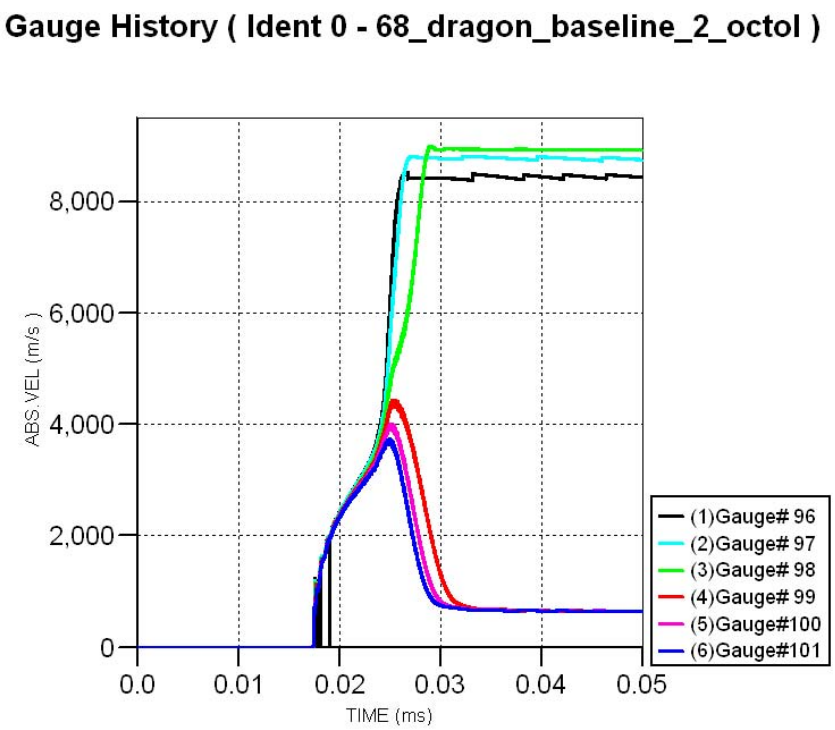

Figure 84: DRAGON baseline gauge 96-101

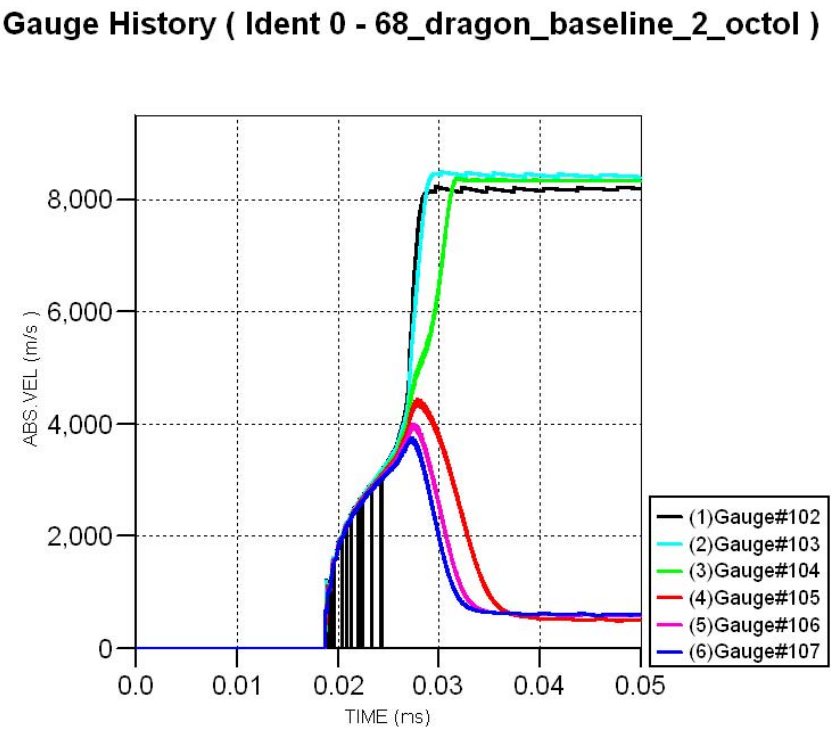

Figure 85: DRAGON baseline gauge 102-107

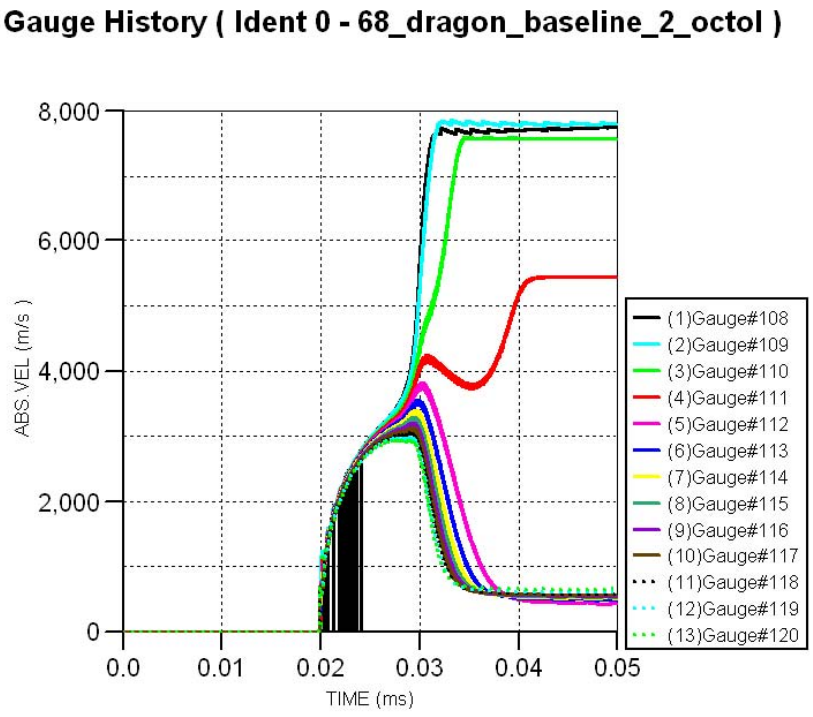

Figure 86: DRAGON baseline gauge 108-120

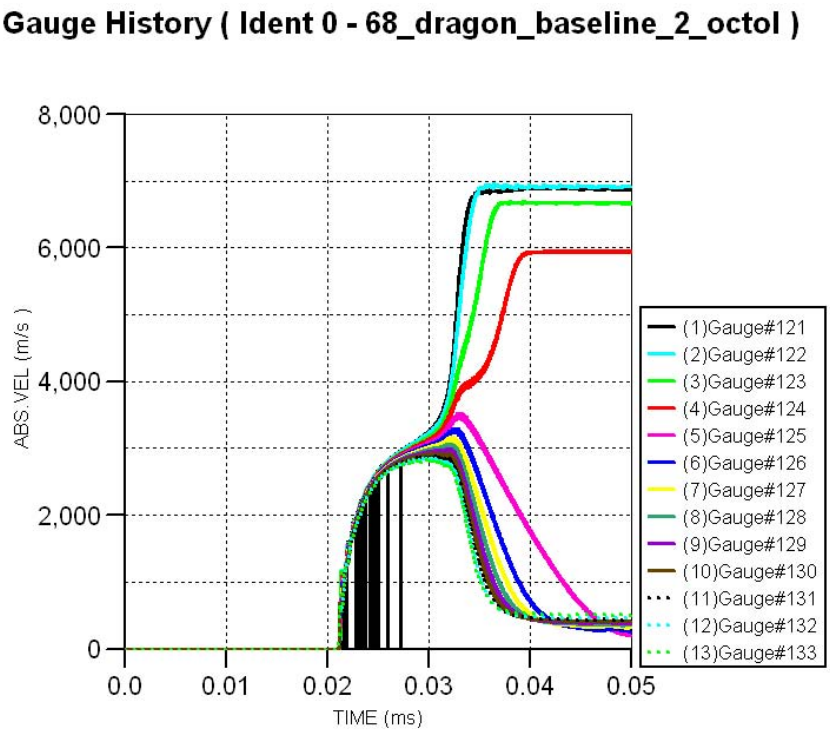

Figure 87: DRAGON baseline gauge 121-133

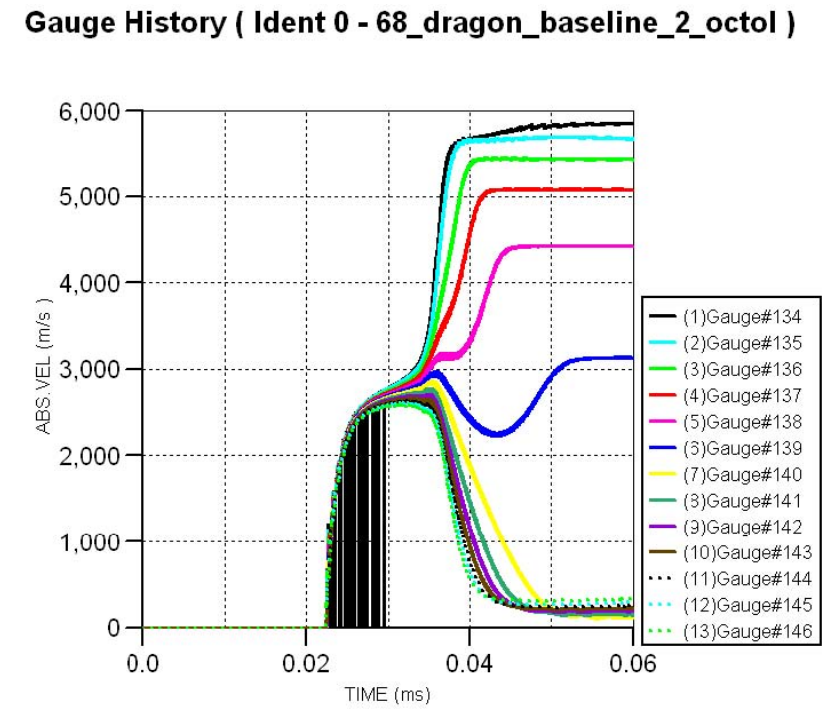

Figure 88: DRAGON baseline gauge 134-146

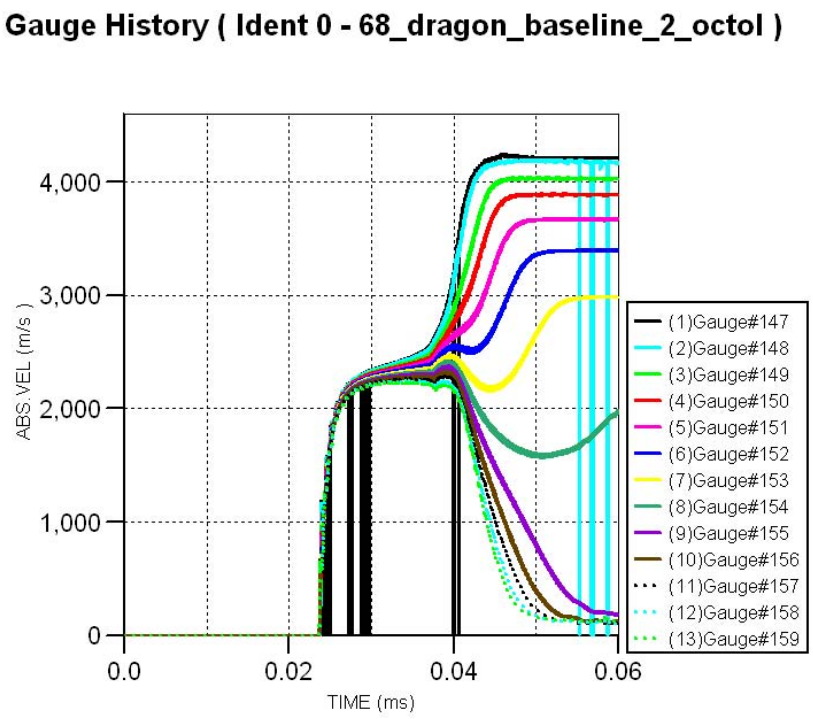

Figure 89: DRAGON baseline gauge 147-159

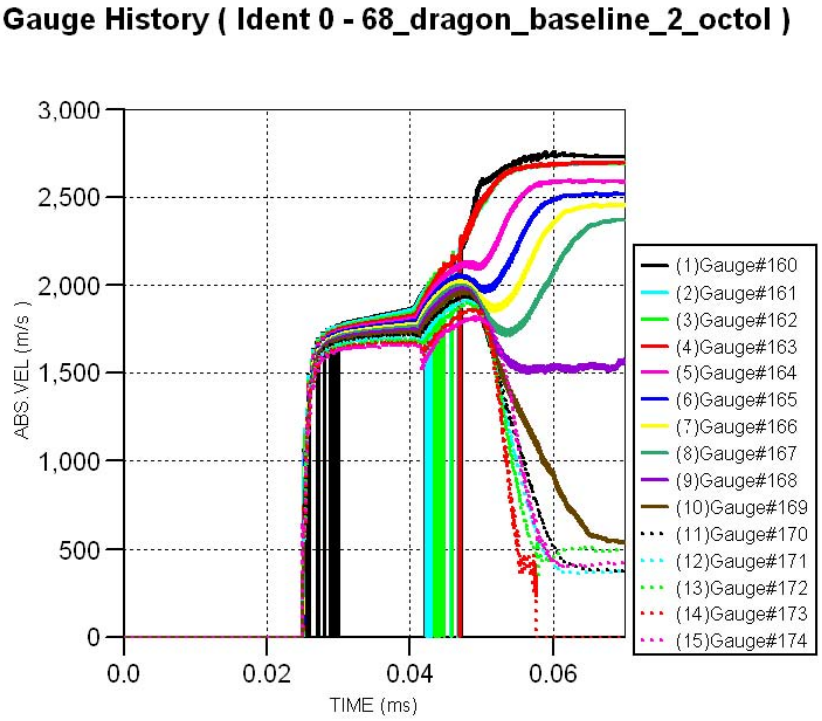

Figure 90: DRAGON baseline gauge 160-174

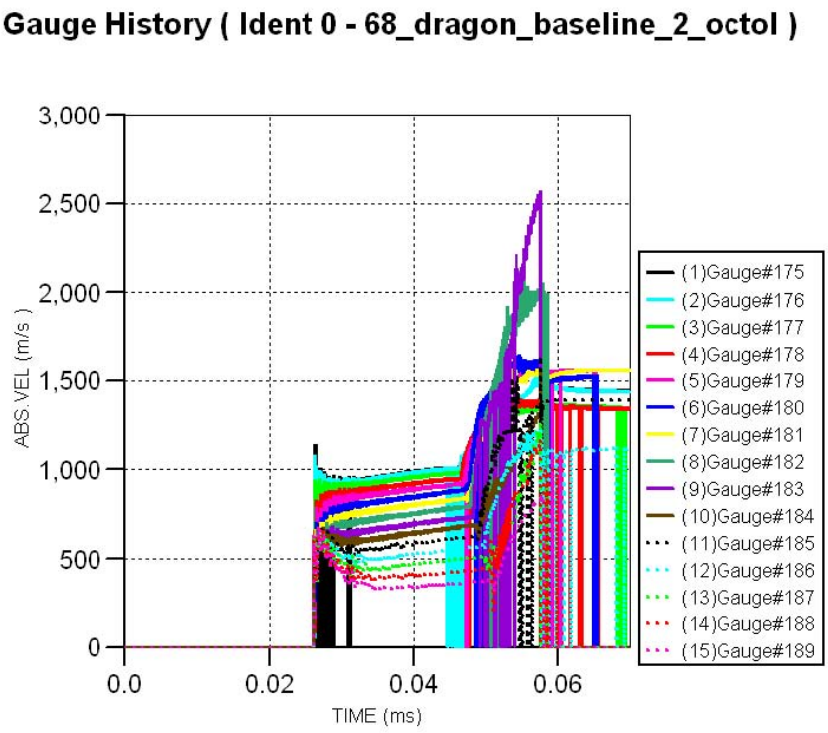

Figure 91: DRAGON baseline gauge 175-189

2. UIUC

The liner partition estimation for a 1 mm copper liner is reported inhere. The simulation setup is shown in Fig. 62, boundaries are applied like in DRAGON simulations. Table 17 shows the gauge positions, the following figures provide the absolute velocity plots for moving gauges.

Fixed gauges	x(mm)	y(mm)	gap(mm)
1-19	-180..0	0	10
20-38	-180..0	2	10
Moving gauges			
39-41	-185	2.329..2.529	0.1
42-44	-180	4.275..4.475	0.1
45-48	-175	6.221..6.521	0.1
49-53	-170	8.167..8.567	0.1
54-58	-165	10.112..10.512	0.1
59-64	-160	12.058..12.558	0.1
65-70	-155	14.004..14.504	0.1
71-77	-150	15.950..16.550	0.1
78-84	-145	17.895..18.495	0.1
85-92	-140	19.841..20.541	0.1
93-101	-135	21.787..22.587	0.1
102-111	-130	23.733..24.633	0.1

Table 17: Gauge position for UIUC copper liner with 1 mm thickness

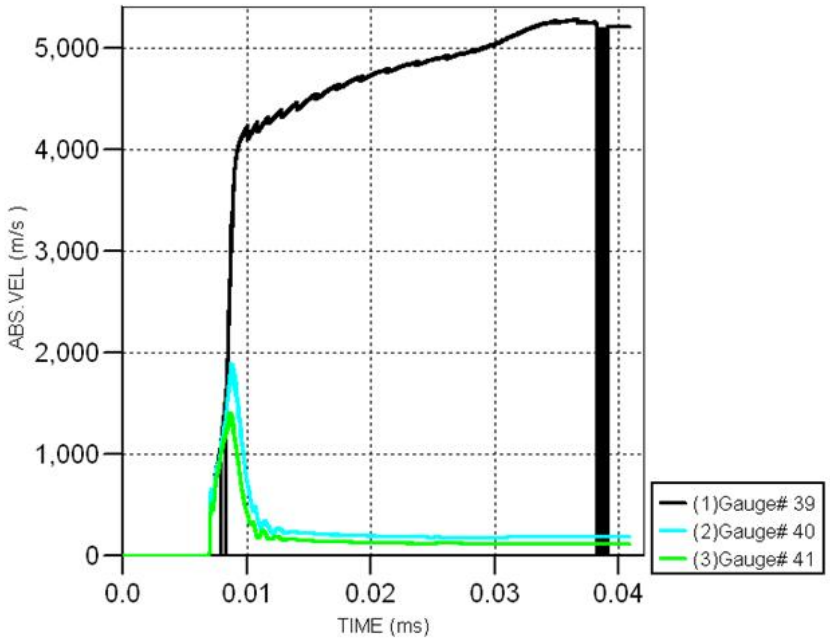

Figure 92: UIUC solid 1 mm copper liner; gauge 39-41

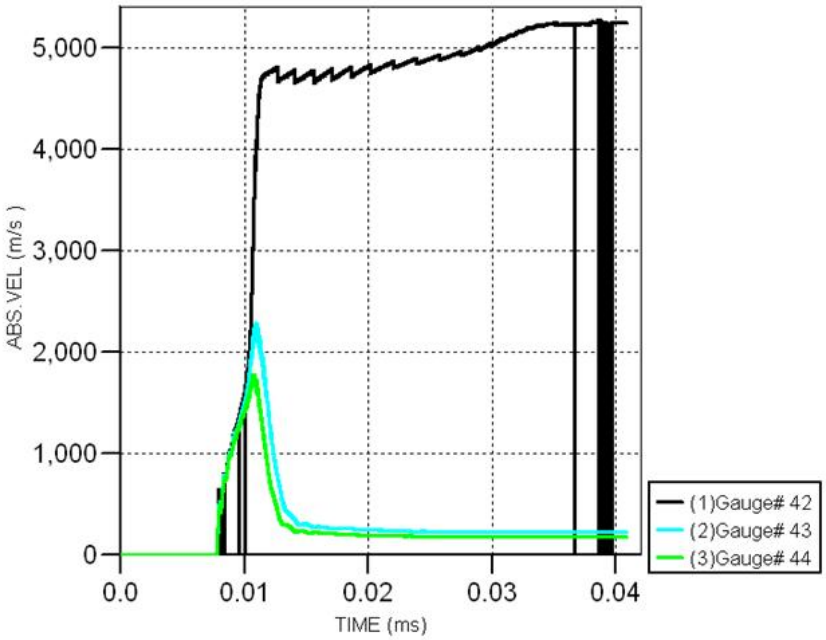

Figure 93: UIUC solid 1 mm copper liner; gauge 42-44

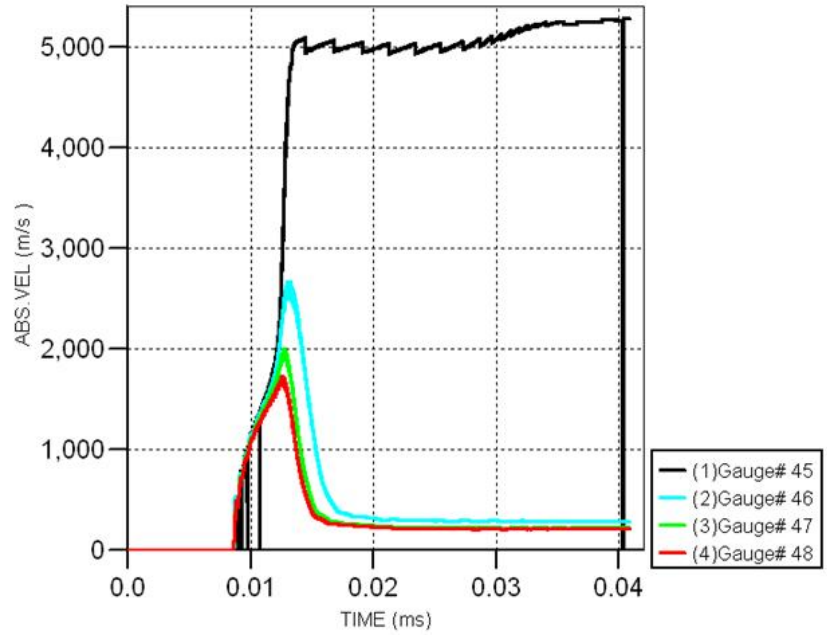

Figure 94: UIUC solid 1 mm copper liner; gauge 45-48

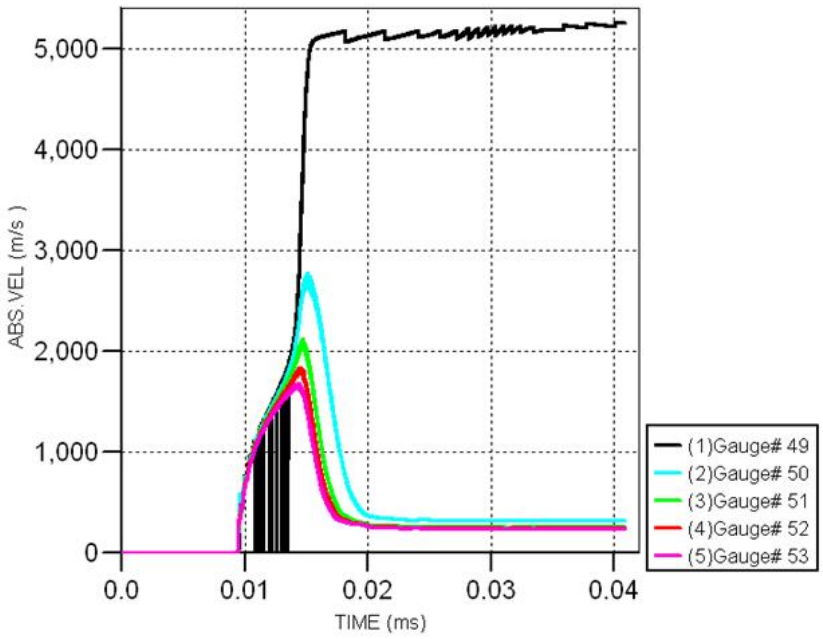

Figure 95: UIUC solid 1 mm copper liner; gauge 49-53

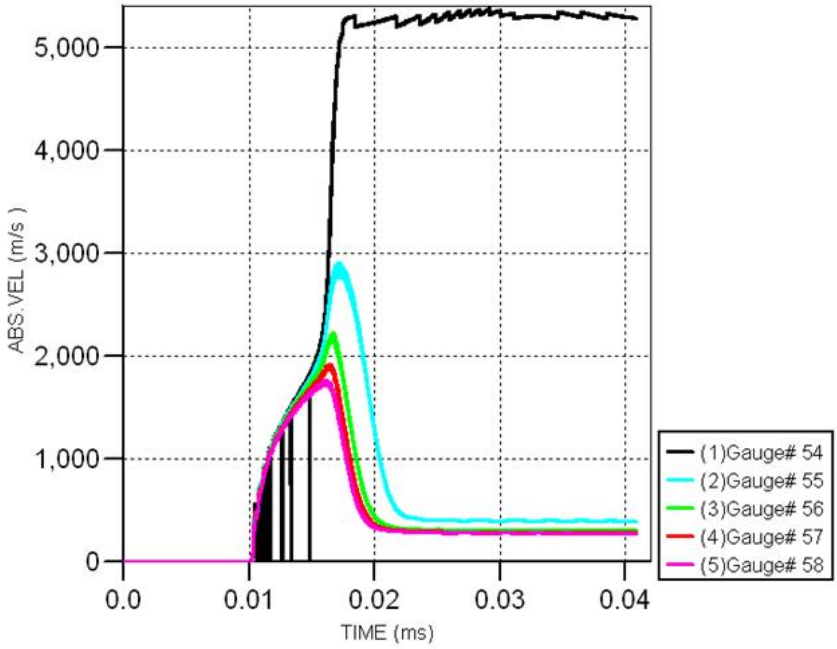

Figure 96: UIUC solid 1 mm copper liner; gauge 54-58

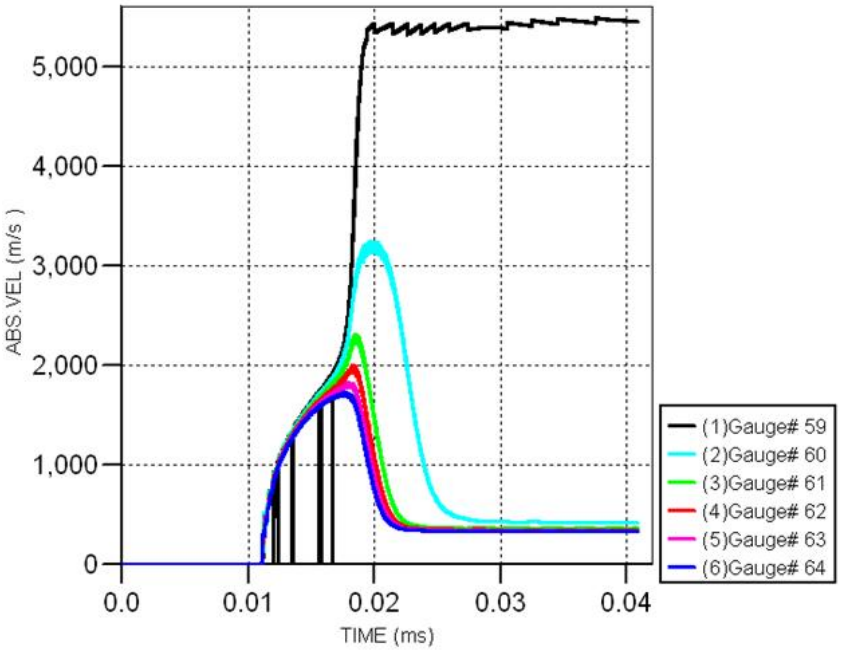

Figure 97: UIUC solid 1 mm copper liner; gauge 59-64

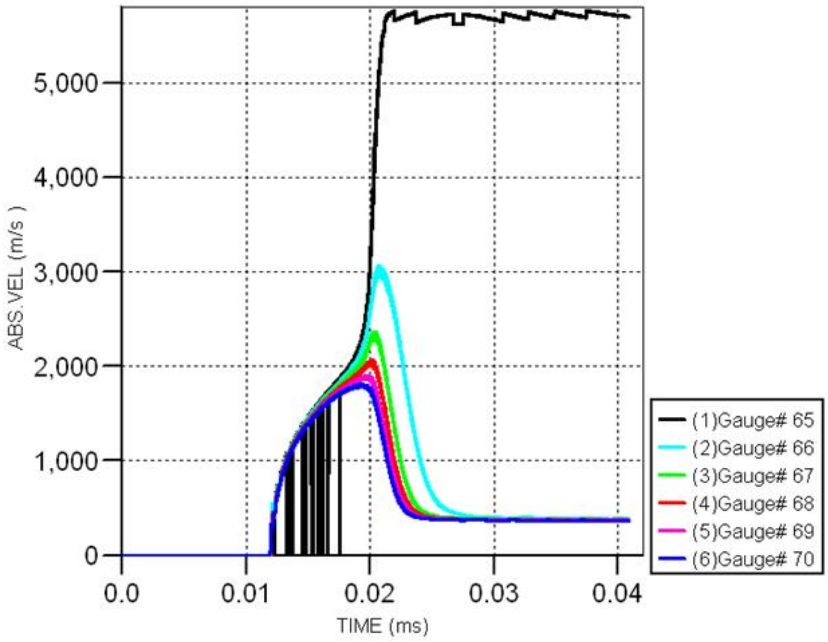

Figure 98: UIUC solid 1 mm copper liner; gauge 65-70

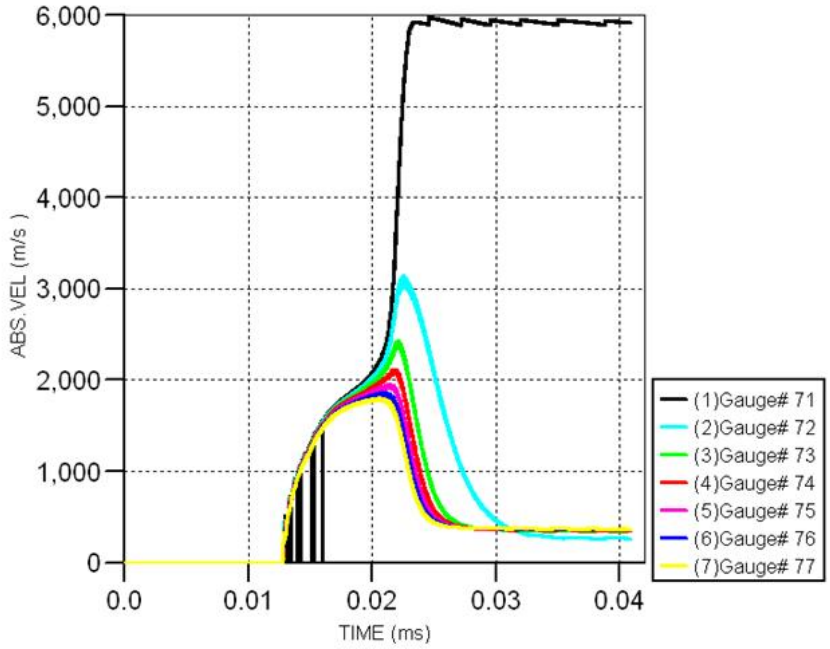

Figure 99: UIUC solid 1 mm copper liner; gauge 71-77

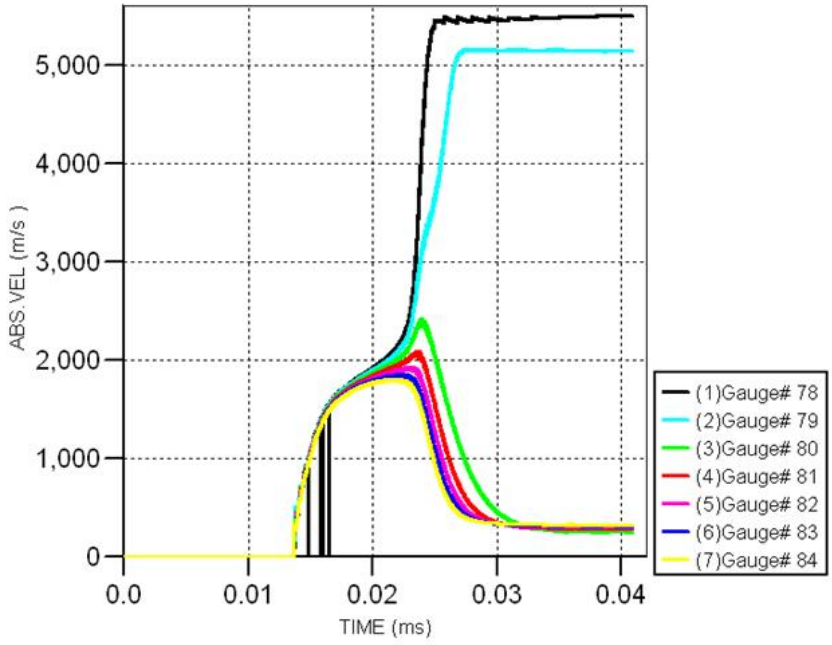

Figure 100: UIUC solid 1 mm copper liner; gauge 78-84

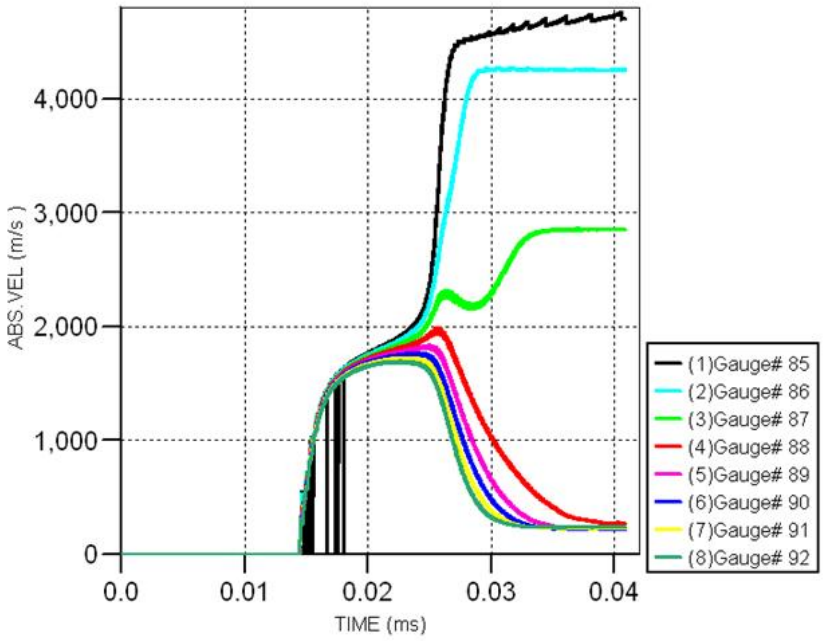

Figure 101: UIUC solid 1 mm copper liner; gauge 85-92

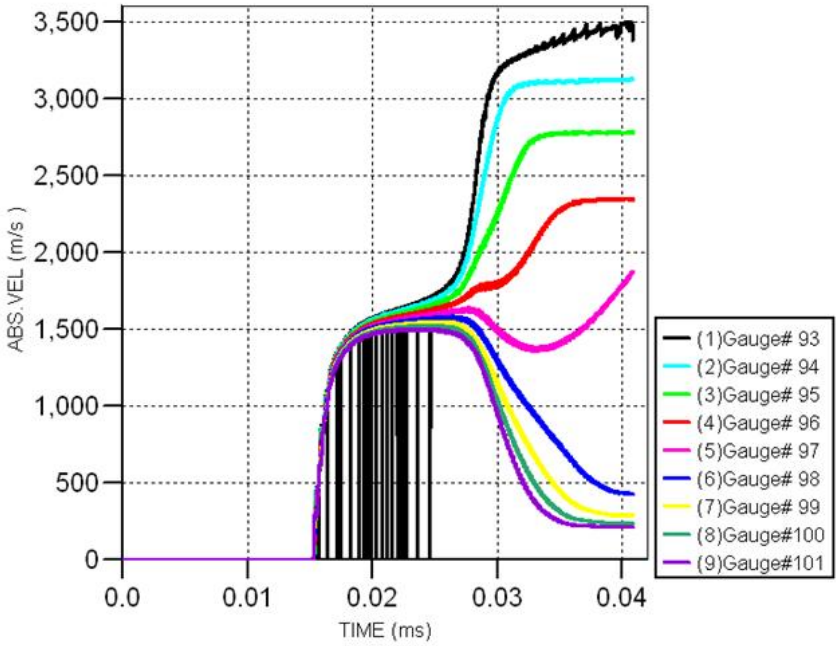

Figure 102: UIUC solid 1 mm copper liner; gauge 93-101

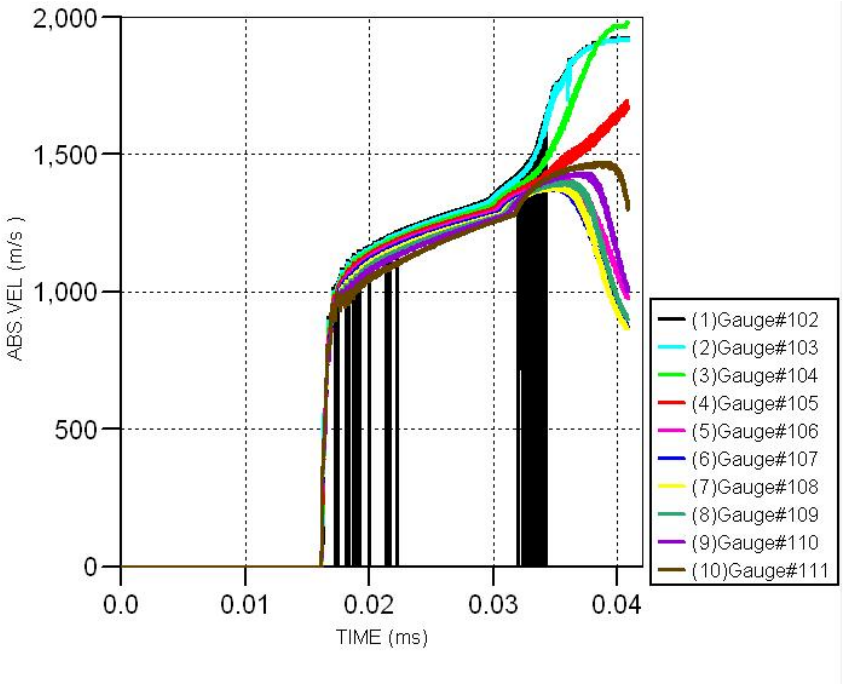

Figure 103: UIUC solid 1 mm copper liner; gauge 102-111

APPENDIX F: LAYOUT DATA

To create the geometry in AUTODYN, the following parameters where used with the ”fill by geometrical space” Fill option. *Space* denotes the dimensions of the part, the following data provide fill parameters. The data in the columns are ordered from top to bottom and left to right.

A. DRAGON BASELINE

Name	**Filltype**
space	RECT
X	-422.65
Y	0
DX	422.65
DY	125
Detonation	point
X	-422
Y	0
body1	RECT
X1	-422.65
X2	-200.4
Y1	0
Y2	52.07
filler1	RECT
X1	-422.65
X2	-209.9
Y1	0
Y2	50.8

liner1	RECT
X1	-209.925
X2	-200.4
Y1	48.6
Y2	50.1
liner2	QUAD
X1	-318.0362
Y1	7.1
X2	-209.925
Y2	48.6
X3	-209.925
Y3	50.1
X4	-318.0362
Y4	8.6
liner3	ELLIPSE
X	-317.8443
Y	0
X-Semi	5.3086
Y-Semi	8.6

air1	RECT
X1	-209.925
X2	-200.4
Y1	0
Y2	48.6
air2	QUAD
X1	-318.0362
Y1	0
X2	-209.925
Y2	0
X3	-209.925
Y3	48.6
X4	-318.0362
Y4	7.1
air3	ELLIPSE
X	-317.8443
Y	0
X-Semi	3.8086
Y-Semi	7.1

B. DRAGON BASE INSERT

Name	**Filltype**
space	RECT
X	-422.65
Y	0
DX	422.65
DY	125
Detonation	point
X	-422
Y	0
body1	RECT
X1	-422.65
X2	-200.4
Y1	0
Y2	52.07
filler1	RECT
X1	-422.65
X2	-209.9
Y1	0
Y2	50.8

liner1	RECT
X1	-209.925
X2	-200.4
Y1	49.34
Y2	50.1
liner2	QUAD
X1	-318.0362
Y1	7.1
X2	-209.925
Y2	48.6
X3	-209.925
Y3	50.1
X4	-318.0362
Y4	8.6
liner3	ELLIPSE
X	-317.8443
Y	0
X-Semi	5.3086
Y-Semi	8.6

insert	QUAD
X1	-221.65
Y1	44.05
X2	-208
Y2	49.34
X3	-209.925
Y3	49.34
X4	-221.825
Y4	44.844

air1	RECT
X1	-209.925
X2	-200.4
Y1	0
Y2	48.6

air2	QUAD
X1	-318.0362
Y1	0
X2	-209.925
Y2	0
X3	-209.925
Y3	48.6
X4	-318.0362
Y4	7.1

air3	ELLIPSE
X	-317.8443
Y	0
X-Semi	3.8086
Y-Semi	7.1

C. ANGLE SERIES FOR COPPER AND NICKEL

1. 20° liner

Name	**Filltype**
space	RECT
X	-550.09
Y	0
DX	550.09
DY	125
Detonation	point
X	-549
Y	0
body1	RECT
X1	-550.09
X2	-200.4
Y1	0
Y2	52.07
filler1	RECT
X1	-509.09
X2	-209.9
Y1	0
Y2	50.8

liner1	RECT
X1	-209.925
X2	-200.4
Y1	48.6
Y2	50.1
liner2	QUAD
X1	-445.2832
Y1	7.1
X2	-209.925
Y2	48.6
X3	-209.925
Y3	50.1
X4	-445.2832
Y4	8.6
liner3	ELLIPSE
X	-445.195
Y	0
X-Semi	5.3086
Y-Semi	8.6

air1	RECT
X1	-209.925
X2	-200.4
Y1	0
Y2	48.6
air2	QUAD
X1	-445.2832
Y1	0
X2	-209.925
Y2	0
X3	-209.925
Y3	48.6
X4	-445.2832
Y4	7.1
air3	ELLIPSE
X	-445.195
Y	0
X-Semi	3.8086
Y-Semi	7.1

2. 25° liner

Name	Filltype
space	RECT
X	-501.85
Y	0
DX	501.85
DY	125
Detonation	point
X	-501
Y	0
body1	RECT
X1	-501.85
X2	-200.4
Y1	0
Y2	52.07
filler1	RECT
X1	-501.85
X2	-209.9
Y1	0
Y2	50.8

liner1	RECT
X1	-209.925
X2	-200.4
Y1	48.6
Y2	50.1
liner2	QUAD
X1	-397.1194
Y1	7.1
X2	-209.925
Y2	48.6
X3	-209.925
Y3	50.1
X4	-397.1194
Y4	8.6
liner3	ELLIPSE
X	-397.0086
Y	0
X-Semi	5.3086
Y-Semi	8.6

air1	RECT
X1	-209.925
X2	-200.4
Y1	0
Y2	48.6
air2	QUAD
X1	-397.1194
Y1	0
X2	-209.925
Y2	0
X3	-209.925
Y3	48.6
X4	-397.1194
Y4	7.1
air3	ELLIPSE
X	-397.0086
Y	0
X-Semi	3.8086
Y-Semi	7.1

3. 42° liner

This design is equal to the DRAGON baseline layout.

D. AB DESIGN

Name	**Filltype**
space	RECT
X	-422.65
Y	0
DX	422.65
DY	125
Detonation	point
X	-422
Y	0
body1	RECT
X1	-422.65
X2	-200.4
Y1	0
Y2	52.07
filler1	RECT
X1	-422.65
X2	-209.9
Y1	0
Y2	50.8

liner1	RECT
X1	-209.925
X2	-200.4
Y1	49.57
Y2	50.1
liner2	QUAD
X1	-318.0362
Y1	7.1
X2	-209.925
Y2	48.6
X3	-209.925
Y3	50.1
X4	-318.0362
Y4	8.6
liner3	ELLIPSE
X	-317.8443
Y	0
X-Semi	5.3086
Y-Semi	8.6

insert	QUAD
X1	-310
Y1	9.8
X2	-208
Y2	49.57
X3	-209.925
Y3	49.57
X4	-310
Y4	10.1

air1	RECT
X1	-208
X2	-200.4
Y1	0
Y2	49.57

air2	QUAD
X1	-318.0362
Y1	0
X2	-208
Y2	0
X3	-208
Y3	49.57
X4	-318.0362
Y4	7.1

air3	ELLIPSE
X	-317.8443
Y	0
X-Semi	3.8086
Y-Semi	7.1

E. ABA DESIGN

Name	Filltype
space	RECT
X	-422.65
Y	0
DX	422.65
DY	125
Detonation	point
X	-422
Y	0
body1	RECT
X1	-422.65
X2	-200.4
Y1	0
Y2	52.07
filler1	RECT
X1	-422.65
X2	-209.9
Y1	0
Y2	50.8

liner1	RECT
X1	-209.925
X2	-200.4
Y1	49.57
Y2	50.1
liner2	QUAD
X1	-318.0362
Y1	7.1
X2	-209.925
Y2	48.6
X3	-209.925
Y3	50.1
X4	-318.0362
Y4	8.6
liner3	ELLIPSE
X	-317.8443
Y	0
X-Semi	5.3086
Y-Semi	8.6

1. insert	QUAD
X1	-310
Y1	10.1
X2	-208
Y2	49.57
X3	-209.925
Y3	49.57
X4	-310
Y4	10.48

2. insert	QUAD
X1	-290
Y1	17.8
X2	-207
Y2	49.57
X3	-208.3
Y3	49.57
X4	-290
Y4	18

air1	RECT
X1	-207
X2	-200.4
Y1	0
Y2	49.57

air2	QUAD
X1	-318.0362
Y1	0
X2	-207
Y2	0
X3	-207
Y3	49.57
X4	-318.0362
Y4	7.1

air3	ELLIPSE
X	-317.8443
Y	0
X-Semi	3.8086
Y-Semi	7.1

F. UIUC LAYOUT

The layout for a 1 mm thick liner is shown in this section. It describes geometric parameters and fill options for AUTODYN; the dimensions for the base insert are also inserted as last step.

Name	**Filltype**
space	RECT
X	-228.73
Y	0
DX	228.73
DY	60
Detonation	point
X	-228
Y	0
Part	**material**
body	steel 1006
filler	NM
liner	CU-OFHC
insert	AL 2024

body1	RECT
X1	-228.65
X2	-200.0
Y1	0
Y2	10.16
body2	QUAD
X1	-218.53
Y1	3.95
X2	-154.94
Y2	24.9
X3	-160.2
Y3	27.95
X4	-211.58
Y4	10.16
body3	RECT
X1	-160.2
X2	-127
Y1	0
Y2	27.95

filler1	QUAD
X1	-218.57
Y1	3.95
X2	-127
Y2	3.95
X3	-127
Y3	24.9
X4	-157.94
Y4	24.9

filler2	RECT
X1	-220
X2	-127
Y1	0
Y2	3.95

liner1	QUAD
X1	-193
Y1	0
X2	-127
Y2	0
X3	-127
Y3	24.9
X4	-131.64
Y4	24.9

air1	QUAD
X1	-186.9
Y1	0
X2	-127
Y2	0
X3	-127
Y3	24.9
X4	-186.9
Y4	1.59

liner2	QUAD
X1	-196.5
Y1	0
X2	-191.9
Y2	0
X3	-127
Y3	24.9
X4	-131.64
Y4	24.9

filler3	QUAD
X1	-197
Y1	0
X2	-193.71
Y2	0
X3	-129.79
Y3	24.9
X4	-135
Y4	24.9

filler4	RECT
X1	-228.73
X2	-191.8
Y1	0
Y2	3.95

insert	QUAD
X1	-175
Y1	6.22
X2	-127
Y2	24.9
X3	-128.7
Y3	24.9
X4	-175
Y4	6.3

THIS PAGE INTENTIONALLY LEFT BLANK

APPENDIX G: ADDITIONAL VISUAL SIMULATION RESULTS

A. AB DESIGN

This appendix shows additional simulation frames from AB design studies with aluminum/ tantalum, tantalum/ aluminum, and copper/ hafnium.

1. Tantalum/ aluminum

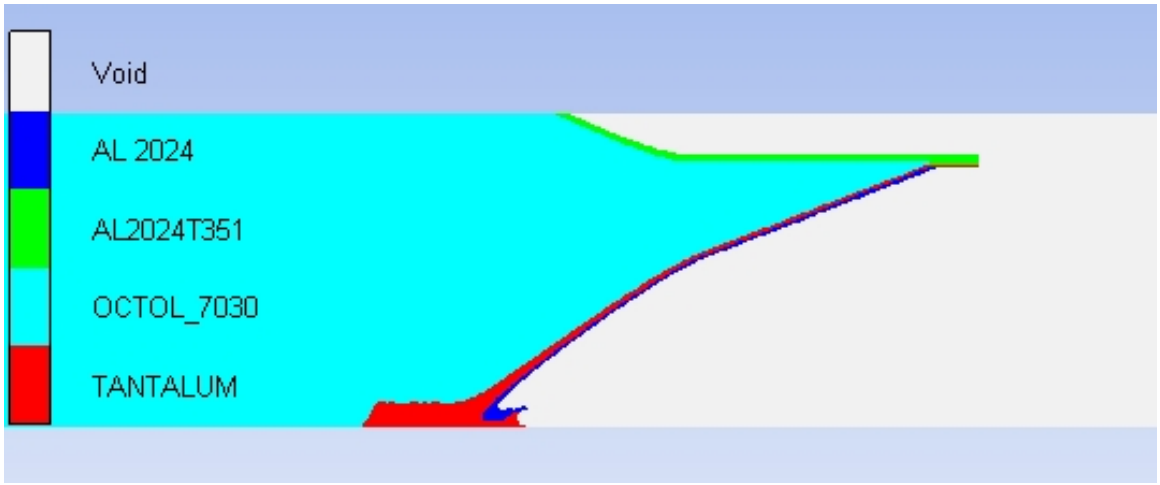

Figure 104: AB: Tantalum/ aluminum jet after 21 μs

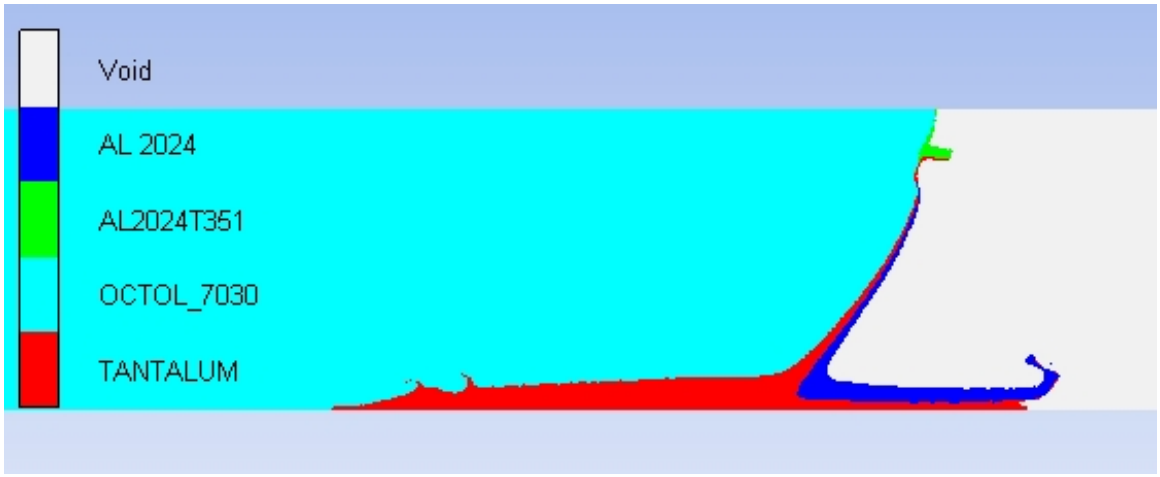

Figure 105: AB: Tantalum/ aluminum jet after 35 μs

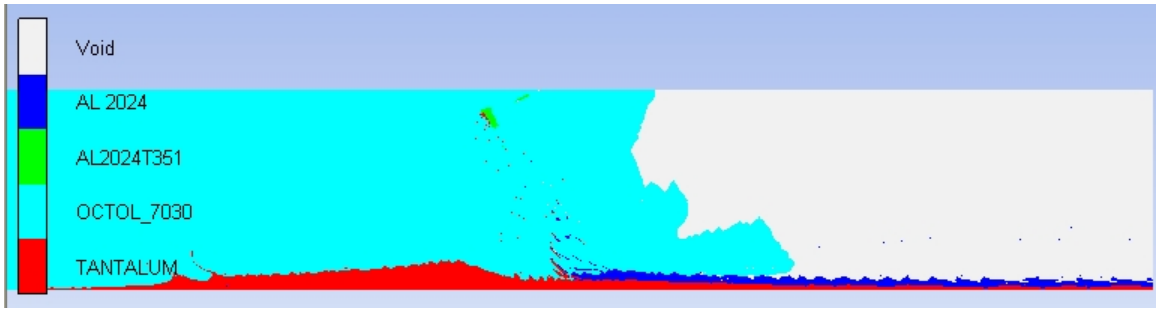

Figure 106: AB: Tantalum/ aluminum jet after 62 μs

2. Aluminum/ tantalum

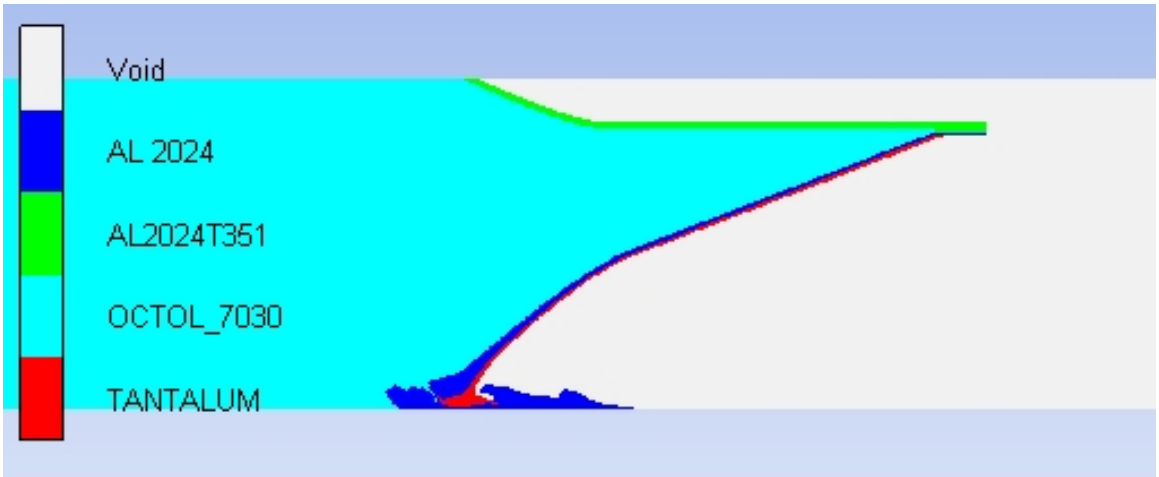

Figure 107: AB: Aluminum/ tantalum jet after 19 μs

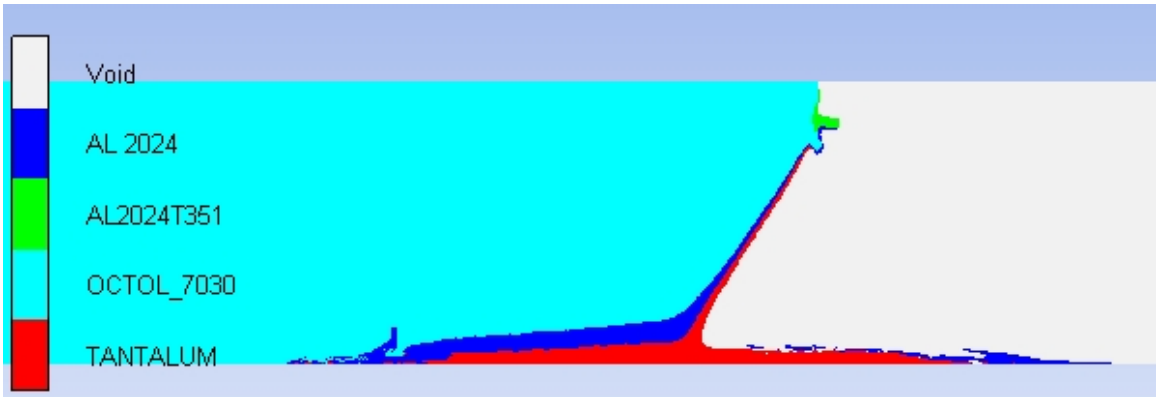

Figure 108: AB: Aluminum/ tantalum jet after 33 μs

3. Copper/ hafnium

Figure 109: AB: Copper/ hafnium jet after 21 μs

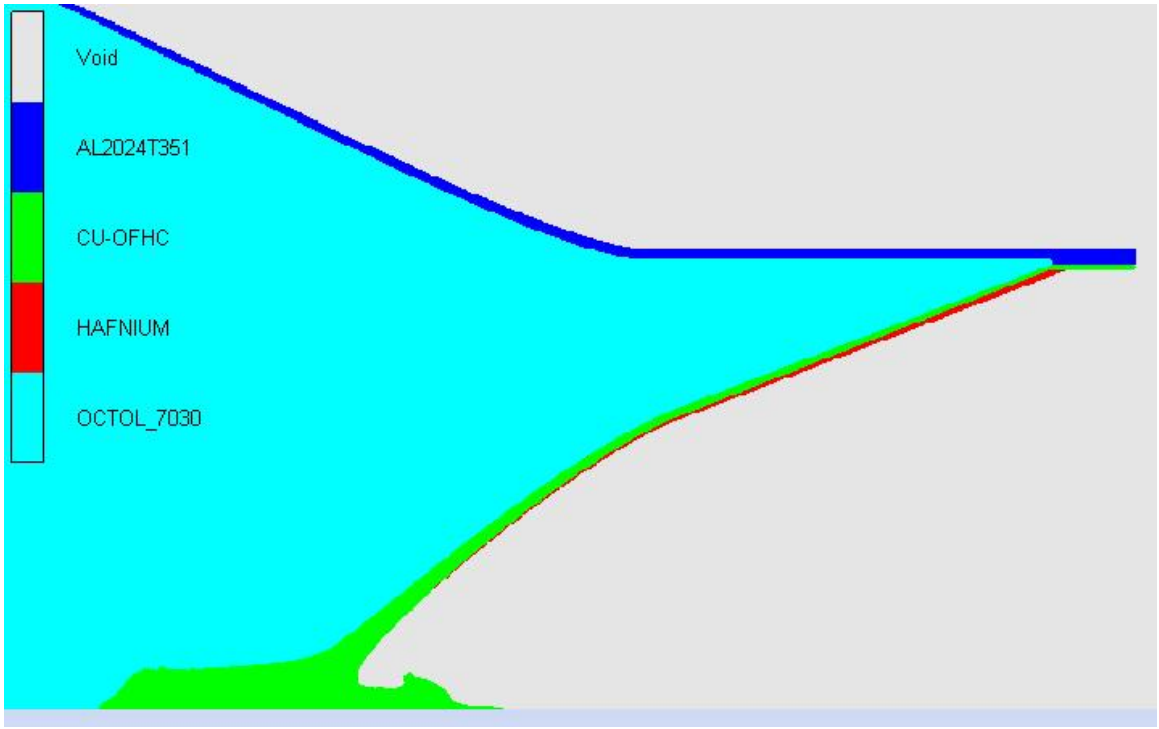

Figure 110: AB: Copper/ hafnium jet after 29 μs

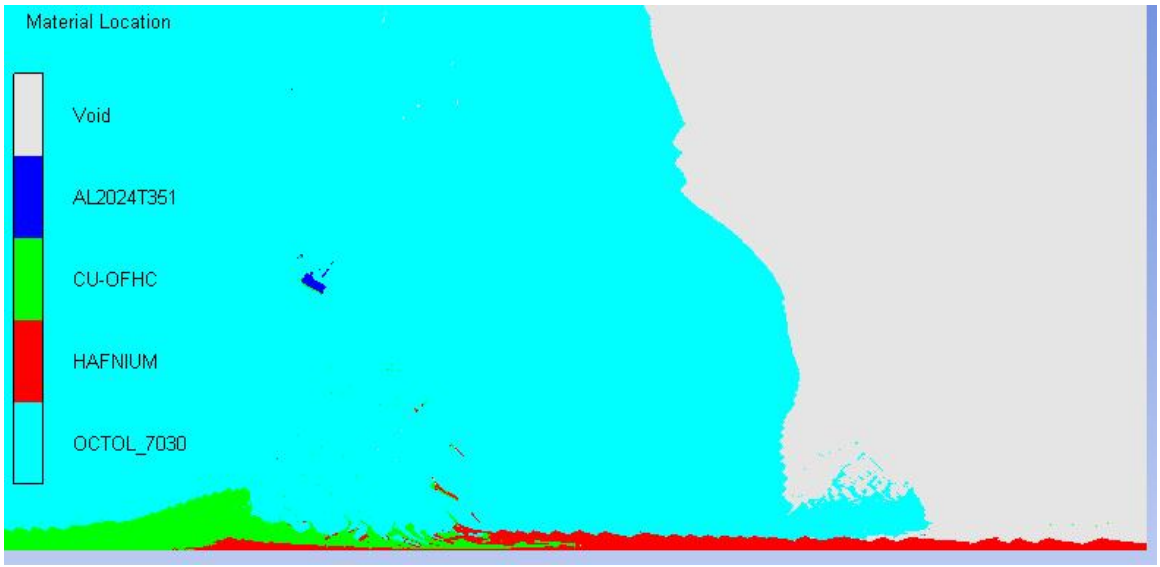

Figure 111: AB: Copper/ hafnium jet after 81 μs

B. ABA DESIGN

This appendix shows additional simulation frames from ABA design studies with copper, aluminum, tantalum, and hafnium

1. Copper/ copper

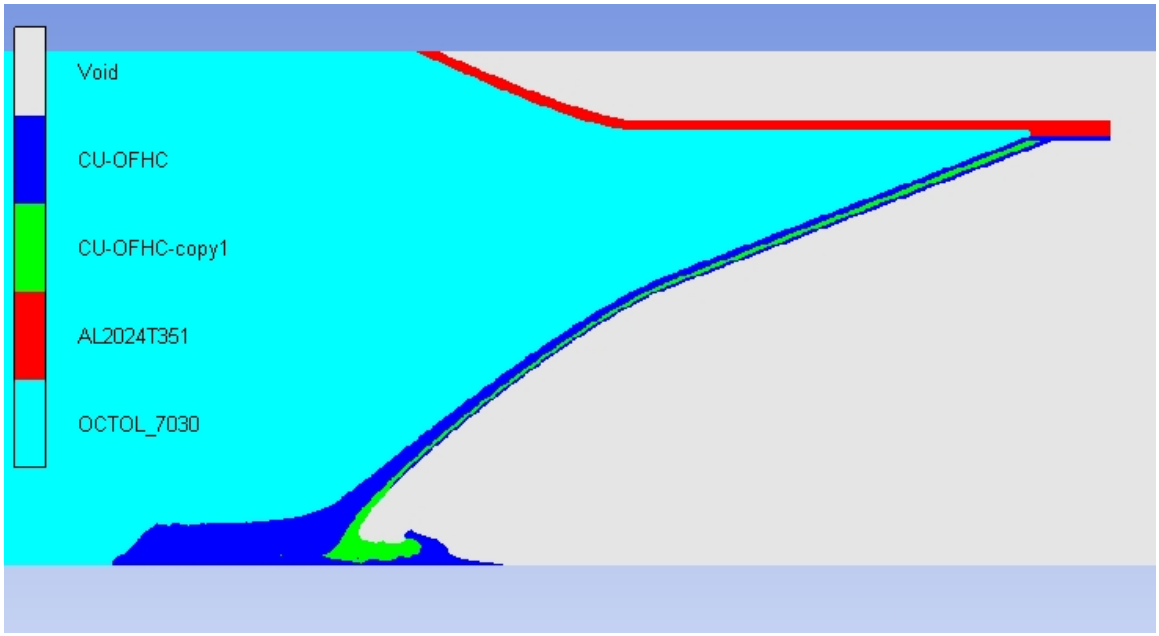

Figure 112: ABA: Copper/ copper jet after 21 μs

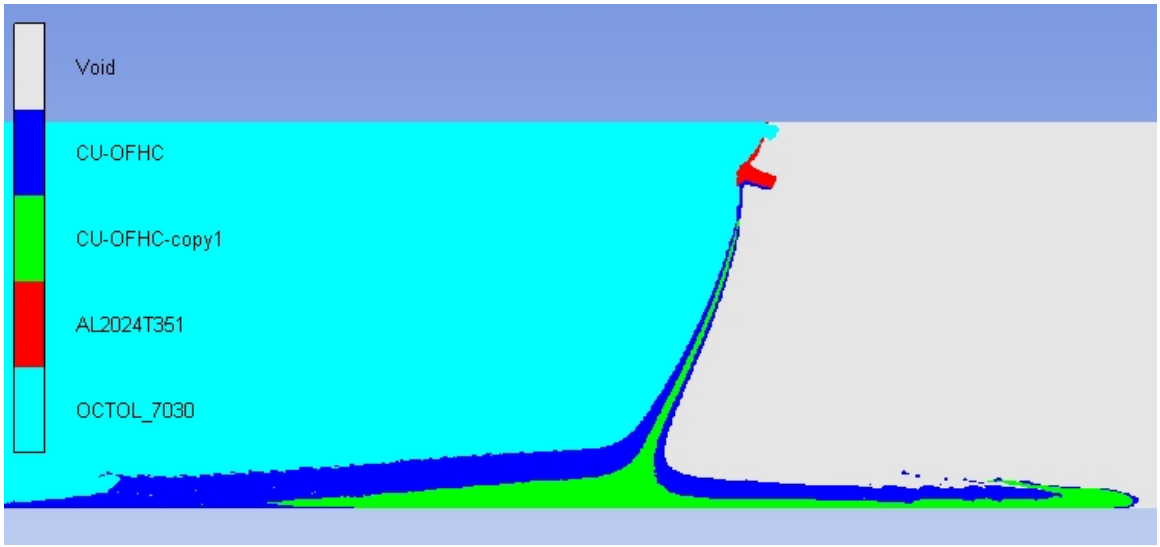

Figure 113: ABA: Copper/ copper jet after 38 μs

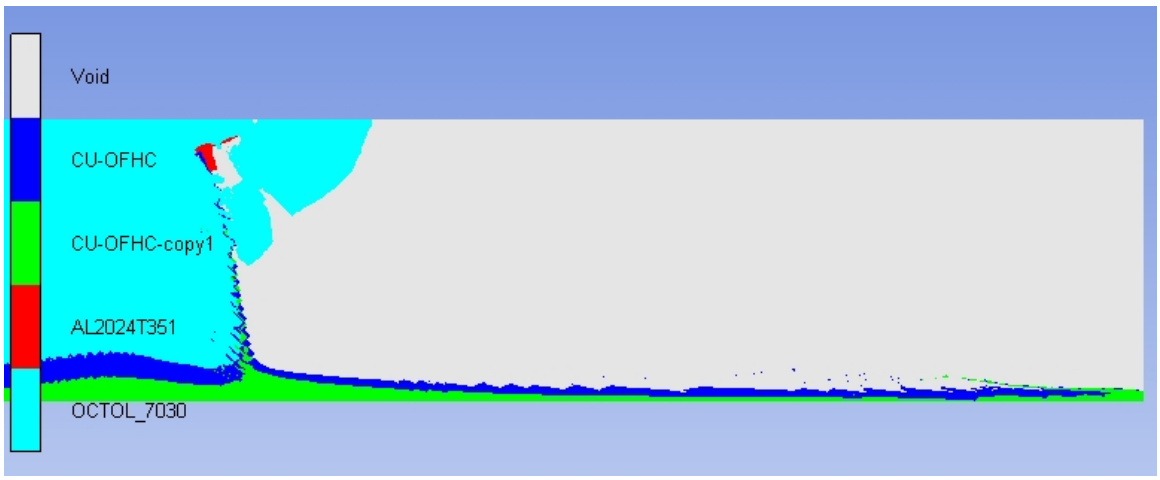

Figure 114: ABA: Copper/ copper jet after 53 μs

2. Aluminum/ tantalum

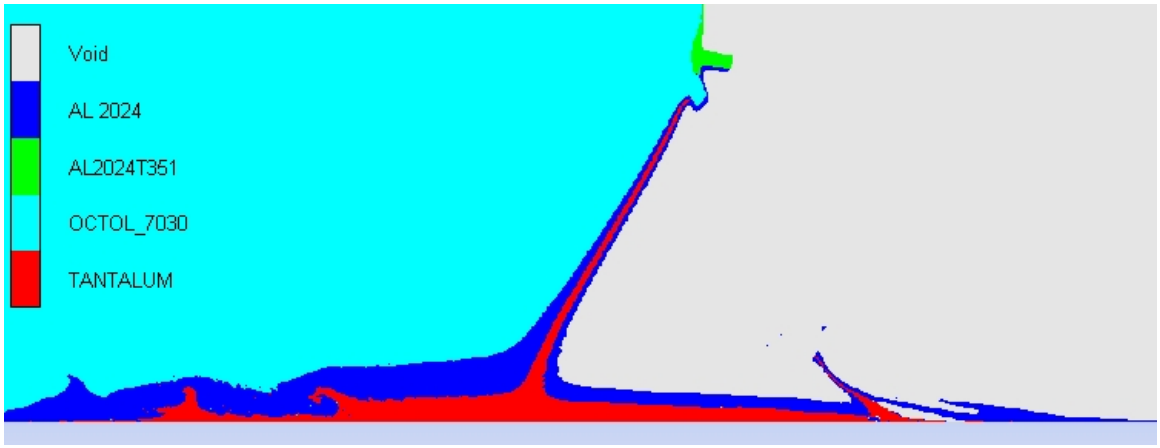

Figure 115: ABA: Aluminum/ tantalum jet after 34 μs

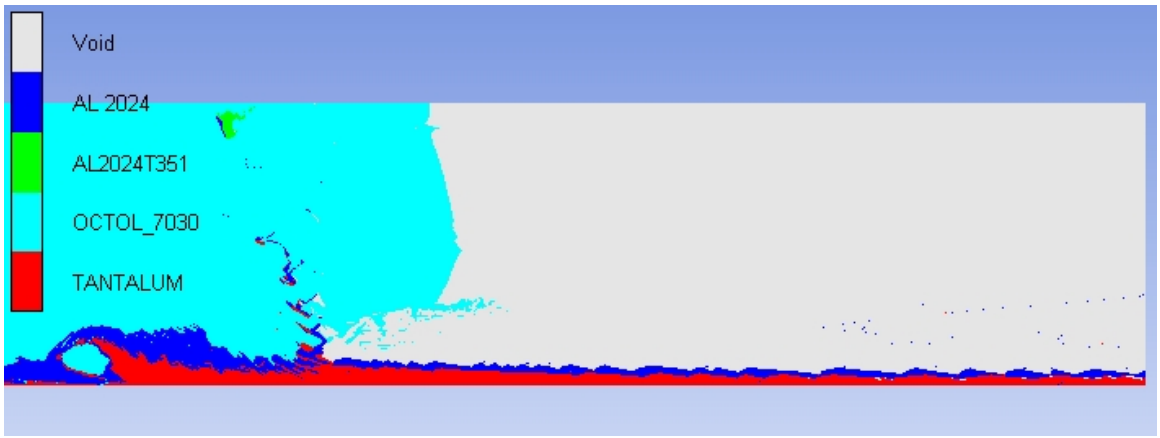

Figure 116: ABA: Aluminum/ tantalum jet after 60 μs

C. UIUC SIMULATION

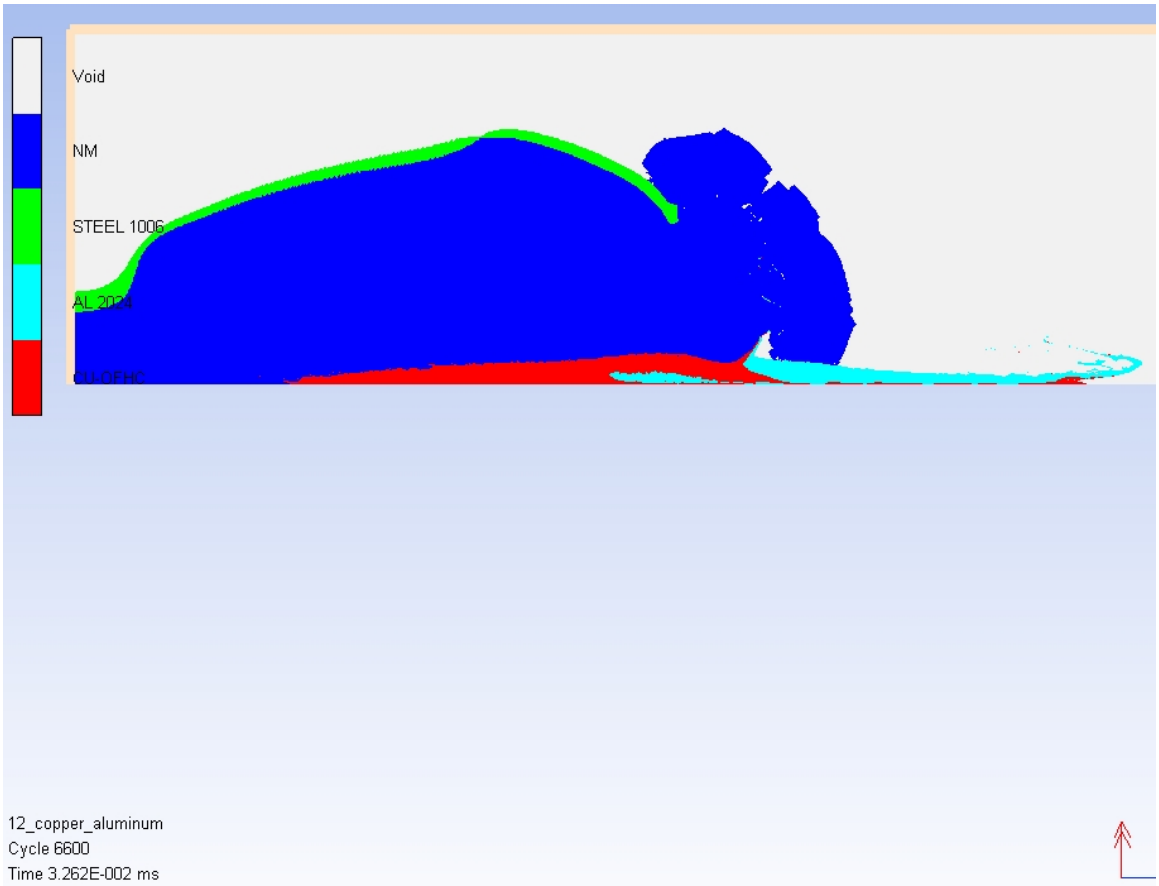

Figure 117: UIUC: Coaxial jet with copper as core and aluminum as shrouding material with a hollow aluminum jet tip; liner thickness: 1 mm

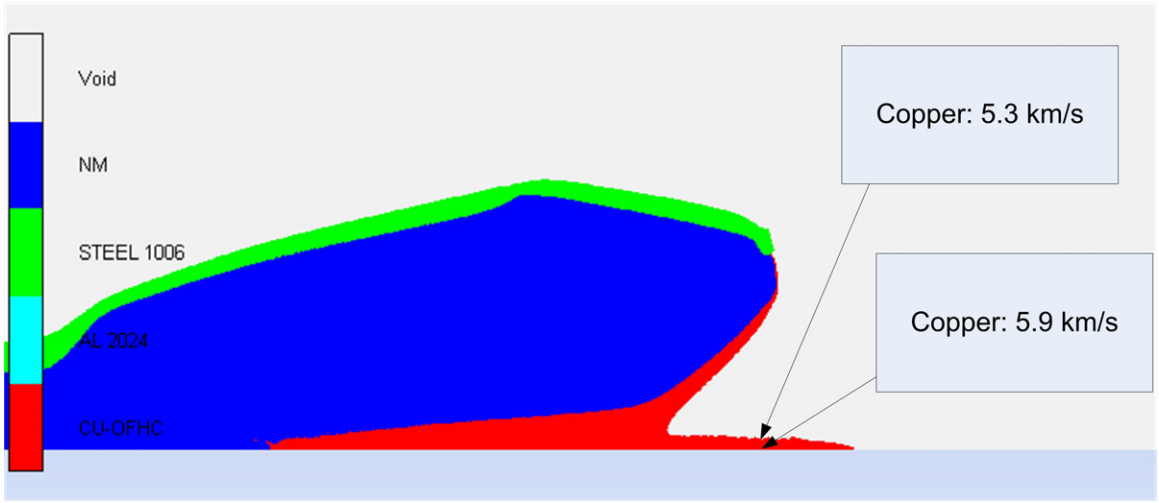

Figure 118: UIUC: Velocity along the radius from a 1 mm liner thickness simulation

APPENDIX H: INITIAL 25MM SIMULATIONS

A. A STATEMENT OF OBJECTIVE

Initial simulations with a 25 mm NM charge, PTFE (Teflon) casing, and a conical copper liner were conducted. The computational setup is shown in Figure 119, note that only the upper half is computed because of cylindrical symmetry. The area of fixed gauges is shown detailed in Fig. 120. The setup is based on the mechanical drawings in appendix C.A.

The fixed gauges are applied to measure the outflowing jet. These are placed equidistant at the right side of the grid (standoff = 2 Cone Diameter (CD)) from y = 0 to 4 mm with a gap of 0.1 mm. Boundary conditions are applied in the same way like in Fig. 66. Another important variable is the mass flowing out of the grid, monitored by the outflow boundary. With the jet velocity and the mass data one can analyze the velocity vs. cumulative mass and compare it to other simulations.

The characteristics of the jet generated from the nitromethane charge was estimated and compared with similar computational results from Haywood and Woody. These results are presented in appendix H.B.

The Teflon body is included in this computational setup. In subsequent simulations the Teflon body was excluded in the computation because an adequate structural failure model was not found and it can be reasonable to assume that the body fails in tension almost immediately after detonation. These simulations have been conducted by Haywood and Woody.

B. CODE VALIDATION

Since, in this research the latest version of ANSYS AUTODYN was used, both, version 11 and 12.0 were compared on the basis of the 25 mm simulation. The resulting

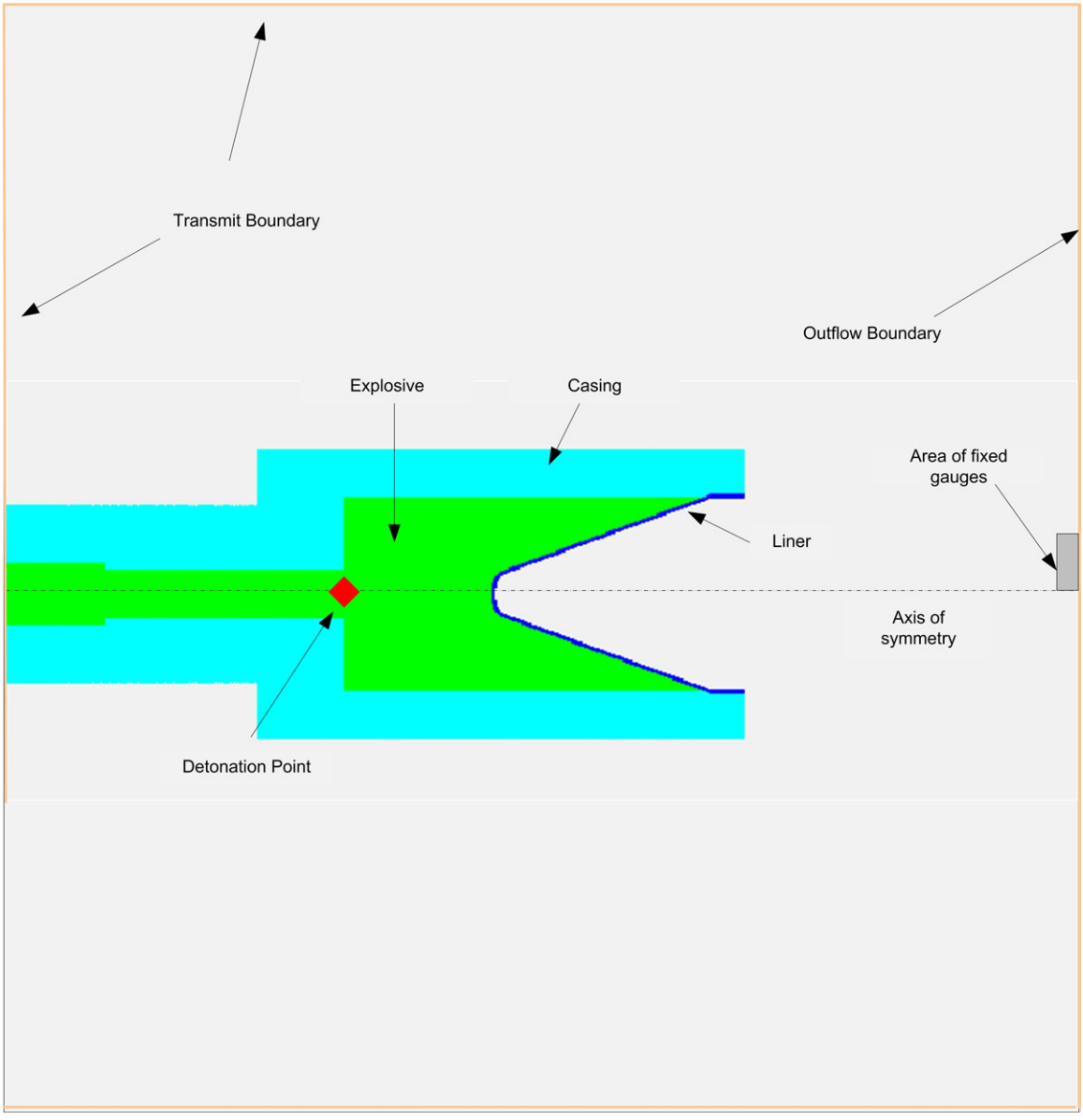

Figure 119: Layout for 25 mm NM charge

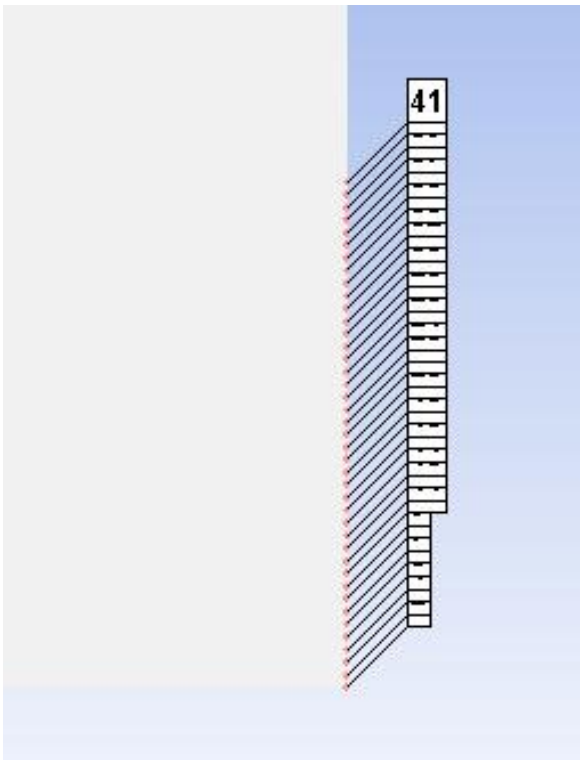

Figure 120: Area of fixed gauges at the right side of the grid

velocity plot (Fig. 121), measured with the fixed gauges, shows few differences which occurred from slightly different material removal times.

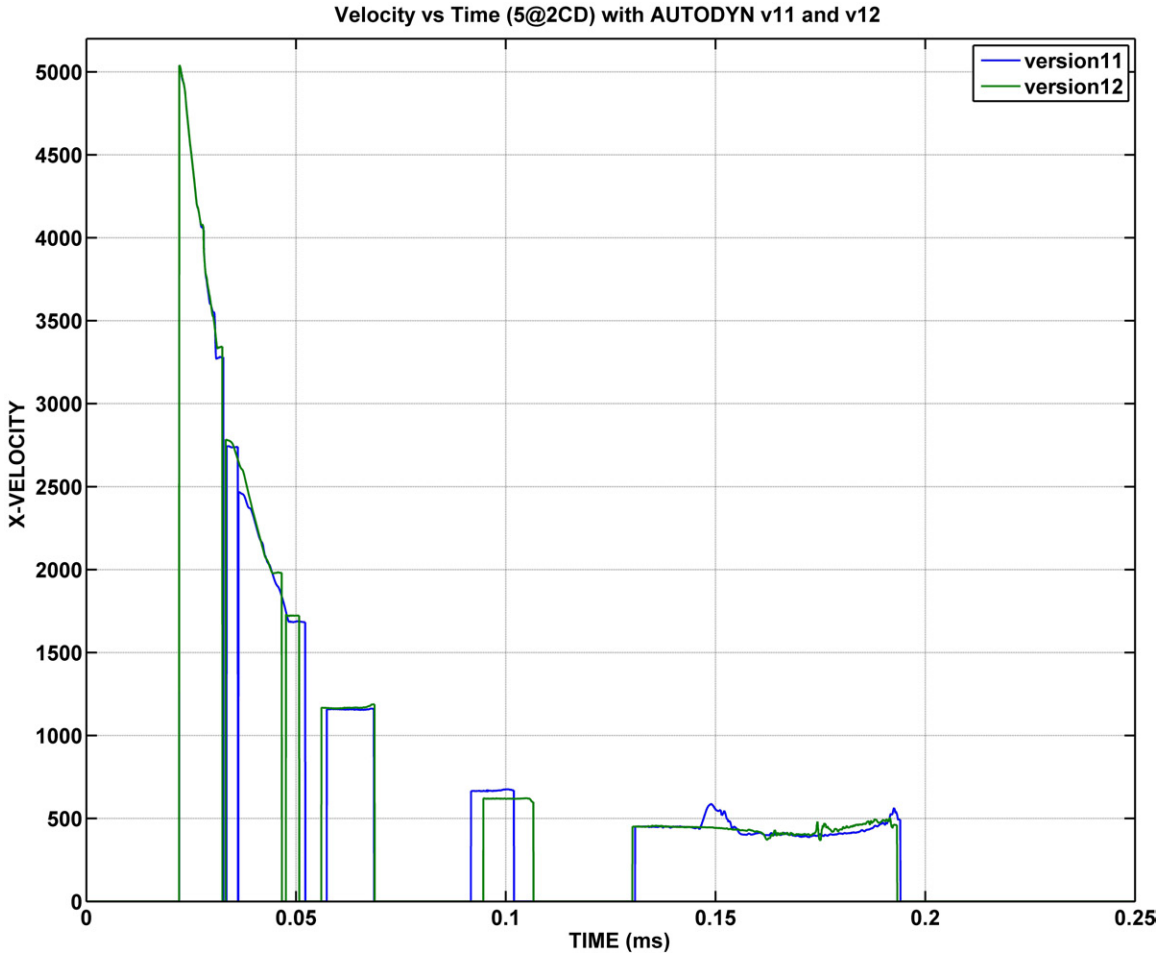

Figure 121: Comparison of X-velocity prediction between AUTODYN versions 11 and 12

The results for the 25 mm charge, described in section H.A were compared with fellow researchers, Haywood and Woody, and found to be almost identical. The velocity vs. time and velocity vs. cumulative mass plots are presented in Fig. 122 - 125. The higher jet tip velocity in the 7@2CD (7 cells/mm, standoff = 2 CD) simulation resulted in a right-shifted velocity vs. cumulative mass graph (Fig. 125). Both 7@2CD simulations setups have been checked a second time and both simulations were each conducted with AUTODYN version 11 and 12.0. The results of these recalculations are identical. Al-

though identical simulations were conducted, one should keep in mind to check anomaly simulation results to increase the statistical significance.

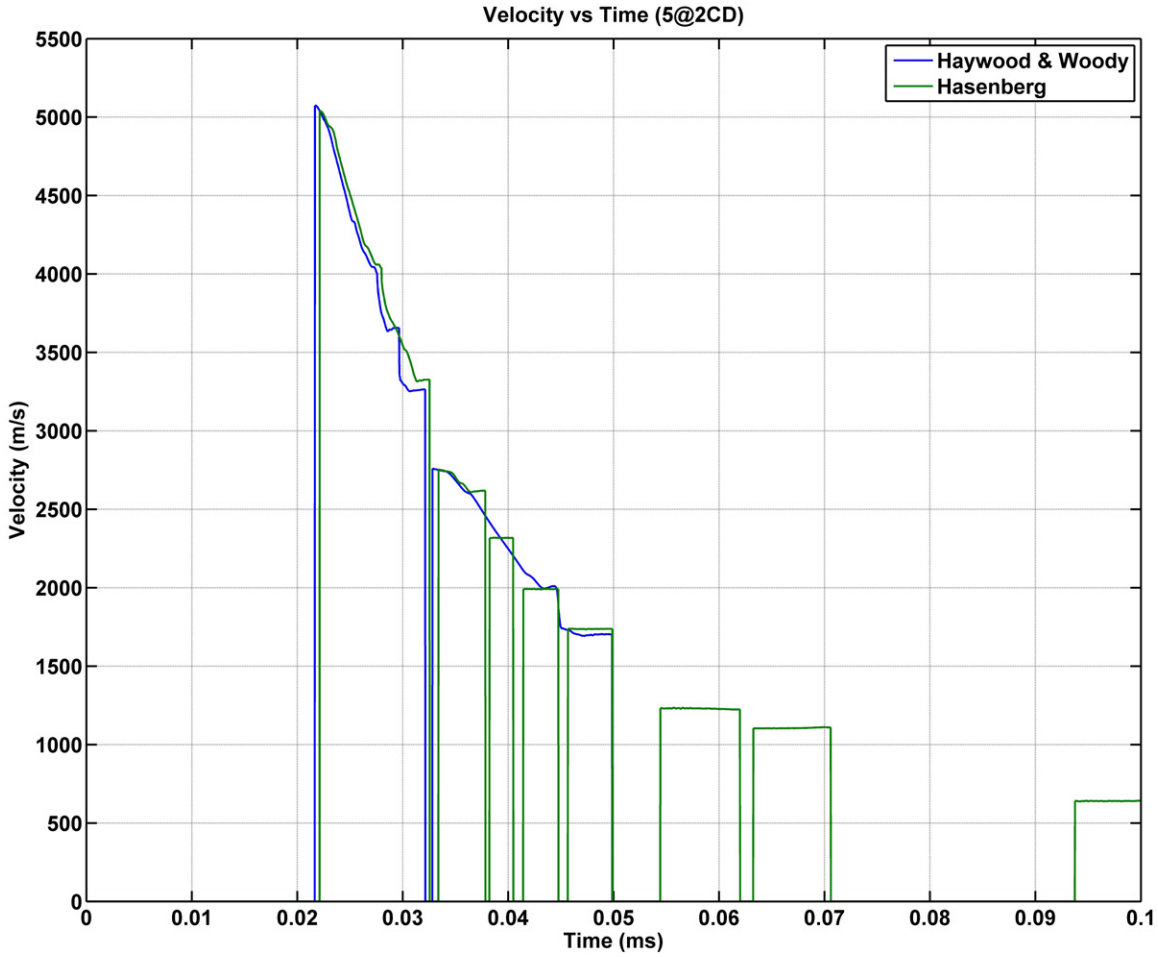

Figure 122: Comparison of Velocity vs. Time prediction between Haywood & Woody and Hasenberg; zoning: 5 cells/mm

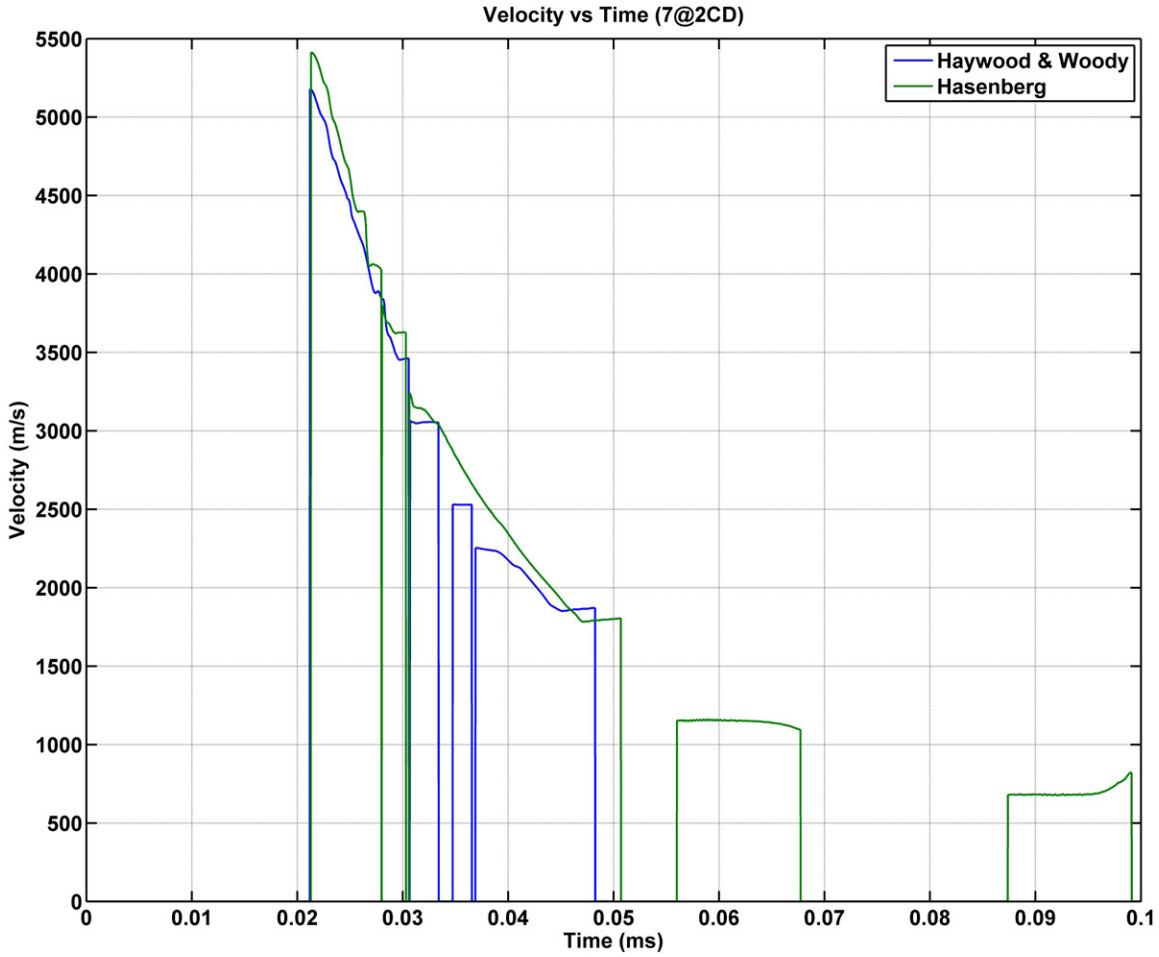

Figure 123: Comparison of Velocity vs. Time prediction between Haywood & Woody and Hasenberg; zoning: 7 cells/mm

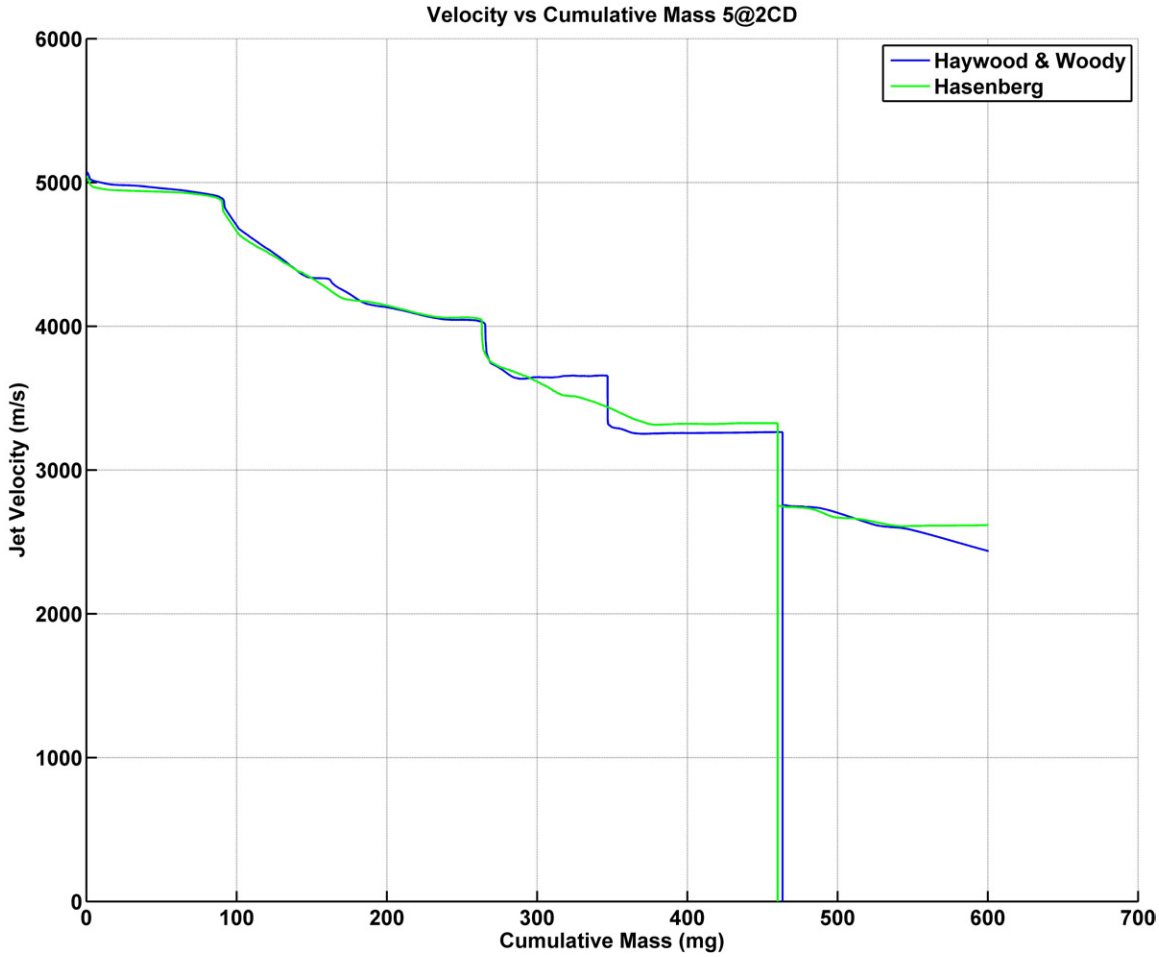

Figure 124: Comparison of Velocity vs. Cumulative Mass prediction between Haywood & Woody and Hasenberg; zoning: 5 cells/mm

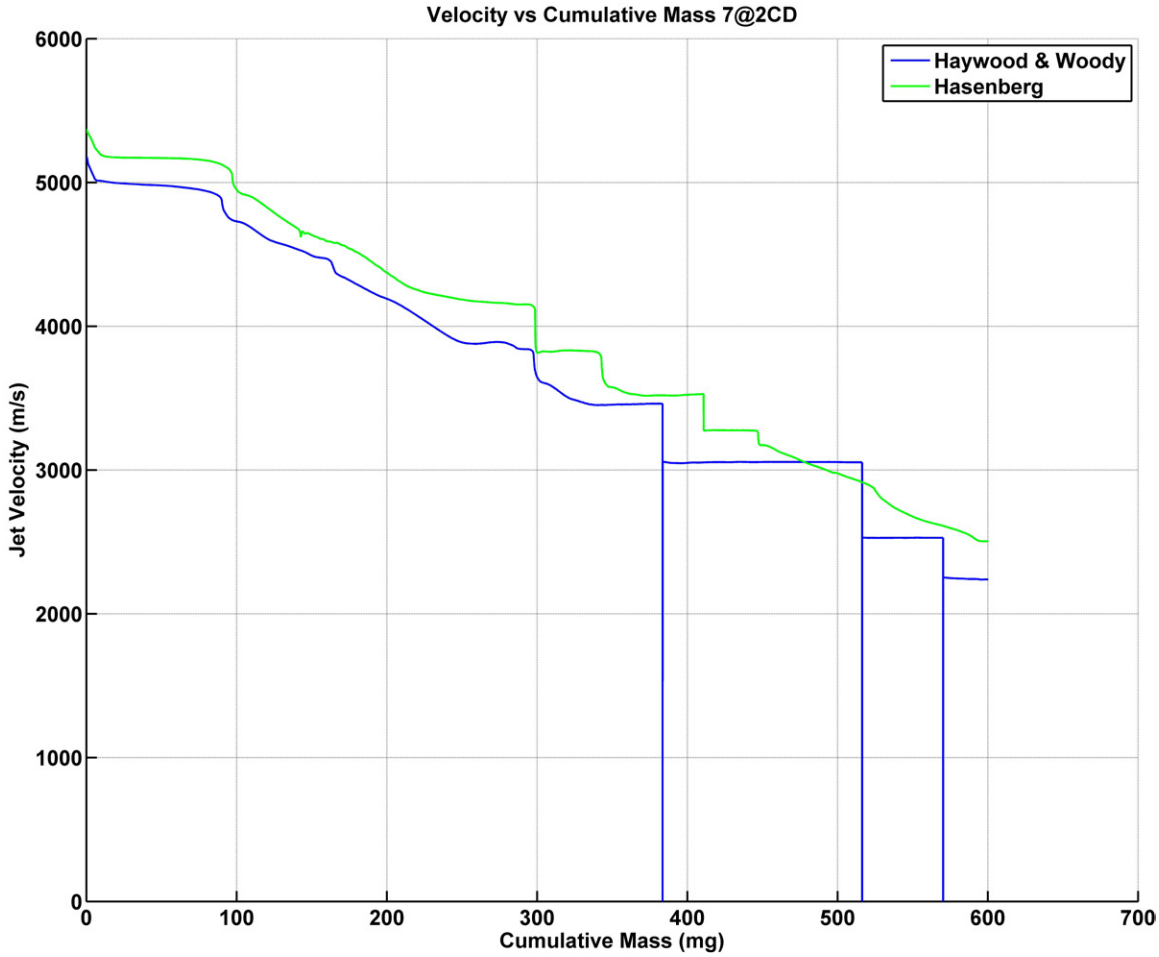

Figure 125: Comparison of Velocity vs. Cumulative Mass prediction between Haywood & Woody and Hasenberg; zoning: 7 cells/mm

LIST OF REFERENCES

[ANS97] Inc. ANSYS. *AUTODYN Technical Note - Euler shaped charge calculation*, 1997.

[ANS07] Inc. ANSYS. *AUTODYN User Manual*, 2007.

[ANS09] Inc. ANSYS. *AUTODYN Training Course*, 2009.

[BML95] R.E. Brown, M.E. Majerus, and J.S. Lewis. Building characteristics into a shaped charge to achieve unique performance requirements. *Int. Journal Impact Engineering*, 17:121–130, 1995.

[Bro10] R.E. Brown, 2010. Private communication, Naval Postgraduate School.

[CC86] Peter Conrad and Ross M. Contiliano. Weight efficient penetration. Technical report, A.R.A.P. Report No. 589, Vought, 1986.

[CCK76] P.E. Chou, J. Carleone, and R.R. Karpp. Criteria for jet formation from impinging shells and plates. *Journal of Applied Physics*, 47, 1976.

[Cha92] Pierre Y Chanteret. Studies of maximum velocities for coherent shaped charge jets. *Proceedings, 13th International Symposium on Ballistics*, 2:327–334, 1992.

[Cha93] Pierre Yves Chanteret. Considerations about the analytical modeling of shaped charges. *Propellants, Explosives, Pyrotechnics*, 18:337–344, 1993.

[CJC77] J. Carleone, R. Jameson, and Pei Chi Chou. The tip origin of a shaped charge jet. *Propellants, Explosives, Pyrotechnics*, 2:126–130, 1977.

[CL95] Pierre Y. Chanteret and Andre Lichtenberger. Bimetallic liners and coherence of shaped charge jets. *Proceedings, 15th International Symposium on Ballistics*, pages 143–150, 1995.

[Coo96] Paul W. Cooper. *Explosives engineering*. Wiley-VCH, New York NY u.a., 1996.

[Duo05] D.V. Duong. Overcoming the effects of supra-pressure detonation on shaped charge performance by liner material substitution. Master's thesis, Naval Postgraduate School, June 2005.

[Har81] John T. Harrison. Improved analytical shaped charge code: Basc. *US Army Ballistic Research Laboratory, Aberdeen, Maryland*, 1981.

[HS87] V. Hohler and AJ. Stiph. Hypervelocity impact of rod penetrators with l/d from 1 to 32. *Int. Journal Impact Engineering*, 5:323–331, 1987.

[HS94] M. Held and W. Schwarz. The importance for jet tip velocity for the performance of shaped charges. *Propellants, Explosives, Pyrotechnics*, 19:15–18, 1994.

[HW10] K. Haywood and J. Woody, 2010. Private communication, Naval Postgraduate School.

[Isb05] William M. Isbell. *Shock waves - Measuring the dynamic response of materials*. Imperial College Press, London, 2005.

[KB81] D.R. Kennedy and R.E. Brown. Unpublished experimental data. 1981.

[Lyn74] Charles T. Lynch. *CRC Handbook of Materials Science - General Properties*, volume 1. CRC Press, Florida, 1974.

[Mas10] J. Mason, January 2010. Private communication, University of Illinois.

[Mur90] M.J. Murphy. Examination of coherency criteria for high velocity jets. *Proceedings, 12th International Symposium on Ballistics*, pages 308–316, 1990.

[Pra06] Rudra Pratap. *Getting started with MATLAB 7 / a quick introduction for scientists and engineers*. Oxford University Press, USA, 2006.

[Wal93] James D. Walker. Incoherence of shaped charge jets. *Proceedings, 14th International Symposium on Ballistics*, 2:165–172, 1993.

[WG87] W.P. Walters and S.T. Golaski. Hemispherical and conical shaped-charge liner collapse and jet formation. 1987.

[ZW89] J.A. Zukas and W.P. Walters. *Fundamentals of Shaped Charges*. CMC Press, Baltimore, 1989.

[ZW98] J.A. Zukas and W.P. Walters. *Explosive Effects and Applications*. Springer, New York NY, 1998.

INITIAL DISTRIBUTION LIST

i. Defense Technical Information Center
Ft. Belvoir, Virginia

ii. Dudley Knox Library
Naval Postgraduate School
Monterey, California

iii. Professor Ronald E. Brown
Naval Postgraduate School
Monterey, California

iv. Professor Jose O. Sinibaldi
Naval Postgraduate School
Monterey, California

v. Professor Hendrik Rothe
Helmut-Schmidt-University
Hamburg, Germany

vi. Prüfungsamt
Helmut-Schmidt-University
Hamburg, Germany

vii. Prüfungsamt
Helmut-Schmidt-University
Hamburg, Germany

viii. Prüfungsamt
Helmut-Schmidt-University
Hamburg, Germany